UNIVERSIDADE FEDERAL DE PERNAMBUCO
CENTRO DE TECNOLOGIA E GEOCIÊNCIAS
DEPARTAMENTO DE GEOLOGIA
PROGRAMA DE PÓS-GRADUAÇÃO EM GEOCIÊNCIAS

MARIA ALCIONE LIMA CELESTINO

EVOLUÇÃO TECTÔNICA DA BORDA NORTE DA BACIA DO ARARIPE, NE DO BRASIL

Recife
2020

MARIA ALCIONE LIMA CELESTINO

EVOLUÇÃO TECTÔNICA DA BORDA NORTE DA BACIA DO ARARIPE, NE DO BRASIL

Dissertação apresentada ao Programa de Pós-Graduação em Geociências da Universidade Federal de Pernambuco, Centro de Tecnologia e Geociências, como requisito parcial para a obtenção do título de Mestre em Geociências. Área de concentração: Geologia Sedimentar e Ambiental.

Orientador: Prof. Dr. Tiago Siqueira de Miranda.

Coorientador: Prof. Dr. Gorki Mariano.

Recife

2020

Catalogação na fonte:
Bibliotecária Sandra Maria Neri Santiago, CRB-4 / 1267

C392e Celestino, Maria Alcione Lima.
Evolução tectônica da borda norte da Bacia do Araripe, NE do Brasil / Maria Alcione Lima Celestino. - 2020.
149 f.: il., figs.

Orientador: Prof. Dr. Tiago Siqueira de Miranda.
Coorientador: Prof. Dr. Gorki Mariano.
Dissertação (Mestrado) – Universidade Federal de Pernambuco. CTG. Programa de Pós-Graduação em Geociências, Recife, 2020.
Inclui referências.

1. Geociências. 2. Zona de dano. 3. Falhas transcorrentes. 4. Datação U-Pb (carbonato). 5. Reativação tectônica. 6. Brechas carbonáticas. I. Miranda, Tiago Siqueira de (Orientador). II. Mariano, Gorki (Coorientador). III. Título.

UFPE

551 CDD (22. ed.) BCTG/2021-211

MARIA ALCIONE LIMA CELESTINO

EVOLUÇÃO TECTÔNICA DA BORDA NORTE DA BACIA DO ARARIPE, NE DO BRASIL

Dissertação apresentada ao Programa de Pós Graduação em Geociências da Universidade Federal de Pernambuco, Centro de Tecnologia e Geociências, como requisito parcial para a obtenção do título de Mestre em Geociências. Área de concentração: Geologia Sedimentar e Ambiental

Aprovada em: 26 / 11 / 2020.

BANCA EXAMINADORA

_____

Prof. Dr. Tiago Siqueira de Miranda (Orientador)
Universidade Federal de Pernambuco

_____

Prof. Dr. Virginio Henrique de Miranda Lopes Neumann (Examinador Interno)
Universidade Federal de Pernambuco

_____

Prof. Dr. Francisco Cézar Costa Nogueira (Examinador Externo)
Universidade Federal de Campina Grande

Dedico este trabalho aos meus pais Maria das Neves e João, aos meus irmãos Alcimar e Alzeny e a Breno Vila Bela.

AGRADECIMENTOS

Primeiramente, agradeço a Deus por ter me concedido vida com saúde e por guiar meus caminhos.

Agradeço aos meus pais, Maria das Neves e João, por sempre acreditarem em mim e por todo apoio concedido todos esses anos, em mais uma jornada longe de casa. Estendo meus agradecimentos aos meus irmãos, Alcimar e Alzeny. Ao meu companheiro Breno Vila Bela, agradeço todo carinho, companheirismo e paciência de sempre.

Aos meus orientadores, Tiago Miranda e Gorki Mariano, pela oportunidade concedida. Muito obrigado pela confiança, por todo conhecimento compartilhado, motivação e por acreditarem em mim desde inicio.

Agradeço a minha amiga e companheira de laboratório, Vivian Silvani, por me escutar e por toda ajuda direta ou indireta.

Agradeço a Márcio e Topan, pela ajuda durante os trabalhos de campo, em especial a Márcio que sempre se dispôs a escutar minhas ideias no pós-campo. A Will, por sempre auxiliar no acesso aos laboratórios em uma época difícil em vivemos esse ano, além de diversas outras situações. Muito obrigada!

Ao Geolab, por preparar nossas amostras em tempo hábil e por tornar muita coisa presente neste trabalho ser possível.

Ao LAGESE (Laboratório de geologia sedimentar e ambiental) e ao ModLab (Laboratório de Modelagem) por todo apoio logístico em geral para as idas ao campo e no trabalho pós- campo.

Agradeço também aos professores que aceitaram participar da banca examinadora deste trabalho, Virginio Neumann e Francisco Cézar, obrigado por participarem desse momento e por contribuírem com o desenvolvimento deste trabalho.

Agradeço também à PETROBRAS pelo financiamento deste trabalho por meio de um projeto de cooperação em P&D FADE/UFPE/PETROBRAS.

RESUMO

Este trabalho apresenta a análise da influência tectônica da zona de cisalhamento Patos no controle estrutural da borda norte da Bacia do Araripe. A área de estudo abrange o contato geológico entre o embasamento (Complexo Granjeiro) e a cobertura sedimentar da Bacia do Araripe (formações Cariri, Barbalha e Crato). Este contato é marcado pela zona de falha Triunfo, que representa a reativação rúptil da zona de cisalhamento Patos. O objetivo deste trabalho foi classificar e quantificar os elementos arquiteturais da Falha Triunfo e analisar suas implicações tectônicas na cobertura sedimentar da Bacia do Araripe. A quantificação da espessura da zona de dano da Falha Triunfo foi realizada com a aplicação da técnica de *scanline*. Além disso, foram utilizados métodos de caracterização petrográfica (descrição de lâmina delgada, EDX e catodoluminescência) e geocronologia (U-Pb, carbonato) de rochas de falha. O núcleo da Falha Triunfo é composto por brechas tectônicas e cataclasitos. As zonas de dano da Falha Triunfo são formadas por: a) ortognaisses miloníticos (*footwall*); e b) arenitos e calcários laminados (*hangingwall*). Foram obtidas duas idades absolutas, 94.9 ± 3.4 Ma e 80.3 ± 2.8 Ma, em veios de carbonato que ocorrem em brechas carbonáticas da Formação Crato. Os resultados deste trabalho indicaram três estágios deformacionais para o desenvolvimento estrutural da borda norte da Bacia do Araripe: a) Dn, Orogênese Brasiliana, deformação dúctil; b) Dn+1, Paleozoico, deformação dúctil-rúptil; e c) Dn+2, Cretáceo, deformação rúptil. Além disso, esta pesquisa propõe que após o evento Dn+2 a Falha Triunfo continuou ativa durante a fase pós-rift da Bacia do Araripe.

Palavras chaves: zona de dano; falhas transcorrentes; datação U-Pb (carbonato); reativação tectônica; brechas carbonáticas.

ABSTRACT

This work presents the analysis of the tectonic influence of the Patos shear zone on the structural control of the northern border of the Araripe Basin. The study area covers the geological contact between the basement (Complex Granjeiro) and the sedimentary cover of the Araripe Basin (Cariri, Barbalha and Crato formations). This contact is marked by the Triunfo fault zone, which represents the brittle reactivation of the Patos shear zone. The objective of this work was to classify and quantify the architectural elements of the Triunfo Fault and to analyze its tectonic implications in the sedimentary cover of the Araripe Basin. The quantification of the thickness of the damage zone of the Triunfo Fault was performed with the application of the scanline technique. In addition, methods of petrographic characterization (petrography in thin section, EDX and cathodoluminescence) and geochronology (U-Pb, carbonate) of fault rocks were used. The core of the Triunfo Fault is composed of tectonic breccias and cataclasites. The damage zones of the Triunfo Fault are formed by a) mylonitic orthogneisses (footwall); and b) sandstones and laminated limestone (hangingwall). Two absolute ages were obtained, 94.9 ± 3.4 Ma and 80.3 ± 2.8 Ma, in carbonate veins that occur in carbonate breccias in the Crato Formation. The results of this work indicated three deformational stages for the structural development of the northern edge of the Araripe Basin: a) Dn, Brasiliano Orogeny, ductile deformation; b) Dn + 1, Paleozoic, ductile-brittle deformation; and c) Dn + 2, Cretaceous, brittle deformation. In addition, this research proposes that after the Dn + 2 event the Fault Triunfo remained active during the post-rift phase of the Araripe Basin.

Keywords: damage zone; strike-slip fault; U-Pb (carbonate) dating; tectonic reactivation; carbonate breccias.

LISTA DE ILUSTRAÇÕES

SUMÁRIO

1 INTRODUÇÃO

Esta dissertação apresenta os resultados obtidos a partir da análise estrutural de um sistema de falhas localizado na borda norte da Bacia do Araripe (BA). A caracterização estrutural foi realizada visando obter uma melhor compreensão sobre a evolução tectônica da borda norte da BA, a partir do estudo da reativação rúptil da zona de cisalhamento Patos, nomeada localmente como zona de falha Triunfo. Este trabalho teve como objetivo específico a análise dos elementos arquiteturais da Falha Triunfo (zona de dano, núcleo e protólito) e sua influência no desenvolvimento estrutural da BA.

Este estudo também possibilitou restringir reativações rúpteis da zona de falha Triunfo a partir do método de geocronologia de U-Pb, através de idades obtidas em veios de calcita e dolomita em brechas carbonáticas da Formação Crato.

O presente estudo foi financiado pelo projeto de pesquisa e desenvolvimento intitulado "ANÁLISE COMPARATIVA ENTRE MODELOS GEOLÓGICOS DE SISTEMAS FRATURADOS (CALCÁRIOS LAMINADOS), EXECUTADOS COM BASE NOS MÉTODOS DE LEVANTAMENTO DE PSEUDOPOÇOS E DE VARREDURA DE SUPERFÍCIES EM AFLORAMENTOS ANÁLOGOS". Este projeto é desenvolvido em cooperação entre a Universidade Federal de Pernambuco (UFPE), Fundação de Apoio ao Desenvolvimento da UFPE (FADE), e financiado pela Petrobras.

1.1 JUSTIFICATIVA E MOTIVAÇÃO

A BA é uma das mais importantes bacias intraplaca do nordeste do Brasil, principalmente devido à grande quantidade de fósseis com excelente estado de preservação (OSÉS *et al*., 2017; VAREJÃO *et al*., 2019). Além disso, esta bacia possui ótimos afloramentos de rochas análogas a sistemas petrolíferos do pré-sal. Portanto, a BA tem sido classificada como uma bacia escola (NEUMANN *et al.,* 2003; MARTILL *et al.,* 2007; ASSINE, 2007).

A sequência sedimentar da borda norte da BA é caracterizada principalmente pela ocorrência de rochas carbonáticas (Formação Crato) e evaporíticas (Formação Ipubi), que fazem parte da fase pós-rifte desta bacia. Estas formações apresentam fácies análogas ao sistema petrolífero presente nas bacias marginais do sudeste brasileiro (e.g., Bacia de Santos e Campos) (CATTO *et al*., 2016; WARREN *et al*., 2017; CABRAL *et al.,* 2019). Por exemplo, os calcários laminados da Formação Crato têm sido investigados em diversos estudos como

um reservatório análogo carbonático de baixa permeabilidade (SANTOS *et al.,* 2015; MIRANDA, *et al*., 2016; MIRANDA *et al.,* 2018). Além disso, este depósito carbonático Aptiano apresenta similaridades em termos deposicionais, geomecânicos e estruturais à uma das fácies das formações Barra Velha e Macabu, bacias de Santos e Campos, respectivamente (MUNIZ & BOSENCE, 2015; CATTO *et al.,* 2016; MIRANDA *et al*., 2018).

Estruturas pré-existentes do embasamento geralmente exercem forte controle estrutural no desenvolvimento de zonas de falha relacionadas a bordas de bacias sedimentares (ROTEVATN *et al.,* 2018). O presente estudo abordou a análise da influência da herança tectônica da zona de cisalhamento Patos na deformação rúptil da sequência sedimentar da borda norte da BA. Zonas de falhas são regiões intensamente fraturadas que podem influenciar no fluxo de fluídos em subsuperfície, incluindo exploração de hidrocarbonetos, água subterrânea, captura e estoque de CO_2 (BILLI *et al*., 2003; BALSAMO *et al*., 2012; SCHUELLER *et al*., 2013; DIMMEN *et al.,* 2017; PEACOCK *et al.,* 2017; TORABI *et al*., 2019; WU *et al*., 2019). Essas regiões apresentam papel importante no controle da distribuição de fluídos ao longo de pacotes sedimentares e diante disso, viu-se a necessidade de quantificar a espessura das zonas de dano da Falha Triunfo e investigar o controle estrutural da ocorrência de brechas carbonáticas dolomitizadas da Formação Crato. Além disso, processos hidrotermais e diagenéticos associados a atividades tectônicas de borda bacia podem afetar a qualidade de reservatórios (LIMA *et al.,* 2020; SALOMON *et al.,* 2020). Por exemplo, em sequencias carbonáticas o hidrotermalismo pode ter uma forte influência na distribuição de porosidade e permeabilidade dessas rochas (BALSAMO *et al*., 2012). Portanto, a caracterização estrutural de zonas de falha é importante para avaliar os impactos da circulação de fluídos hidrotermais dentro de reservatórios carbonáticos (LIMA & De ROS, 2019; LIMA *et al*., 2020; SALOMON *et al.,* 2020).

A partir deste contexto, observa-se que a compreensão sobre padrões estruturais (direções das estruturas rúpteis e dúcteis, e relação temporal entre elas) que controlaram a evolução tectônica de zonas de falha associadas à borda de bacias sedimentares possui grande relevância na caracterização de reservatórios carbonáticos.

1.2 OBJETIVOS

Os objetivos dessa pesquisa se dividem em gerais e em específicos, visando detalhar de forma precisa o que foi buscado durante esta pesquisa.

1.2.1 Objetivos Gerais

O objetivo principal desta pesquisa é a realização da análise da reativação tectônica da zona de cisalhamento Patos (zona de falha Triunfo) e sua relação com a deformação rúptil que ocorre na sequência sedimentar da borda norte da BA, visando obter uma melhor compreensão sobre a evolução tectônica da borda norte da BA. Desta forma, esta pesquisa utilizou como ferramenta a geologia estrutural e geocronologia, com enfoque no controle estrutural da zona de falha Triunfo na geração de brechas carbonáticas da Formação Crato.

1.2.2 Objetivos Específicos

a) Caracterização morfotectônica para identificação das estruturas em escala regional e correlaciona-las com os padrões das estruturas vistas em campo;
b) Mapeamento geológico-estrutural de detalhe (1:25.000) e análise cinemática das estruturas tectônicas presentes no embasamento cristalino e cobertura sedimentar;
c) Elaborar perfis topográficos 2D perpendiculares às principais estruturas tectônicas;
d) Quantificar a espessura das zonas de danos da Falha Triunfo;
e) Elaborar modelo digital de afloramento com uso de veículo aéreo não-transportado (VANT) para amparar a identificação de estruturas tectônicas;
f) Realizar o estudo de microtectônica das rochas de falha com uso de catodoluminescência, microscopia óptica (transmitida e refletida) e Energia Dispersiva de Raio-X (EDX) para identificação dos conteúdos mineralógicos, texturais e estruturais;
g) Caracterização mineralógica dos preenchimentos das falhas através do método de Difração de Raio X (DRX);
h) Caracterização geocronológica dos veios carbonáticos de rochas de falhas, utilizando o método de U-Pb.

1.3 LOCALIZAÇÃO DA ÁREA DE ESTUDO

A área de estudo abrange as cidades de Santana do Cariri e Nova Olinda, microrregião do Cariri, estado do Ceará. Estes municípios estão localizados a cerca de 540 km de Fortaleza, capital do estado do Ceará e aproximadamente 650 km do Recife, capital do estado de Pernambuco. A região estudada está inserida na BA, mais precisamente na borda norte (Fig.

1). Esta bacia é classificada como uma bacia interior do nordeste do Brasil e está inserida no Domínio Central (ou Zona Transversal) da Província Borborema.

A BA é limitada ao norte pela terminação oeste da zona de cisalhamento Patos, na área de estudo este trecho da zona de cisalhamento é classificada como Falha Triunfo que ocorre no contato entre as rochas do embasamento cristalino (Complexo Granjeiro) e cobertura sedimentar (Formações Cariri e Crato) (ALENCAR, 2014) (Fig. 1).

O embasamento Pré-Cambriano que ocorre na área estudada consiste em ortognaisses (Trondemitos-Tonalitos-Granodioritos– TTG) milonitizados, devido à proximidade da zona de cisalhamento Patos, do Complexo Granjeiro (Arqueano). Estas rochas apresentam forte foliação milonítica subvertical, lineação de estiramento mineral sub-horizontal, falhas dúcteis-rúpteis transcorrentes, falhas normais, veios e juntas (ALENCAR, 2014; CELESTINO *et al*., 2020). Além de metassedimentos do Grupo Cachoeirinha (Neoproterozóico) que ocorrem na porção sudeste da área. A cobertura sedimentar da BA na área de estudo é composta por arenitos da Formação Cariri (Siluro-Devoniano?), sequência pré-rifte (NEUMANN, 1999; ASSINE, 2007). Calcários laminados da Formação Crato (Aptiano-Albiano), sequência pós-rifte (NEUMANN, 1999; ASSINE, 2007; ASSINE *et al*., 2014). Esses arenitos ocorrem intensamente deformados por bandas de deformação, falhas e juntas, enquanto que os calcários apresentam juntas, veios, falhas transcorrentes, shear fractures sin-sedimentares, microslumps, *pipes* brechas e estilolitos (SILVA, 2003; MARTILL *et al*., 2008; ALENCAR *et al*., 2013; ALENCAR, 2014, ALENCAR *et al*., 2020).

Figura 1- Mapa aeromagnetométrico, com filtro de redução ao polo, da região da Bacia do Araripe. Detalhe para área de estudo (retângulo azul).

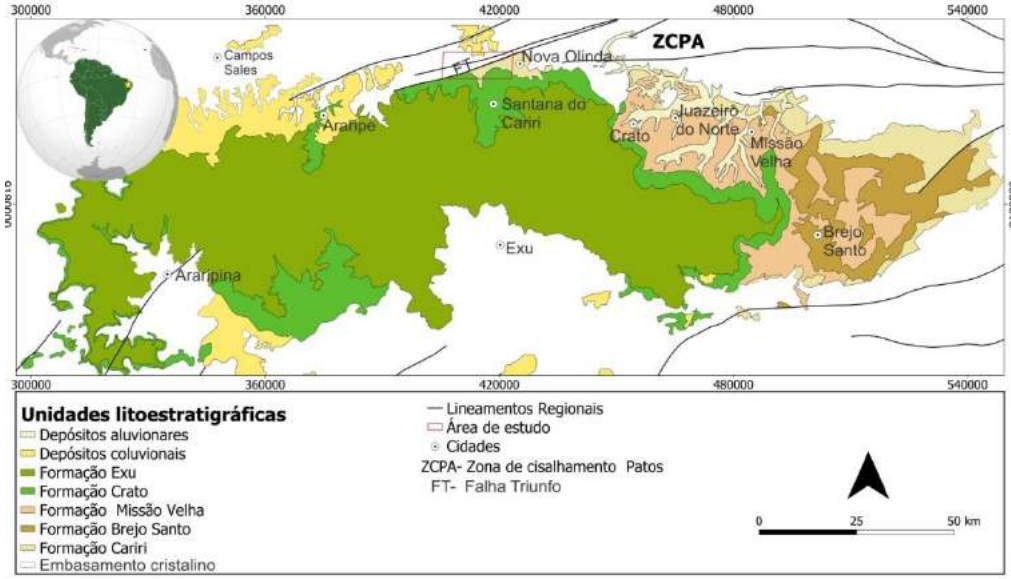

Fonte: Modificado de dados do GEOBANK/CPRM

1.4 MATERIAIS E METÓDOS

A sistemática adotada para elaboração do presente trabalho consistiu em 8 etapas: a) revisão bibliográfica; b) compilação da base de dados; c) análise de lineamentos; d) mapeamento geológico- estrutural; e) construção de modelos digitais de afloramento; f) caracterização petrográfica e microtectônica; g) análises física e química; e h) integração, análise dos dados e elaboração de manuscrito (Fig. 2). Cada etapa será detalhada abaixo.

Figura 2- Fluxograma das etapas realizadas durante a realização do trabalho.

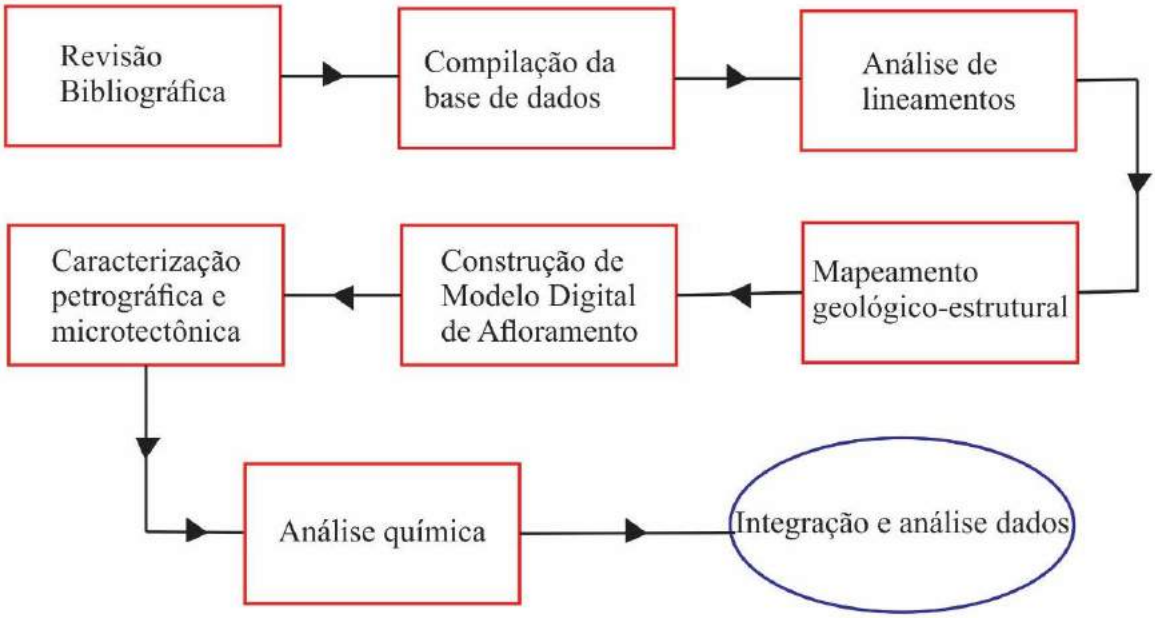

Fonte: Autor (2020).

1.4.1 Revisão Bibliográfica

O levantamento bibliográfico foi realizado com o intuito de reunir todo material de pesquisas realizadas anteriormente (artigos, livros e mapas), a fim de adquirir um conhecimento prévio sobre a área em escala regional e local. Essa etapa se estendeu até a fase final da elaboração da presente dissertação. Foram levantados temas centrados na evolução tectônica da BA, Província Borborema, nos complexos gnáissicos que compõem o embasamento cristalino da bacia, além de trabalhos sobre caracterização de zonas de dano, rochas de falha, análise morfotectônica e das demais técnicas utilizadas, objetivando dar um maior suporte para as etapas posteriores.

1.4.2 Compilação da base de dados

Durante esta etapa foi realizada a compilação das bases cartográficas disponíveis para a área de estudo, como: mapas geológicos, estruturais, dados aerogeofísicos (aeromagnetometria), do Serviço Geológico do Brasil (CPRM - http://geosgb.cprm.gov.br/), dados de satélite do *United States Geological Survey* (USGS), obtidos a partir do portal *EarthExplorer* (https://earthexplorer.usgs.gov/). Os dados de satélite utilizados compreendem as imagens de SRTM (*Shuttle Radar Topography Mission*) com resolução espacial de 30m. Estes dados auxiliaram na interpretação de estruturas regionais da área. Também foram coletados relatórios de poços perfurados na área de estudo por meio da plataforma do SIAGAS (Sistema de Informações de Águas Subterrâneas - http://siagasweb.cprm.gov.br/layout/) para um melhor entendimento do topo do embasamento cristalino.

1.4.3 Análise de Lineamentos Topográficos

A obtenção de lineamentos topográficos se deu a partir de imagens SRTM, com resolução espacial de 30m. Com o auxílio do *software* QGis 3.4.7 essas imagens foram processadas e possibilitaram a produção de Modelos Digitais de Elevação (MDE).

Quatro MDE foram produzidos a partir da técnica de iluminação interativa em quatro direções de iluminação (0Az, 45Az, 90Az e 315Az), que auxilia a identificação dos lineamentos estruturais conforme os diferentes ângulos de sombreamento. Para extração dos lineamentos topográficos foram utilizados dois critérios: a) cristas e b) vales (ONORATI *et al.*, 1992; SALAMUNI *et al.*, 2004; DE LIMA *et al.*, 2017; CELESTINO *et al.*, 2018; CELESTINO *et al.*, 2020) (Fig. 3).

A identificação dos lineamentos foi realizada para dois setores distintos: a) embasamento adjacente; e b) cobertura sedimentar da BA. Com auxílio do *software* GIS foi calculado o azimute e comprimento de todos os lineamentos identificados, no embasamento e na cobertura sedimentar da bacia. Em seguida foram construídos diagramas de roseta, com intervalo de classe (*bin size*) de 10Az, para as atitudes dos lineamentos extraídos de cada MDE de iluminação diferente. Posteriormente, todos os lineamentos extraídos de cada MDE, foram reunidos em duas rosetas para cada setor estudado: a) embasamento adjacente; e b) cobertura sedimentar da BA e critério utilizado.

Por fim, para a análise dos padrões de orientação e comprimento dos lineamentos foram produzidos diagramas de rosetas, para cada setor estudado, com intervalo de classe de 10Az. Em cada diagrama de rosetas foram inseridos dados de direções associados a intervalos de comprimentos definidos a cada 500 m.

Figura 3- Fluxograma das etapas realizadas durante a análise dos lineamentos topográficos.

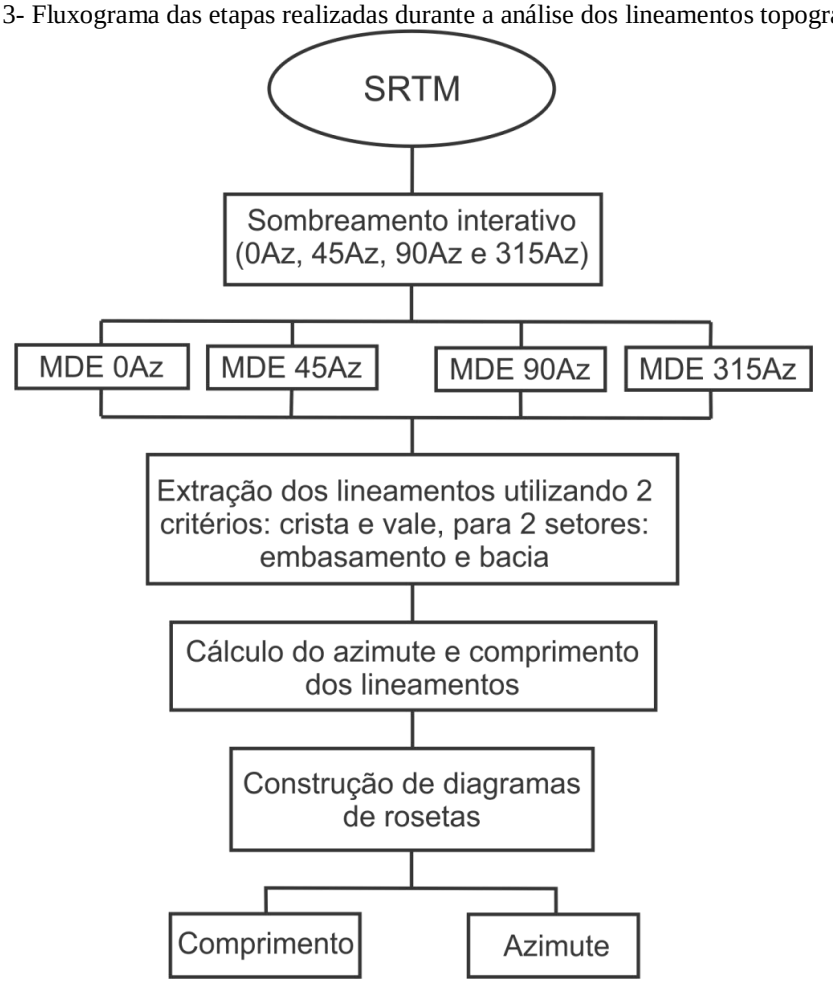

Fonte: Modificado de Celestino *et al.* (2020).

1.4.4 Mapeamento Geológico-Estrutural

Durante a etapa de mapeamento estrutural foram realizados trabalhos de campo na escala de 1:25.000, com objetivo de coletar dados estruturais associados as falhas que ocorrem na área de estudo.

Para realização do trabalho de campo previamente foram definidos seis perfis transversais a principal estrutura da área, Falha de Triunfo, que apresenta uma orientação preferencial NE-SW. Estes perfis encontram-se dispostos ao longo de redes de drenagens e estradas não pavimentadas.

Ao longo dos perfis foram realizadas *scanlines* que consistem na contagem de fraturas por metro ao longo de uma linha (e.g., P10) (DERSHOWITZ & EINSTEIN, 1988), a fim de identificar a frequência das estruturas rúpteis e definir a espessura de zonas de danos. Ao longo das *scanlines* foram coletados: número de estruturas, orientação, relação de interseção entre as estruturas e preenchimento (ORTEGA *et al*., 2006; BISDOM *et al*., 2014; SANTOS *et al*., 2015; MIRANDA *et al*., 2018). As *scanlines* foram posicionadas de forma perpendicular as orientações preferenciais das estruturas rúpteis. Foram coletadas atitudes das diversas estruturas tectônicas encontradas na área (juntas, falhas e bandas de deformação) o que permitiu a elaboração de diagramas de rosetas, estereogramas e histogramas. Foram utilizados para coleta dos dados estruturais, bússolas geológicas *Clar* e *Brunton*, e os aplicativos *Fieldmove Clino* e *StereoNet* por meio de *smartphones*.

Também foi realizada a coleta de amostras de mão que foram devidamente enumeradas e orientadas, para posterior confecção de seções delgadas para estudo de microtectônica e datação geocronológica. Ao longo dos planos de falhas encontrados foram coletadas amostras do preenchimento da falha para análise de difratometria de raio X (vide tópico 1.5.7).

1.4.5 Modelo Digital de Afloramento

Durante esta etapa foram produzidos Modelos Digitais de Afloramento (MDA) de áreas selecionadas em função da sua representatividade. Para coleta das imagens foi utilizado um Veículo Aéreo Não Tripulado (VANT), Mavic Pro, DJI. As imagens foram processadas no *software* Agisoft para produção de ortomosaicos. Através dos ortomosaicos as estruturas tectônicas foram identificadas e digitalizadas para melhor exposição dos dados de campo.

Os afloramentos escolhidos para elaboração do MDA foram cuidadosamente selecionados com foco na ocorrência de um ou mais tipos litológicos, extensão e uma diversidade de estruturas. O MDA foi elaborado preferencialmente em locais em que foram coletados os dados de *scanlines* para melhor visualização da distribuição das estruturas.

1.4.6 Caracterização Petrográfica e Microtectônica

Para a análise petrográfica e microtectônica foram confeccionadas seis seções delgadas, em seguida foram descritas no Laboratório de Petrografia Sedimentar, do Departamento de Geologia (DGEO – Litpeg - UFPE). A partir dessas seções delgadas foi

possível realizar a caracterização mineralógica, textural e estrutural das rochas da área, utilizando microscópio de luz transmitida, catodoluminescência e EDX.

A catodoluminescência foi utilizada como uma ferramenta complementar na caracterização estrutural e nas relações de temporalidade de preenchimento do cimento das rochas de falha, visto que essa técnica realça feições que não são facilmente identificadas na microscopia óptica convencional. A análise foi realizada em imagens cedidas pela Petrobrás e também em seções delgadas analisadas no Laboratório de Catodoluminescência do DGEO-Litpeg- UFPE. Após esta etapa, foram selecionadas seções delgadas para posterior análise de EDX.

1.4.7 Análises físico-química

As análises realizadas consistiram em: DRX (físico) (a) e geocronológicas de U-Pb em calcita (química) (b). As amostras para análise de DRX foram preparadas no Laboratório de Preparação de Amostras (LPA) do Departamento de Geologia da UFPE (DGEO/UFPE) e as amostras para datação foram preparadas pelo GEOLAB- Soluções em Geologia.

As análises de DRX foram elaboradas em materiais coletados ao longo de planos de falhas e analisadas através do método do pó. As amostras inicialmente foram coletadas e pulverizadas até a fração argila e a composição química desse material foi determinada a partir da análise do pó, no laboratório de Cristaloquímica e micromorfologia do solo (UFRPE-UAG). O aparelho utilizado para análise foi o XRD 6100 Shimadzu, Volt 40, Amp 20, 2º theta por minuto, e amplitude de varredura do 2º theta de 3 a 50 graus. As amostras na fração argila não foram submetidas à pré-tratamentos para caracterização do tipo de argila. As caracterizações das amostras foram realizadas a partir do software X'Pert High Score Plus da PANalytical, por meio da comparação dos difratogramas gerados com padrões de referência disponíveis no trabalho de Chen (1977).

a) Amostras de carbonatos foram preparadas para análise geocronológicas a partir do método U-Pb. Foram produzidos blocos polidos com 5 cm de comprimento e espessura de cerca de 1,5 cm. As análises geocronológicas de U-Pb em calcita foram realizadas utilizando *Laser Ablation Inductively Coupled Mass Spectometry* (LA-ICP-MS) do *Geochronology and Tracers Facility, British Geological Survey* (Nottingham, UK), usando o método descrito em Roberts & Walker (2016) e Roberts *et al*. (2017). Com os resultados obtidos foram construídos diagramas de Tera-Wasserburg.

1.4.8 Integração, Análise dos Dados e Elaboração de Manuscritos

Nessa última etapa foi realizada a integração, processamento e interpretação dos dados obtidos das fases anteriores e a redação de manuscritos e da presente dissertação. A partir do trabalho de campo foi possível fazer uma análise multiescalar da área, identificar a orientação das estruturas, suas relações temporais, quantificar a espessura de zonas de danos das falhas e classificar rochas de falha.

2 CONTEXTO TECTÔNICO DA BACIA DO ARARIPE

A BA é a mais extensa das bacias intraplaca do nordeste brasileiro. Esta bacia encontra-se limitada ao norte pela zona cisalhamento Patos e a sul pela zona cisalhamento Pernambuco (MIRANDA, 2015).

O embasamento adjacente da BA compreende a rochas dos subdomínios Granjeiro-Seridó e Araripina, suítes intrusivas Prata, Itaporanga (batólito Bodocó), Conceição e por rochas metassedimentares do Grupo Cachoeirinha (MEDEIROS, 2004; SCHOBBENHAUS *et al*., 2004; OLIVEIRA, 2008).

Internamente a BA foi dividida em duas sub-bacias, inicialmente chamadas de sub-bacia E e W (RAND, 1983 e RAND & MANSO, 1984), a partir de dados magnetométricos e gravimétricos. Estes autores observaram a existências de anomalias gravimétricas associadas às sub-bacias e definiram profundidades para esses dois setores (depocentros): 2400 m (leste) e 2000 m (oeste). Ponte & Ponte Filho (1996) denominaram estas sub-bacias como Cariri (oeste) e Feitoria (leste) separadas por um alto estrutural, chamado alto Dom Leme. Posteriormente, Castro & Castelo Branco (1999) realizaram levantamento gravimétrico na BA com um total de 999 estações distribuídas numa malha irregular, estes autores comprovaram a existência dessas sub-bacias a partir da modelagem 3D. Alguns trabalhos propõem que a origem tectônica das bacias interiores do NE do Brasil está associada com a abertura do Atlântico Sul, que consiste em um evento de rifteamento (Neocomiano) (MATOS, 1992, 1999; FRANÇOLIN et al., 1994).

Chang *et al*. (1988) propuseram a existência de estágios de rifteamento associados a abertura do Atlântico Sul, estes foram classificados como: sin-rifte I (Jurássico Superior), sin-rifte II (Neocomiano) e sin-rifte III (Barremiano). O estágio sin-rifte II estaria associado ao desenvolvimento dos *trends* Recôncavo-Tucano-Jatobá, Gabão-Sergipe-Alagoas e Cariri-Potiguar, este último está ligado a formação das bacias do Araripe, Rio do Peixe, Iguatu, Malhada Vermelha, Lima Campos, Icó e Potiguar (MATOS, 1999). Dois modelos se destacam no estudo desses rifteamentos desenvolvidos durante a abertura do Atlântico Sul no Eocretáceo, modelos propostos por Matos (1992, 1999) e Françolin *et al*. (1994).

Matos (1992, 1999) propôs que as bacias tipo rifte intracontinentais apresentam geometrias em três direções de sistemas de riftes e que foram controladas pelo arcabouço estrutural do embasamento, estas bacias consistem em riftes abortados. De acordo com estes autores à medida que Atlântico Sul abria de sul para norte ocorria uma deformação que é reconhecida a partir de três estágios deformacionais: sin- rifte I, II, III (Fig. 4). Estes estágios

são caracterizados pela formação de meio grábens distribuídos ao longo dos três *trends* anteriormente citados: Recôncavo-Tucano-Jatobá, Gabão-Sergipe-Alagoas e Cariri-Potiguar.

Segundo Matos (1992, 1999) a fase sin-rifte I (final do Jurássico- início do Berriasiano) é caracterizada por uma sedimentação de idade Jurássica associada à depressão Afro-brasileira que se estendia desde o sul da Bahia até a região do Cariri (Fig. 4- A). A fase sin-rifte II foi dividia em sin-rifte IIa e sin-rifte IIb, a partir de dados bioestratigráficos observou-se que a abertura do Atlântico sul ocorreu do sul para o norte. Durante a fase sin-rifte IIa (início do Berriasiano) os *trends* Recôncavo-Tucano-Jatobá e Gabão-Sergipe-Alagoas se desenvolveram e é marcado por uma distensão de direção E-W que pôde ser comprovada por meio de indicadores cinemáticos (Fig. 4- B). Durante a fase sin-rifte IIb (Neocomiano) as zonas de cisalhamento Pernambuco (Brasil) - e Ngaoundere (África) serviram como zona de acomodação à medida que se desenvolvia o *trend* Cariri- Potiguar, caracterizado por uma extensão de direção NW-SE (Fig. 4- C). Uma série de bacias com *trends* preferenciais NE-SW (bacias do Araripe, Rio do Peixe, Iguatu, Malhada Vermelha, Lima Campos, Icó e Potiguar), controladas por zonas de cisalhamentos adjacentes de direção NE-SW, teriam se desenvolvido (MATOS (1992, 1999)). Durante a fase sin-rifte III (Barremiano superior) a sedimentação das bacias do vale do Cariri e porção onshore da Bacia Potiguar é abortada e se inicia a abertura do Atlântico equatorial (MATOS (1992, 1999)) (Fig. 4- D).

Figura 4- Modelo proposto por Matos (1999) ilustra os três estágios deformacionais desenvolvidos durante a abertura do Atlântico Sul, as setas indicam as direções de extensão. A) Fase sin-rifte I ((final do Jurássico e início do Berriasiano), desenvolvimento da depressão Afro-Brasileira; B) Sin-rifte IIa (Início do Berriasiano), início do fraturamento crustal nos *trends* Recôncavo-Tucano-Jatobá e Gabão-Sergipe-Alagoas; C) Sin-rifte IIb (Neocominiano), desenvolvimento do *trend* Cariri-Potiguar; e D) Sin-rifte III (Barremiano Superior).

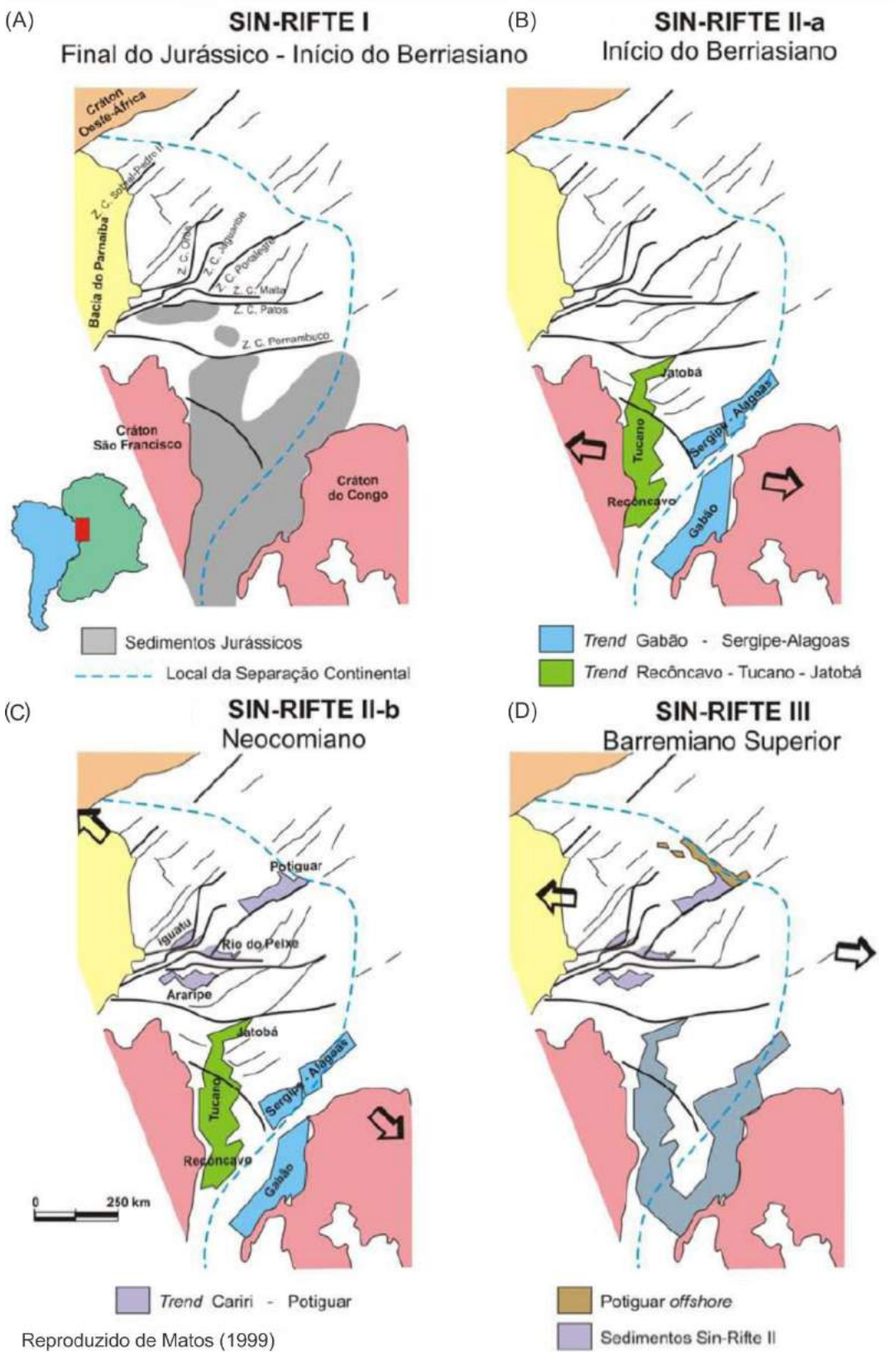

Fonte: Modificado de Oliveira (2008).

O segundo modelo foi proposto por Françolin *et al*. (1994), estes sugeriram que durante a abertura do Atlântico Sul ocorreu reativação rúptil das zonas de cisalhamento de direção E-W sinistrais e NE-SW dextrais, que levaram ao desenvolvimento de grábrens e semi-grábens, estes estudos foram realizados na Bacia Rio do Peixe.

Trabalhos mais recentes têm sugeridos novos aspectos sobre a evolução tectônica da BA, como o modelo proposto por Marques *et al*. (2014). Estes autores propuseram que a bacia passou por uma fase de inversão tectônica após a fase de rifteamento durante o Cretáceo (Fig. 5). Esta inversão resultou na inversão de falhas normais para falhas inversas e geração de novas falhas inversas, que foram causadas por esforços compressivos, de direção ENE-WSW, resultantes do afastamento da cadeia Meso-atlântica na porção leste da América do sul e na porção oeste seria resultado dos esforços compressivos associados à Cordilheira dos Andes. Porém para que essa inversão seja possível a placa teria que apresentar um comportamento elástico para suportar tais esforços. Segundo os autores acima citados, durante o Cretáceo seria difícil manter um relevo associado à inversão devido à fase extensional atuante, o que é diferente nos tempos mais recentes onde essa inversão passa a ser bem preservada nas rochas. Para estes autores a BA consiste em um horst com 500 m acima do embasamento adjacente.

Figura 5- Evolução tectônica da BA proposta por Marques *et al*. (2014). A) Estágio inicial do rifteamento, com um gráben estreito resultante de esforços distensivos NW-SE; B) Gráben mais largo e profundo com desenvolvimento de falhas normais; C) Estágio final do rifteamento contemporâneo com a abertura do Atlântico Sul; D) Inversão tectônica da bacia resultado de esforços compressivos de direção ENE-WSW, com reativação das falhas normais e injeção de rochas dúcteis ao longo dos planos de falha. A linha branca tracejada indica a topografia atual da BA.

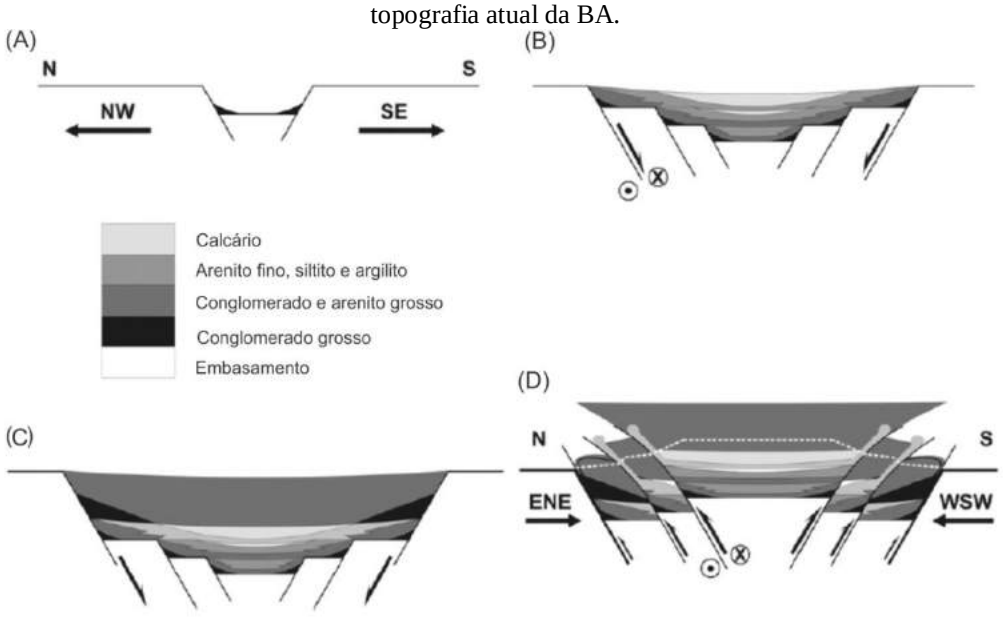

Fonte: Modificado de Marques *et al*. (2014).

Peulvast & Bétard (2015) sugeriram que topografia atual da BA está associada a um processo de erosão diferencial combinado ao soerguimento do Planalto da Borborema, e não a um processo de inversão tectônica como proposto por Marques *et al*. (2014). As rochas do topo da BA (Formação Exu) apresentam camadas de concreções de ferro que funcionaram como camadas resistentes aos processos intempéricos, enquanto que o embasamento composto em sua maioria por rochas metassedimentares, menos resistentes ao intemperismo, sofreu uma taxa de erosão maior do que a região da cobertura sedimentar. Estes fatores foram importantes para o desenvolvimento da atual topografia da BA. Mais recentemente Garcia *et al*. (2019) utilizaram o método magnetotelúrico, que consiste em método eletromagnético passivo, e observaram que sob a bacia ocorre um material astenosférico que favoreceu a inversão topográfica da bacia por meio de um empurrão vertical local. Este material é resultado do afinamento da crosta (devido os esforços extensionais, Mesozoico), que favoreceu a ascensão do material astenosférico.

Miranda *et al*. (2014) e Miranda (2015) propuseram que a BA passou por duas fases de evolução tectônica: a primeira do tipo *pull apart* (Paleozoico) e segunda uma tectônica do tipo rifte (Eocretáceo). Está última fase coerente com o modelo proposto por Matos (1992, 1999). Os autores utilizaram dados gravimétricos e topográficos para o estudo de lineamentos estruturais, a partir desses dados observaram a ocorrência de *trends* preferenciais NE-SW, E-W, NW-SE e N-S. Os *trends* NW-SE e N-S foram interpretadas como falhas normais e/ou transcorrentes (R e R'), como estruturas nucleadoras da quebra do embasamento com geometria do tipo *pull apart*, associadas à primeira fase tectônica (Fig. 6). As direções NE-SW estariam associadas à distensão NW-SE que ocorreu durante a fase rifte (Eocretáceo), os *trends* E-W estariam associados a reativações da zona de cisalhamento Patos. Segundo esses autores a zona cisalhamento Patos compreende a estrutura principal associada à formação da bacia, esta é composta por depocentros romboédricos (sub-bacias E e W).

Figura 6- Mapa de anomalias gravimétricas residuais da BA ilustrando os lineamentos no interior da bacia (linhas verdes) e no embasamento adjacente (linhas branca) com suas respectivas rosetas. Diagrama de Riedel mostrando as principais estruturas geradas durante a formação do possível sistema *pull-apart* que originou a bacia. As anomalias que mostram lineamentos NW-SE e N-SE podem ser explicadas pela geração de falhas transcorrentes, conforme previsto no diagrama de Riedel.

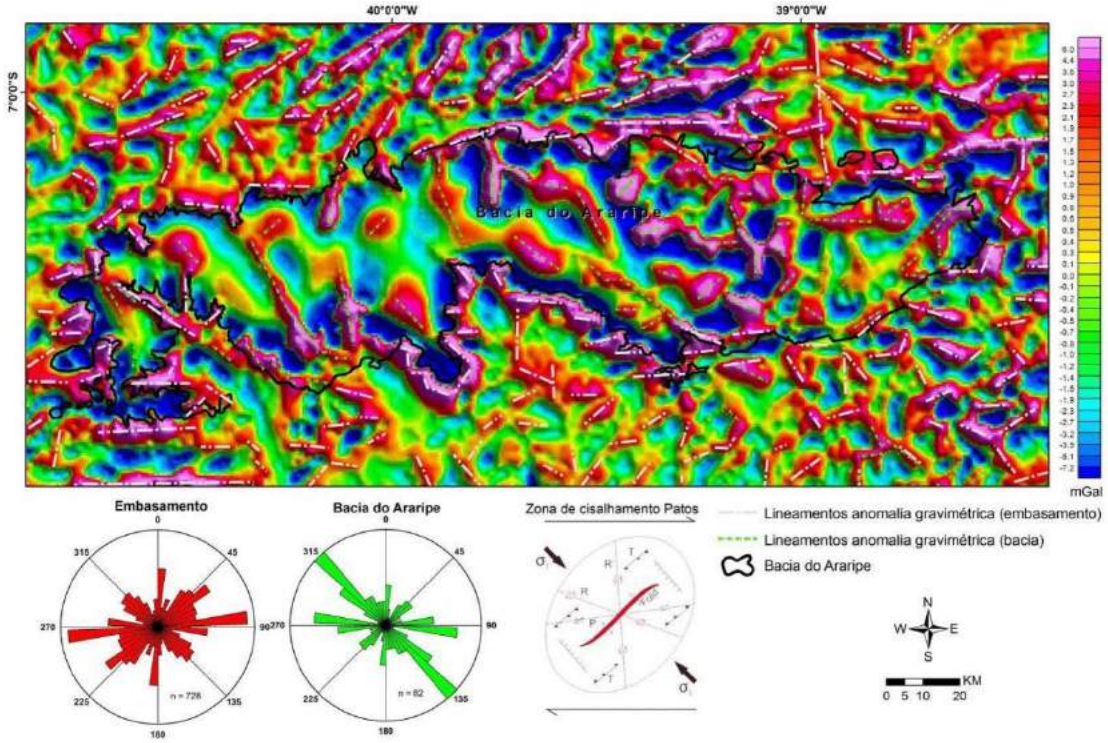

Fonte: Miranda (2015).

3 RESULTADOS

Parte dos resultados desta dissertação encontra-se na forma de dois artigos científicos. O primeiro artigo é intitulado "*Fault Damage Zones Width: Implications for the Tectonic Evolution of the Araripe Basin, Brazil, NE Brazil".* Este artigo foi publicado no *Journal of Structural Geology*, nele é abordado a quantificação dos elementos arquiteturais da Falha Triunfo e suas implicações tectônicas na cobertura sedimentar da Bacia do Araripe.

O segundo artigo é intitulado *"Structural control and geochronology of Cretaceous carbonate breccia pipes, Crato Formation, Araripe Basin, NE Brazil"*. Este artigo foi submetido para a *Marine and Petroleum Geology*, e apresenta uma análise do controle estrutural na origem e desenvolvimento de brechas carbonáticas da Formação Crato, acompanhado de uma análise petrográfica (EDX, catodoluminescência) e geocronológica (U-Pb).

A sessão 3.3 apresenta a caracterização estrutural e análise de DRX das rochas de falha associadas à zona de falha Triunfo.

3.1 FAULT DAMAGE ZONES WIDTH: IMPLICATIONS FOR THE TECTONIC EVOLUTION OF THE ARARIPE BASIN, NE BRAZIL

Maria Alcione Lima CELESTINO[a] (alcionelimma22@gmail.com)

Tiago Siqueira de MIRANDA[b]* (tiago.smiranda@ufpe.br)

Gorki MARIANO[b] (marianogorki@gmail.com)

Marcio Alencar de LIMA[a] (mlimaalencar@gmail.com)

Bruno Raphael Barbosa Melo de CARVALHO[c] (brcarvalho@petrobras.com.br)

Thiago da Cruz FALCÃO[c] (tfalcao@petrobras.com.br)

João Gabriel TOPAN[a] (gabrieltopan@gmail.com)

José Antonio BARBOSA[b] (barboant@hotmail.com)

Igor Fernandes GOMES[d] (gomes@ufpe.br)

[a]Geosciences Graduate Program, Federal University of Pernambuco, Recife, PE, 50740-530, Brazil

[b]Department of Geology, Federal University of Pernambuco, Recife, PE, 50740-530, Brazil

[c]Petrobras Research Center (CENPES), Rio de Janeiro, 21941-915, Brazil

[d]Department of Civil Engineering, Federal University of Pernambuco, Recife, PE, 50740-530, Brazil

*Corresponding author; e-mail: tiago.smiranda@ufpe.br; tiagogeoufpe@gmail.com; telephone: +55 81 98743-9197; postal address: Av. da Arquitetura, 953-995 - Cidade Universitária, Recife - PE, 50740-540, Brazil.

Author contributions:

Maria Alcione Lima Celestino: Conceptualization; Data acquisition; Investigation; Methodology; Supervision; Validation; Visualization; Writing-Original draft preparation. **Tiago Siqueira de Miranda:** Supervision; Conceptualization; Methodology; Review and editing; Investigation. **Gorki Mariano:** Review and editing; **Marcio Alencar de Lima**:

Investigation; Review**;** **Bruno Raphael Barbosa Melo de Carvalho:** Methodology, Validation; Review and editing. **Thiago da Cruz Falcão:** Validation; Review and editing. **João Gabriel Topan:** Investigation; Review. **José Antonio Barbosa:** Funding acquisition; Review and editing. **Igor Fernandes Gomes:** Review and editing.

Abstract

Fault zones commonly have spatially variable fault rocks and brittle structures. Differing fault-rock attributes may retard or increase cross- and along-fault permeability. Our work analyzed brittle deformation of a segment of the Patos shear zone, Triunfo Fault, which is located in the northern border of the Araripe Basin, NE Brazil. We investigated the structural evolution and tectonic implications of the Triunfo Fault by mapping damage zone width patterns and the types and distributions of breccia and brittle structure arrays within the fault zone using scanline fracture analysis techniques and topographic and aeromagnetometric data. Fractured rocks of the damage zone mainly comprise: mylonitic orthogneiss (footwall); and sandstone and carbonate rocks (hangingwall). The fault core is composed of tectonic breccia and cataclasites occurring as lenses, with calcite-filled veins. Due to fault sinuosity and rheology heterogeneities, the width of the damage zone ranges from 240- 290m (footwall), and 372- 610m (hangingwall). Our analysis obtained from the topographic and gravimetric data combined with field data indicate the following sequential deformation phases: a) Dn, Brasiliano Orogeny, dextral shear zone; b) Dn+1, Paleozoic time, brittle-ductile deformation; and c) Dn+2, Lower Cretaceous time, brittle deformation.

Keywords: Brittle Deformation; Fault damage zone; Fault Core; Strike-slip

1. Introduction

Structural characterization of fault zones is key for a better understanding of the evolution of sedimentary basins (e.g. Rio do Peixe Basin; Araujo et al, 2018), in addition, is important in the study of subsurface fluid flow including geothermal, groundwater and hydrocarbon production, and CO_2 storage, which can be directly influenced by fault zones (Billi et al., 2003; Schueller et al., 2013; Dimmen et al., 2017; Peacock et al., 2017; Celestino et al., 2019a; Torabi et al., 2019; Wu et al., 2019). Fault zones are commonly described as to their architectural elements: a) damage zone, b) core, and c) protolith (host rock) (Caine et al., 1996; Kim et al., 2004; Lin and Yamashita, 2013; Laubach et al., 2014; Choi et al., 2016; Liao et al., 2019; Mayolle et al., 2019) (Fig. 1).

The damage zone occurs involving a fault core and is characterized by increasing frequency of fault related brittle structures. In this zone, the original characteristics of the protolith are preserved, although with a greater degree of brittle deformation (Gudmundsson et al., 2010; Choi et al., 2016). A range of brittle structures including smaller, faults, joints, vein, or deformation bands may be associated with damage zone. The fault core accommodates most of slip. They vary from is cm- to m-thick, and is characterized by the presence of slip surfaces, breccias, cataclasites, and fault gouges, variably interspersed with less deformed fault rocks and undeformed host rock lenses. The protolith corresponds to non-fractured or poorly fractured rock, that surrounding the damage zones (Caine et al., 1996; Cello et al., 2001). These architectural elements of fault zones affect the fluid flow, influencing the permeability of the rock units, and can act as conduits, barriers or a combination of both (Antonellini and Aydin, 1994; Caine et al., 1996; Gudmundsson et al., 2010; Reyer et al., 2012; Fossen et al., 2017; Torabi et al., 2018).

An important component of fault zone characterization is documenting the widths and width distributions of fault zone elements. In this study, we applied the nomenclature suggested by Choi et al. (2016), which defines the width of damage zones by considering a

change in the slope gradients of the cumulative frequency curves of brittle structures measured of fault zone damage as a marker of zone boundaries. Some authors propose other methods for defining the width of a damage zone, such as arbitrarily identifying a fracture density background, as limiting a damage zone (Lin and Yamashita, 2013). Schueller et al. (2013) mark the boundary of the damage zone in the first interval along a scanline without the occurrence of brittle structures. A superior method might be the statistical that define of deviations from background by some rigorous statistical methods (e.g., O'Hara et al., 2017; Marrett et al., 2018). Another more recent statistical method was proposed by Balsamo et al. (2019), which quantified deformation intensity of fault zones using fracture density, fracture spacing, and fracture height / spacing ratio also could have value.

Our study presents an integrated analysis of structural field data acquired using one-dimensional scanline sampling method, satellite and aeromagnetometry data, for the structural characterization of the Triunfo Fault, located on the northern border of the Araripe Basin, NE Brazil (Fig. 2). The Triunfo Fault marks the contact between crystalline basement rocks (Granjeiro Complex), and sedimentary cover (Cariri and Crato formations). The analysis of this fault zone allows a better understanding of the tectonic processes that were responsible for the tectonic evolution of the northern border of the basin.

This paper quantifies the Triunfo fault damage zone width pattern and patterns of structures within the damage zone. Width variation is due to fault sinuosity and rheology heterogeneities in the host rocks. Our research is the first to propose a tectonic evolution model for the Araripe Basin. We show that the Triunfo Fault evolved in a strike-slip regime and our findings infer that a strike-slip regime characterizes the evolution of the basin.

Figure 1 here

2. Geological Context

The Araripe Basin is classified as an intraplate basin of northeastern Brazil (Fig. 2). It is located in the Central Domain (Transversal Zone) of the Borborema Province, NE Brazil. The Triunfo Fault is located on the northern border of the Araripe Basin. The fault represents one of the west termination splays of the Neoproterozoic age Patos shear zone (PASZ) that underwent brittle reactivation during the Cretaceous. The PASZ is approximately 600 km long, and is characterized by mylonites and ultramylonites related to the Neoproterozoic Brasiliano Orogeny, which represent the crystalline basement of the northern border of the Araripe Basin. The PASZ correlates with the East Nigeria shear zone, in West Africa, within the Gondwana paleo-continent (Viegas et al., 2014), from which it was separated by the opening of the South Atlantic.

Based on magnetometric and gravimetric data the Araripe Basin is divided into two sub-basins: a) Cariri, in the east; and b) Feitoria, in the west (Rand, 1983 and Rand & Manso, 1984) (Fig. 2). Matos (1992, 1999) proposed that the tectonic origin of the interior basins of NE Brazil is associated with the opening of the South Atlantic Ocean. Three deformational stages are recognized. These stages are characterized by the formation of half-grabens distributed along three trends: that of Recôncavo-Tucano-Jatobá (N-S), Gabon-Sergipe-Alagoas (NE-SW), and Cariri-Potiguar (ENE-WSW). Another tectonic model that stands out was proposed by Françolin et al. (1994). This model suggests that brittle reactivation of the shear zones influenced the tectonic evolution of some intraplate basins in the NE Brazil (e.g. Rio do Peixe, Araripe and Fátima basins). Nogueira et al (2015) also proposed a model based on studies carried out in the Rio do Peixe Basin. This model proposes that the basin was formed from an approximately NW–SE extension.

Recent work suggests other aspects of the evolution of the Araripe Basin. Two tectonic phases have been identified: a) pull apart phase, during Paleozoic time, characterized by conjugate pairs of NW-SE and N-S strike-slip faults; and b) rift-type phase in Cretaceous

time, marked by normal faults striking NE-SW (Miranda et al., 2014). This last phase is consistent with the model proposed by Matos (1992, 1999). Peulvast and Bétard (2015) proposed that the Araripe Basin underwent a topographic inversion, caused by the uplift of the Borborema Province and subsequent differential erosion processes. Garcia et al. (2019) based on magnetotelluric evidence, inferred that under the Araripe Basin there is asthenospheric material. Magnetotelluric observations favor a model of topographic inversion of the basin through a local vertical push. This inversion is the result of the crustal thinning, due to extensional stress, during Mesozoic time, which favored the ascent of asthenospheric material.

Figure 2 here.

3. Materials and Methods

We mapped structures at two scales. Macroscale characterization used aerogeophysics and satellite data and mesoscale outcrop scale using one-dimensional scanline data. Aerogeophysical data are from the aeromagnetometry database of the Geological Survey of Brazil (CPRM) (http://geosgb.cprm.gov.br/). Satellite is from Earth Explorer portal of the United States Geological Survey (USGS) (https://earthexplorer.usgs.gov/). For mesoscale interpretation, digital outcrop models were produced, and scanlines surveys were carried out in well-exposed outcrops.

3.1. Aeromagnetometry

Magnetic lineaments were interpreted from the aeromagnetometric map (first derivative), which was used to highlight the centers of the magnetic sources. Magnetic lineaments were extracted using positive anomaly centers as criteria, which had their azimuth calculated with the QGIS software (https://qgis.org/en/site/). Then, the lineament azimuth data were compiled in a rose diagram with bin size 10Az.

3.2. Digital Elevation Model (DEM)

The use of Shuttle Radar Topography Mission (SRTM) images for the investigation of topographic lineament data was based on the interactive shading technique (Onorati et al., 1992; Salamuni et al., 2004; De Lima and De Sá, 2017; Celestino et al., 2018). This technique allows the creation of Digital Elevation Model (DEM) with different lighting directions.

DEM for the study area was performed using SRTM imagery, with spatial resolution of 30m (Fig. 3). Four DEM maps with different illumination parameters were used (0Az, 45Az, 90Az, and 315Az), which helped in the identification of perpendicular topographic lineaments to different shading direction. The choice of lighting directions was based on the directions of the main structures that occur in the study area (e.g. Triunfo Fault and PASZ).

To identify and extract topographic lineaments, two criteria were used: a) crest (topographic highs); and b) valley (topographic lows). Lineament identification was performed for two distinct sectors: a) basement; and b) sedimentary cover. With the aid of the GIS software, azimuths and lengths of all identified lineaments were calculated. Then, rose diagrams were constructed, with bin size of 10Az, for the attitudes of lineaments extracted from each DEM map created with different illumination. Finally, for the analysis of the orientation patterns and length of the lineaments, rose diagrams associated with 500m length intervals were produced.

Figure 3 here

3.3. Digital Outcrop Model

The construction of the digital outcrop model was based on three stages: a) outcrop selection; b) geological-structural characterization; and c) digital image processing.

The selection of outcrops was based on the following criteria: (1) representative outcrop of the damage zone; (2) good exposure and (3) a diversity of structures, in terms of different types and number of structures (Cawood et al., 2017).

The outcrop geological-structural characterization was based in the identification of the lithological types and their spatial distribution in relation to the context of damage zone. During the fieldwork, both ductile (foliation and lineation) and brittle (fault, joints and shear fractures) structures were measured. The faults were classified hierarchically according to the degree of deformation, the presence of fault rocks associated with their planes and the displacement associated with these structures.

We produce a digital outcrop model in our analysis with 35 photographs covering the entire outcrop, using an Unmanned Aerial Vehicle (UAV), Mavic Pro, DJI. The images were processed through Agisoft software (https://www.agisoft.com/). The final products were orthomosaics that helped in the identification and digitalization of the structures observed in the field.

3.4. Scanlines

A scanline, or linear line of observation measurement, is a standard method for collecting one-dimension structural data (e.g., Ortega et al., 2006). We counted fractures per meter along the sampling line, corresponding to the P10 value (Dershowitz and Einstein, 1988). The scanlines were oriented orthogonal to the strike of the dominant brittle structures and the following attributes were recorded: (1) number of structures; (2) orientation; (3) crosscutting relationships between fractures and (4) composition of the fracture fills (Ortega et al., 2006; Bisdom et al., 2014; Santos et al., 2015; Miranda et al., 2018). Based on Triunfo Fault's geometry and exhibitions in the study area 6 profiles oriented perpendicular to the fault were selected for measuring scanlines (Fig 7).

The scanline technique was applied to map fault and fracture occurrence within and adjacent to the damage zone associated with the Triunfo Fault. This analysis helped to estimate the width of the damage zone.

4. Results

4.1. Macroscale

4.1.1. *Aeromagnetometry*

Magnetic lineaments (positive anomalies) occurring in the northern border of the Araripe Basin have a preferential ENE-WSW trend. These lineaments were extracted from two sectors, basement rocks and sedimentary cover of the Araripe Basin (Fig. 4). The lineaments correspond to the main ductile deformation, represented by the PASZ and its splay mapped in the study area. Furthermore, the magnetic anomalies in the Araripe Basin represent the splay of PASZ beneath the sedimentary cover.

Figure 4 here

4.1.2. *Digital Elevation Model (DEM)*

The DEM general lineaments (crest and valley) within the study area (Fig. 5) are distributed in the basement sector with two preferred directions: E1) ENE-WSW; and E2) NW-SE; and one secondary direction: E3) N-S. The lineaments identified within the sedimentary cover sector are distributed into two main directions: B1) N-S; B2) NE-SW and one secondary direction: B3) NW-SE (Fig. 5). It is possible to observe from the DEM lineament analysis that the preferential lineaments in the basement sector are associated with positive (crest) and negative (valley) lineaments, with higher concentration of data linked to positive features. The basin sector presents lineaments common to both criteria, without predominance of one over the other.

Figure 5 here

Analysis of the orientation patterns and lengths of the topographic lineaments was performed form adjacent basement and sedimentary cover. Lineaments extracted were classified into three scale categories, based on their length: 1) small (0 to 500 m); 2) medium (500 to 1000 m); c) larges (> 1000 m). The total distribution of the lineament length has a minimum of 13 m, a maximum of 2975 m, and an average of 222 m, with a higher density of

small-scale lineaments, followed by medium scale and by large scale with the lowest density in the area.

The basement sector has lineaments ranging in length from 63 to 2975 m (Fig. 6- A). The small lineaments range from 63 to 500 m, this range has the highest concentration of lineaments (n = 1971), with a preferential direction of ENE-WSW, and secondary directions NW-SE and N-S. The medium sized lineaments (500 to 1000 m) show an ENE-WSW main direction and two secondary directions NW-SE and N-S. Long lineaments (1000 to 2975 m) have preferential NE-SW and secondary NW-SE trends.

Lineaments in the sedimentary cover sector range in length from 13 to 2223 m (Fig. 6-B). Small alignments ranging in length from 13 to 500 m occur with preferred directions NE-SW and N-S and one NW-SE secondary direction. In this range are the largest number of lineaments are concentrated (n = 1672). Medium length lineaments (500 to 1000 m) have a main trend of N-S and two secondary trends NE-SW and NW-SE. Finally, the long lineaments (1000 to 2223 m) occur with a NE-SW main direction and two secondary directions NW-SE and N-S.

Figure 6 here

Throughout the six profiles, a topographic analysis was also performed (Figs. 7 and 8), aiming to analyze the points in which the Triunfo Fault occur. The profiles have preferred N-S directions and extend from the crystalline basement to the sedimentary cover. From this analysis, we observed throughout the profiles that the crystalline basement generally occurs associated with high altitudes (560 m). In the profiles, 02 and 04 the basement occurs as structural highs within the Araripe Basin sector. The Cariri Formation generally occurs at lower altitudes, except for profile 2, where it occurs at the same level as the crystalline basement. The Crato Formation commonly occurs associated with median altitudes 520 m.

The Triunfo Fault tends to occur marking the contact between the crystalline basement and the Cariri and Crato Formation. In profiles 03 and 05 this contact is marked by topographic lows. Profile 01 is located at the Triunfo Fault splay and it showed that the portions where occur faults (NE-SW) are generally associated with topography drops. Profile 02 stands out because there are two faults involved, the Triunfo Fault, restricted to the crystalline basement, and a branch of the Triunfo Fault that marks the contact between the basement and the Cariri Formation. In this location, both lithologies occur at the same topographic level. Finally, profile 04 is also marked by the occurrence of a high basement, being limited to the north and south by inferred normal faults. The Triunfo Fault at this point occurs at the contact between basement and sedimentary cover, but without the common topographic difference observed in other profiles, as well as profile 06.

Figure 7 here

Figure 8 here

4.2. Mesoscale (Outcrop)

The Triunfo fault Zone occurs at the contact between mylonitic orthogneiss (Granjeiro Complex), sandstones (Cariri Formation) and carbonate rocks (Crato Formation) throughout the studied area (Fig. 7). The mylonitic foliation of the orthogneiss generally strikes ENE-WSW with a dip oscillating from medium to high angle towards SE, and locally NW, due to the regional fold that occur in this region (Fig. 9-A). Mylonitic foliation planes carry a horizontal stretching lineation with plunge to SW (Fig. 9-B). This mylonitic orthogneisses show mesoscopic kinematic indicators that indicate dextral shearing of the PASZ (Fig. 9-C). In addition, to the Triunfo fault Zone, the crystalline basement presents a conjugate system of oblique faults with preferential directions (Fig.9-D): N-S, sinistral (Fig.9-E), and NW-SE (N60W), dextral, with average dip sub-vertical (Fig. 9-F). Slickenside on polished surfaces filled by epidote and calcite plunging NW at 27° (Fig. 9-G). A negative flower structure is

observed along an oblique fault, with NNW-SSE direction (Fig. 9-H). This structure was classified as an oblique sinistral fault locally filled with epidote and calcite along the fault planes. The system of conjugate pairs characterizes the brittle-ductile tectonics and are interpreted as the R (NW-SE) and R' (N-S) faults of the Riedel system (MacClay, 1987).

In this paper, we classified the Triunfo Fault as a normal fault characterized by fault rocks and well-developed slip. The Triunfo Fault has strikes N60E and dip to the SE at 65°. Slickenside on the main fault planes plunge SE at 64°, indicating that the Fault Triunfo has a predominantly dip-slip component (Fig. 9 cont.- I, J, K). The nucleation of this fault occurred by the brittle reactivation of the mylonitic foliation and axial planes of parasitic folds. Throughout the Triunfo Fault, fault rocks such as cataclasites and breccias occur in both the crystalline basement and in the sandstones of the Cariri Formation (Fig. 9 cont. - L and 10–D).

The sandstones have conjugated pairs of deformation bands with preferential directions N-S and ENE-WSW with moderate to strong dip (Fig. 9 cont. L and 10-B). These structures occur as single and clusters, their kinematic movements are marked mainly by the displacement between them. The carbonate rocks that occur bordering to the Triunfo Fault are tilted with bedding plunging towards NE and NW and have a higher degree of fractures (Fig. 9 cont. M).

Figure 9 here

Figure 9 (cont.) here

4.2.1. *Architectural Elements of the Triunfo Fault*

In the Triunfo fault Zone, we observe the three architectural elements of fault zones: damage zones, fault cores (Fig. 10) and protolith. The rocks of the footwall, mylonitic orthogneiss, have a well-developed mylonitic foliation formed during Neoproterozoic ductile deformation (Brasiliano Orogeny). These rocks also have veins and joints (preferred direction

N-S), as well as normal faults (direction NE-SW), strike-slip faults and shear fractures (Fig. 9-D-I and 10-A). The strike-slip faults, oriented NW-SE and N-S are the most common structures in the footwall of the Triunfo Fault. The hangingwall of the fault exhibits deformation bands (preferred direction NE-SW), joints and faults (preferred direction NE-SW) in the sandstones of the Cariri Formation (Fig. 10- B). The Crato Formation is represented by naturally fractured laminated limestones (Fig. 10- C). The core of the Triunfo Fault is bounded by the damage zones on both sides of the fault and consists of breccias and cataclasites, composed of fragments of orthogneiss and/or sandstone of various sizes (Fig. 9-L and 10 -D). Non-foliated cataclasites were observed only in the crystalline basement. These cataclasites also show calcite veins.

Figure 10 here

4.2.2. *Frequency of Structures in Damage Zone*

In this section, we present the data of the frequency of brittle structures obtained through scanlines along the Triunfo Fault (profiles P01 to P06, Fig. 7). Profiles 03 and 05 have less outcrop gaps, were therefore selected to quantify the width of the damage zone of the Triunfo Fault.

The damage zones and the fault core are zones that have been subject to distinct deformation intensities. The crystalline basement rocks that occur near the fault core have a higher degree of deformation relative to the more distant rocks. Furthermore, are subject to the effects of rheologic control (mechanical) on the intensity of structures. The digital outcrop model of the mylonitic orthogneiss (Fig. 11) is located near the core of Triunfo Fault. This rock has two facies: felsic (rich in quartz and feldspar) and mafic facies (rich in amphibole). In this outcrop, we performed a 23 m scanline to analyze the intensity of deformation in relation to each facies. The mafic facies occurs over 16 m, and shows a density of brittle

structures of approximately 21 brittle structures/m. The felsic facies shows a density of approximately 30 brittle structures/m over 7 m (Fig. 11D).

Figure 11 here

To calculate the damage zone width, bar diagrams of frequency versus cumulative frequency versus distance from fault core were produced (Fig. 12). The bar diagrams allowed us to estimate the width of the damage zone from the change in slope of the cumulative frequency curve, which marks an increase and decrease in the frequency of brittle structures, indicating the outer limits of a damage zone (Choi et al., 2016). The width of the damage zone was calculated as follows: a) footwall, 240 to 290 m; b) hangingwall, 372 to 610 m. These data show an asymmetry associated with the Triunfo Fault.

Profile 01 is located on the portion of the splay of the Triunfo Fault, where the NE-SW Tatajuba Fault occurs (Fig. 12 - A). This splay marks the contact between the orthogneiss of the Granjeiro Complex and the limestones of the Crato Formation. The width of the damage zone in this region is thicker than the one associated with the Triunfo Fault, which is about 509 m. Profiles 02, 03 and 05 illustrate a decrease in the frequency of brittle structures with increasing distance from Triunfo Fault (Fig. 12- B, C, E). The fault core width was estimated locally in the profile 03 to be approximately 30 m. In profile 04 the decay in the frequency of brittle structures is observed only in the fault hangingwall (Fig. 12- D). Profile 06 the decay of structures is not continuous in the fault footwall, marked by brittle structures frequency peaks, similar to what occurs in the footwall of profile 01 (Fig. 12- F).

The bar diagrams made it possible to estimate density of the brittle structures. The density was obtained through the limits of the damage zone, from which it was possible to identify the density of the structures inside and outside the damage zone. Thus, it is observed that the density within the damage zone is approximately 25 brittle structures/m (footwall and

hangingwall), while outside the damage zone there is a decrease in density values to 3 brittle structures/m in the footwall and 8 brittle structures/m in the sedimentary cover (hangingwall).

Figure 12 here

5. Discussion

5.1. Structural Lineaments

The correlation between structural lineaments and structural field data has been proposed to analyze structural patterns and correlate them with deformational phases associated with the tectonic evolution of sedimentary basins (e.g. De Lima and De Sá, 2017; Celestino et al., 2018). The topographic basement lineaments with a direction of ENE-WSW (E1, Fig. 5-C) are associated with the mylonitic foliation (N75E) that occurs in the Granjeiro Complex (basement rocks) (Fig. 9-A). Lineaments striking NW-SE (E2, Fig. 5-C) are correlated to faults and joints with a preferential direction of N45W (Fig. 10-A). Basement joints preferentially strike N-S (Fig. 10- A) that is consistent with N-S (E3, Fig. 5-C) trend lineaments. The topographic lineaments with N-S (B1, Fig. 5-B) direction occurring in the sedimentary cover sector could be correlated to the joints in the sandstone of the Cariri Formation and faults in the limestone of the Crato Formation (Fig. 10-B, C). The lineaments with NE-SW (B2, Fig. 5-B) direction show a strong correlation with the faults (N50E), joints (N25E and N70E) and deformation bands (N50E) of the Cariri Formation (Fig. 10-B) and joints in the Crato Formation, with preferential trends N45E and N70E (Fig. 10-C). The NW-SE (B3, Fig. 5-B) direction of secondary lineaments can be correlated to the deformation bands and joints of the Cariri Formation with N70W and N45W, respectively (Fig. 10-B).

Analysis of the length of the topographic lineaments shows that the lineaments in the basement sector that vary between medium and long corresponding to the brittle structures, mostly, and to a lesser extent the ductile structures. On the other hand, short lineaments can be correlated to ductile structures (foliation, shear zones) and subordinately to brittle structures

(faults and joints). In the sedimentary cover sector, short to long topographic lineaments comprise brittle structures (faults, joints, and veins) and are characterized by the recurrence of preferential trends (N-S, NE-SW, NW-SE) in the short, medium and long lengths of the lineaments (Fig. 5).

The correlation of field data and lineaments made it possible to observe that the topographic lineaments show that the ENE-WSW trends in the basement are associated with the ductile fabric (mylonitic foliation) generated during the Brasiliano Orogeny. These lineaments mark well the occurrence of the PASZ, E-W direction and adjacent NE-SW shear zones. The main topographic lineaments within the Araripe Basin show NE-SW trend possibly associated with normal faults formed during the Cretaceous (e.g. Triunfo Fault). The NW-SE and NNE-SSW trends may be associated with a deformation that occurred during the Paleozoic, which according to Riedel's model may represent nucleating structures of the pull-apart geometry basement breaking system, which originate from a dextral transtensional tectonic regime (Miranda et al., 2014).

Magnetic lineaments show a preferential ENE-WSW trend (Fig. 4), consistent with the structural fabric associated with shear zones and the Triunfo Fault. In other words, the magnetic data suggest that the PASZ shows a strong correlation and thus possible structural control on the northern border of Araripe Basin. These alignments agree with the topographic lineaments that occur in the basement sector, mainly associated with the ductile fabric ENE-W-SW direction.

5.2. Brittle structure intensity

It is generally accepted that the intensity of deformation in fault zones tends to decrease with increasing distance from the fault core, towards the protolith (e.g. Caine et al., 1996, Wilson et al., 2003; Liao et al., 2019; Mayolle et al., 2019). Fault zones are also subject to the effects of rheologic control (mechanical) on the intensity of brittle structures. In this

work, the brittle deformation associated with crystalline rocks located in the footwall and sedimentary rocks of the Triunfo Fault's hangingwall were analyzed. The minimum density values of zero brittle structures/m in the footwall and three brittle structures/m in the-hangingwall occur, at approximately 2.0 km from the fault core. Maximum density values of 57 brittle structures/m (footwall) and 47 brittle structures/m (hangingwall) occur about 22 m and 125 m from the fault core, respectively (Fig. 13).

Generally, brittle structures decay can be fit by a power function or an exponential function (Cowie et al., 1995; Wilson et al., 2003; Liao et al., 2019). The power-laws represent the best fit for the density of brittle structures in linear-log plots with a coefficient of determination of 0.74 for the Triunfo Fault footwall and hangingwall (Fig. 13). Exponential function shows coefficients of determination of 0.70 and 0.43 to hangingwall and footwall, respectively. We also use the linear function to evaluate behavior. This function shows coefficients of determination of 0.58 and 0.37 to hangingwall and footwall, respectively. Thus, it does not represent a good fit of the data.

The effect of rheological control is observed in the crystalline basement, which presents two facies, mafic and felsic (Fig. 11). The orthogneiss (felsic facies, rich in quartz and feldspar) of the Triunfo Fault footwall show higher density of brittle structures (~21 brittle structures/m) compared to the mafic facies (rich in amphibole) (~30 brittle structures/m) (Fig. 11-D, E). This behavior reflects the rheologically distinct characteristics of quartz and feldspar versus amphibole. The digital outcrop model (Fig. 11-A) illustrates this rheological behavior, with the mafic portion showing a greater development of foliation and faults, while the felsic facies shows a more cataclastic character. This difference in rheological behavior within the same unit may reflect variations in the frequency of brittle structures, and consequently, may influence the width of the damage zone.

Figure 13 here

5.3. Triunfo Fault displacement

The damage zone width data obtained from the scanline analysis allowed infer the Triunfo Fault displacement (Fig. 12 and 14). Figure 14 compiles damage zone width versus fault displacement data acquired for each lithological type (orthogneiss, sandstone and limestone). To infer the fault displacement of the Triunfo Fault, we used the best-fit equation from the literature data (e.g. Choi et al, 2016; Mitchell and Faullkner, 2016; Ellingsen, 2017; Mayolle et al, 2019).

The power law function illustrates the best fit with a coefficient of determination of 0.75 with an exponent $\alpha = 0.74$ (Fig. 14). Data from this study and from the literature (Choi et al, 2016; Mitchell and Faullkner, 2016) follow a near-linear (less dispersed) trend, different from the others.

Inferred displacements show an increase in value as the damage zone width within each lithological type increases. In the limestone, where the width of the damage zone is less thick, the fault displacement is inferred to be 196 m. On the other hand, in sandstone and orthogneiss, the inferred displacements are: a) 4728 m (sandstone) and b) 2621 m (orthogneiss). The different damage zone width values show an asymmetry associated with the Triunfo Fault. This asymmetry is possibly caused by mechanical heterogeneities of the different lithological types occurring on both sides of the fault (Gudmundsson et al., 2010; Lin and Yamashita, 2013). Other factors can also influence the asymmetry of a damage zone, such as fault geometry, variations in the stress field during the process of faulting (Berg and Skar, 2005; Lin and Yamashita, 2013) and tectonic environment and burial depth of deformation (Balsamo et al., 2019). Furthermore, the polyphasic deformations superimposed on the orthogneiss and sandstone, and the physical properties of these rocks probably affected the damage zone width. The mylonitic orthogneiss underwent two deformational events (see section 5.4), which led to a thicker damage zone (i.e. secondary peak of brittle structures, Fig.

12). Porosity in the order of 10 to 15% in sandstones commonly is considered an important factor for the development of deformation bands (Wong et al. 1997; Fossen et al., 2007). Due to its porosity, the sandstone rocks favored the development of deformation bands generated during nucleation of the Triunfo Fault. While the carbonate (Crato Formation), post-rift sequence, may have suffered only the last deformation event associated with the Triunfo Fault (see section 5.4). Thus, we observed that the values of the damage zone width have a positive correlation with the inferred displacement values. The variations of inferred displacement can be associated with different lithological types, fault reactivations and fault geometry (e.g. Kim and Sanderson, 2005).

Figure 14 here

5.4. Tectonic Implications

According to the geological- structural data collected in this work, it was possible to identify transcurrent dextral shear zones (E-W), strike-slip faults with N-S and NW-SE directions; and normal-oblique faults striking NE-SW (Fig. 15). The spatial organization, kinematics and temporal relationship suggest that the structures mentioned above were generated in different deformational phases. Oblique faults of N-S direction have predominantly sinistral kinematics and NW-SE faults have dextral kinematics (Fig. 9- D-G). These structures occur superimposed to the mylonitic fabric and could be respectively correlated to the R' and R faults of the Riedel Model (MacClay, 1987). This conjugate pair of faults was generated under a brittle-ductile deformation of dextral strike-slip regime (PASZ), with maximum extension ($\sigma 3$) in the NE-SW direction. Conversely, the normal-oblique faults oriented NE-SW, and the deformation bands within the basin, suggest a maximum extension ($\sigma 3$) in the NW-SE direction (Fig. 16).

From the field data, we suggest that the study area has at least three deformational phases (Fig. 16). The first phase/deformational stage (Dn) occurred during the Brasiliano

Orogeny (Neoproterozoic), characterized by a ductile and dextral kinematic deformation (PASZ). These deformations occur imprinted in the rocks of the Granjeiro Complex as high angle mylonitic foliation (75/sub-vertical) and horizontal mineral lineation (250/06) (Fig. 9-A,D).

The second deformational phase (Dn + 1) is inferred to have occurred during the Paleozoic (e.g. Castro et al., 2014; De lima and De Sá, 2017; Miyouna et al., 2018; Cerri et al., 2020; Oha et al., 2020). This phase caused the development of sinistral and dextral strike-slip faults oriented N-S and NW-SE, respectively. During this deformational stage, the dominant tectonic was strike-slip with the same kinematics as the ductile deformation of Brasiliano age (Dn), but at shallow crustal levels. Several structural highs occurring within the basin must have been formed during this stage (Dn + 1).

The third deformational phase (Dn + 2) was responsible for the generation of the Triunfo Fault and is interpreted to have occurred during the opening of the South Atlantic in the Lower Cretaceous. During this period, the northeastern intraplate basins began to nucleate and the shear zones underwent brittle reactivation (Françolin et al. 1994). At this stage, the PASZ was reactivated with sinistral kinematics (Nogueira et al., 2015). In the study area this deformation occurs imprinted as NE-SW normal-oblique faults (e.g. Triunfo Fault), as well as conjugate pairs of deformation bands that occur in the Cariri Formation (Fig. 9 cont. I-K).

In summary, the preexisting shear zones in the crystalline basement, developed during the Brasiliano Orogeny, acted as areas of weakness and were reactivated during the Cretaceous as brittle structures (faults, fractures and deformation bands). This brittle fabric is characterized by a preferential NE-SW trend, with maximum extension ($\sigma 3$) in the NW-SE direction, as suggested by basin boundary faults (Araujo et al., 2018, Rio do Peixe Basin; Celestino et al., 2019b, Fátima Basin). In the Araripe Basin, the Triunfo Fault represents the brittle deformation that occurred during the Cretaceous, relating to the Dn + 2 phase.

Our results suggest that the northern border of the Araripe Basin presents a transitional brittle tectonics involving two deformational stages: Dn + 1 and Dn + 2. The Dn + 1 phase associated with dextral transtensional (pull apart) tectonics, marked by an NE-SW distension, and the Dn + 2 phase associated with sinistral transtensional tectonics, characterized by an oblique distension of the NW-SE direction, with normal fault development (NE-SW). In addition, our data suggest that the Triunfo Fault remained active during the post-rift phase under an extensional regime. With the limestone tilted and with higher degrees fracturing near the faults registering the post-rift deformation (Fig. 9 cont. M).

Figure 15 here

Figure 16 here

6. Conclusions

Concerning the brittle deformation of the PASZ in the north border of the Araripe Basin, NE Brazil, we documented following the structural characteristics of architectural elements of the Triunfo Fault and its control in the tectonic evolution of the Araripe Basin:

1- Topographic and magnetic lineaments are strongly correlated with ductile (basement) and brittle (basement and sedimentary cover) structures;

2- The main topographic lineaments within the basin show NE-SW trend, and are possibly associated with the tectonic event of the maximum extension (σ3) in the NW-SE direction (Cretaceous). The trends NW-SE and NNE-SSW may be associated with brittle-ductile deformation that occurred during the Paleozoic, with maximum extension (σ3) in NE-SW direction;

3- The width of the damage zone of the Triunfo Fault ranges from 240 to 290m in the footwall and from 372 to 610m in the hangingwall. These regions are marked by a density of approximately 25 brittle structures per meter;

4- Topographic control allowed the identification of faults, since these structures occur mostly associated with topographic falls and lithological contacts;
5- The damage zone of the Triunfo Fault has an asymmetry, which can be attributed to mechanical heterogeneities. At the Triunfo Fault splay sector, the greater width of the damage zone may result from the geometric pattern of the fault;
6- Three deformational events with distinct ages were identified: Dn (Neoproterozoic), Dn+1 (Paleozoic) and Dn+2 (Cretaceous);
7- The structural evolution of the northern border of Araripe Basin occurred between the deformational stages Dn + 1 (dextral transtensional) and Dn + 2 (sinistral transtensional);
8- The events Dn + 1 and Dn + 2 are imprinted in the crystalline basement rocks causing an overlap of the deformations and influencing the width of the damage zone in the fault footwall.

7. Acknowledgments

We warmly thank the Editor Stephen Laubach and the reviewers Fabrizio Balsamo, Sonja Philipp and the two anonymous reviewers for their helpful comments, which greatly improved the early version of this manuscript. This study was carried out with financial support provided Project Pseudopoços – Petrobras/Federal University of Pernambuco (UFPE). We are grateful to Petrobras, National Agency of Petroleum, Natural Gas and Biofuels of Brazil (ANP) and Department of Geology UFPE. We thank Gabriel Matos for the fieldwork and fruitful discussions and everyone who directly or indirectly contributed to the elaboration of this work. We also thank Nick Roberts for the helpful English review. This work is part of a MSc of Maria Alcione under the postgraduate program in Geosciences of the Federal University of Pernambuco (PPGEOC- UFPE) and represents the contribution N. 01 of the Laboratório de Modelagem de Bacias (ModLad-UFPE).

References

Antonellini, M., and Aydin, A., 1994, Effect of faulting on fluid flow in porous sandstones: Petrophysicial properties: American Association of Petroleum- AAPG Bulletin', 78, 355–377.

Araujo, R.E.B., Bezerra, F.H.R., Nogueira, F.C.C., Balsamo, F., Carvalho, B.R.B.M., Souza, J.A.B., Sanglard, J.C.D., de Castro, D.L., Melo, A.C.C., 2018. Basement control on fault formation and deformation band damage zone evolution in the Rio do Peixe Basin, Brazil. Tectonophysics 745, 117–131. https://doi.org/10.1016/j.tecto.2018.08.011

Balsamo, F., Clemenzi, L., Storti, F., Solum, J., & Taberner, C., 2019. Tectonic control on vein attributes and deformation intensity in fault damage zones affecting Natih platform carbonates, Jabal Qusaybah, North Oman. Journal of Structural Geology, 122, 38-57.

Berg, S.S., Skar, T., 2005. Controls on damage zone asymmetry of a normal fault zone: Outcrop analyses of a segment of the Moab fault, SE Utah., Journal of Structural Geology. https://doi.org/10.1016/j.jsg.2005.04.012

Billi, A., Salvini, F., Storti, F., 2003. The damage zone-fault core transition in carbonate rocks: implications for fault growth, structure and permeability. Journal of Structural geology, 25(11), 1779-1794.

Bisdom, K., Gauthier, B.D.M., Bertotti, G., Hardebol, N.J., 2014. Calibrating discrete fracture-network models with a carbonate three-dimensional outcrop fracture network: Implications for naturally fractured reservoir modeling. AAPG Bulletin 98, 1351–1376. https://doi.org/10.1306/02031413060

Caine, J.S., Evans, J.P., Forster, C.B., 1996. Fault zone architecture and permeability structure (supplemental data). Geology 24, 1049. https://doi.org/10.1130/0091-7613(1996)024<1025

Castro, D. L., Fuck, R. A., Phillips, J. D., Vidotti, R. M., Bezerra, F. H. R., Dantas, E. L.,

2014. Crustal structure beneath the Paleozoic Parnaíba Basin revealed by airborne gravity and magnetic data, Brazil. Tectonophysics, 614, 128-145.

Cawood, A.J., Bond, C.E., Howell, J.A., Butler, R.W.H., Totake, Y., 2017. LiDAR, UAV or compass-clinometer? Accuracy, coverage and the effects on structural models. Journal of Structural Geology 98, 67–82. https://doi.org/10.1016/j.jsg.2017.04.004

Celestino, M.A.L., Miranda, T., Correia Filho, O., Barbosa, J., 2018. Aspectos Tectônicos Da Borda Ne Da Bacia De Fátima, Província Borborema- Ne Do Brasil. Estudos Geológicos 27, 3–19. https://doi.org/10.18190/1980-8208/estudosgeologicos. 27(2),3-19.

Celestino, M.A.L., Miranda, T.S., Matos, G., Mariano, G., Topan, J. G., Carvalho, B.R.B.M., Falcão, T., Oliveira, G.M., 2019a. Resultados preliminares da análise multiescalar de zona de falha: Borda Norte Da Bacia Do Araripe. In: Simpósio de Estudos Tectônicos, 27. Bento Gonçalves, Rio Grande do Sul, Brasil, Anais, 738 176.

Celestino, M.A.L., Miranda, T., Correia Filho, O., Passos, V.S.A., 2019b. Evolução tectônica da borda nordeste da bacia de fátima, província borborema, ne brasil. In: Simpósio de Geologia do Nordeste, 28. Aracaju, Sergipe, Brasil, Anais.

Cello, G., Tondi, E.,Micarelli, L., Invernizzi, C., 2001. Fault zone fabrics and geofluid properties as indicators of rock deformation modes. J. Geodynamics. 32, 543–565.

Cerri, R. I., Warren, L. V., Varejão, F. G., Marconato, A., Luvizotto, G. L., Assine, M. L., 2020. Unraveling the origin of the Parnaíba Basin: Testing the rift to sag hypothesis using a multi-proxy provenance analysis. Journal of South American Earth Sciences, 102625. https://doi.org/10.1016/j.jsames.2020.102625

Choi, J.H., Edwards, P., Ko, K., Kim, Y.S., 2016. Definition and classification of fault damage zones: A review and a new methodological approach. Earth-Science Reviews 152, 70–87. https://doi.org/10.1016/j.earscirev.2015.11.006

Cowie, P. A., D. Sornette, and C. Vanneste, 1995. Multifractal scaling properties of a growing fault population: Geophysical Journal International, 122(2), 457–469. https://doi:10.1111/j.1365-246X.1995.tb07007.x.

Dershowitz, W. S., and H. H. Einstein, 1988. Characterizing rock joint geometry with joint system models: Rock Mechanics and Rock Engineering, v. 21, p. 21–51, doi:10 .1007/BF01019674.

De Lima, F.G.F., De Sá, E.F.J., 2017. Controle estrutural da borda sudeste da Bacia do Parnaíba, Nordeste do Brasil: relação com eventos geodinâmicos no Gondwana. Geologia USP - Serie Cientifica 17, 3–21. https://doi.org/10.11606/issn.2316-9095.v17-125909

Dimmen, V., Rotevatn, A., Peacock, D.C.P., Nixon, C.W., Nærland, K., 2017. Quantifying structural controls on fluid flow: Insights from carbonate-hosted fault damage zones on the Maltese Islands. Journal of Structural Geology 101, 43–57. https://doi.org/10.1016/j.jsg.2017.05.012

Ellingsen, T. S. S., 2017. Fault damage zone architecture and its scaling laws: Master thesis, University of Bergen.

Françolin, J.B.L., Cobbold, P.R., Szatmari, P., 1994. Faulting in the Early Cretaceous Rio do Peixe 753 Basin (NE Brazil) and its significance for the opening of the Atlantic. Journal. Structural Geology, 16, 647-661.

Fossen, H., Schultz, R. A., Shipton, Z. K., Mair, K., 2007. Deformation bands in sandstone: a review. Journal of the Geological Society, 164(4), 755-769.

Fossen, H., Soliva, R., Ballas, G., Trzaskos, B., Cavalcante, C., & Schultz, R. A., 2017. A review of deformation bands in reservoir sandstones: geometries, mechanisms and distribution. Geological Society, London, Special Publications, 459(1), 9-33.

Garcia, X., Julià, J., Nemocón, A.M., Neukirch, M., 2019. Lithospheric thinning under the Araripe Basin (NE Brazil) from a long-period magnetotelluric survey: Constraints for

tectonic inversion. Gondwana Research 68, 174–184. https://doi.org/10.1016/j.gr.2018.11.013

Gudmundsson, A., Simmenes, T.H., Larsen, B., Philipp, S.L., 2010. Effects of internal structure and local stresses on fracture propagation, deflection, and arrest in fault zones. Journal of Structural Geology 32, 1643–1655. https://doi.org/10.1016/j.jsg.2009.08.013

Oha, I.A., Okonkwo1, I.A., Dada, S.S., 2020. Wrench Tectonism and Intracontinental Basin Sedimentation: A Case Study of the Moku Sub-Basin, Upper Benue Trough, Nigeria. Journal of Geography and Geology 12 (1), 65-75.

Kim, Y.S., Peacock, D.C.P., Sanderson, D.J., 2004. Fault damage zones. Journal of Structural Geology 26, 503–517. https://doi.org/10.1016/j.jsg.2003.08.002

Kim, Y.-S., Sanderson, D.J., 2005. The relationship between displacement and length of faults: a review. Earth Sci. Rev. 68, 317–334.

Laubach, S.E., Eichhubl, P. Hargrove, P., Ellis, M.A., Hooker, J.N., 2014. Fault core and damage zone fracture attributes vary along strike owing to interaction of fracture growth, quartz accumulation, and differing sandstone composition. Journal of Structural Geology 68, Part A, 207-226. doi: 10.1016/j.jsg.2014.08.007.

Liao, Z., Liu, H., Carpenter, B.M., Marfurt, K.J., Reches, Z., 2019. Analysis of fault damage zones using three-dimensional seismic coherence in the Anadarko Basin, Oklahoma. AAPG Bulletin 103, 1771–1785. https://doi.org/10.1306/1219181413417207

Lin, A., Yamashita, K., 2013. Spatial variations in damage zone width along strike-slip faults: An example from active faults in southwest Japan. Journal of Structural Geology 57, 1–15. https://doi.org/10.1016/j.jsg.2013.10.006

Marrett, R., Gale, J.F.W., Gomez, L., and Laubach, S.E., 2018. Correlation analysis of fracture arrangement in space. Journal of Structural Geology 108, 16-33. doi.org/10.1016/j.jsg.2017.06.012.

Matos R.M.D., 1992. The Northest Brasilian rift system. Tectonics, 11(4), 776-791.

Matos R.M.D., 1999. History of the Northeast Brazilian rift system: kinematic implications for the break-up between Brazil and West Africa. In: N.R. Cameron, R.H. Bate, V.S. Clure (eds.). The Oil and Gas Habitats of the South Atlantic. Geol. Soc., London, Spec. Publ., 153, 55-73.

Mayolle, S., Soliva, R., Caniven, Y., Wibberley, C., Ballas, G., Milesi, G., Dominguez, S., 2019. Scaling of fault damage zones in carbonate rocks. Journal of Structural Geology, 124, 35-50. https://doi.org/10.1016/j.jsg.2019.03.007.

McClay, K. R., 1987. The mapping of geological structures. Geological Society of London handbook. 161p.

Miranda, T.S. De, Magalhães, J.R.G., Barbosa, J.A., Correia Filho, O., Alencar, M.L., 2014. Araripe Basin , NE Brazil : A rift basin implanted over a previous pull-apart system ? 4th Atlantic Conjugate Margins Conference 3.

Miranda, T. S., Santos, R. F., Barbosa J. A., Gomes I. F., Alencar M. L., Correia O. J., Falcão T. C., Gale J. F. W., Neumann V. H., 2018. Quantifying aperture, spacing and fracture intensity in a carbonate reservoir analogue: Crato Formation, NE Brazil. Marine and Petroleum Geology, v. 97, p. 556-567, 2018.

Mitchell, T. M., & Faulkner, D. R., 2009. The nature and origin of off-fault damage surrounding strike-slip fault zones with a wide range of displacements: A field study from the Atacama fault system, northern Chile. Journal of Structural Geology, 31(8), 802-816. https://doi.org/10.1016/j.jsg.2009.05.002

Miyouna, T., Dieu-Veill Nkodia, H. M., Essouli, O. F., Dabo, M., Boudzoumou, F., Delvaux, D., 2018. Strike-slip deformation in the Inkisi Formation, Brazzaville, Republic of Congo. Cogent Geoscience, 4(1), 1542762.

Nogueira, F.C.C., Marques, F.O., Bezerra, F.H.R., de Castro, D.L., Fuck, R.A., 2015.

Cretaceous intracontinental rifting and post-rift inversion in NE Brazil: Insights from the Rio do Peixe Basin. Tectonophysics 644, 92–107. https://doi.org/10.1016/j.tecto.2014.12.016

O'Hara, A.P., Jacobi, R.D., Sheets, H.D., 2017. Predicting the width and average fracture frequency of damage zones using a partial least squares statistical analysis: Implications for fault zone development. Journal of Structural Geology 98, 38–52. https://doi.org/10.1016/j.jsg.2017.03.008

Onorati, G., Pascolieri M., Ventura R., Chiarini V., Crucillà U., 1992. The digital elevation model of Italy for geomorphology and structural geology Catena, 147-178

Ortega, O.J., Marrett, R.A., Laubach, S.E., 2006. A scale-independent approach to fracture intensity and average spacing measurement. AAPG Bulletin 90, 193–208. https://doi.org/10.1306/08250505059

Peacock, D.C.P., Dimmen, V., Rotevatn, A., Sanderson, D.J., 2017. A broader classification of damage zones. Journal of Structural Geology 102, 179–192. https://doi.org/10.1016/j.jsg.2017.08.004

Peulvast, J.P., Bétard, F., 2015. A history of basin inversion, scarp retreat and shallow denudation: The Araripe basin as a keystone for understanding long-term landscape evolution in NE Brazil. Geomorphology 233, 20–40. https://doi.org/10.1016/j.geomorph.2014.10.009

Rand, H.M., 1983. Levantamento gravimetrico e magnetometrico da Bacia Araripe. Relatório interno da PETROBRAS, 11 p., caderno de dados e mapas.

Rand, H.M. and Manso, V.A.V., 1984. Levantamento gravimétrico e magnetométrico da Bacia do Araripe. In: SBG, Congresso Brasileiro de Geologia, 4, Anais, 2011-2016.

Reyer, D., Bauer, J.F., Philipp, S.L., 2012. Fracture systems in normal fault zones crosscutting sedimentary rocks, Northwest German Basin., Journal of Structural

Geology. https://doi.org/10.1016/j.jsg.2012.06.002

Salamuni, E., Ebert, H.D., Hasui, Y., 2004. Morfotectônica Da Bacia Sedimentar De Curitiba. Revista Brasileira de Geociências 34, 469–478. https://doi.org/10.25249/0375-7536.2004344469478

Santos, R.F.V.C., Miranda, T.S., Barbosa, J.A., Gomes, I.F., Matos, G.C., Gale, J., Neumann, V.H., Guimarães, L.J., 2015. Characterization of natural fracture systems: analysis of uncertainty effects in linear scanline results. AAPG (Am. Assoc. Pet. Geol.) Bull. 99 (12), 2203–2219. https://doi.org/10.1306/05211514104.

Schueller, S., Braathen, A., Fossen, H., Tveranger, J., 2013. Spatial distribution of deformation bands in damage zones of extensional faults in porous sandstones: Statistical analysis of field data. Journal of Structural Geology 52, 148–162. https://doi.org/10.1016/j.jsg.2013.03.013Torabi, A.; Alaei, B.; Ellingsen, T. S. S. 2018. Faults and fractures in basement rocks, their architecture, petrophysical and mechanical properties. Journal of Structural Geology, v. 117, p. 256-263.

Torabi, A.; Johannessen, M. U.; Ellingsen, T. S. S. 2019. Fault Core Thickness: Insights from Siliciclastic and Carbonate Rocks. Geofluids, v. 2019.

Viegas, L.G.F., Archanjo, C.J., Hollanda, M.H.B.M., Vauchez, A., 2014. Microfabrics and zircon U-Pb (SHRIMP) chronology of mylonites from the Patos shear zone (Borborema Province, NE Brazil). Precambrian Research 243, 1–17. https://doi.org/10.1016/j.precamres.2013.12.020

Wilson, J.E., Chester, J.S., Chester, F.M., 2003. Microfracture analysis of fault growth and wear processes, Punchbowl Fault, San Andreas system, California. Journal of Structural Geology 25, 1855–1873. https://doi.org/10.1016/S0191-8141(03)00036-1

Wong, T.-f., David, C. & Zhu, Q. 1997. The transition from brittle faulting to cataclastic flow in porous sandstones: mechanical deformation. Journal of Geophysical Research, 102,

3009–3025.

Wu, G., Gao, L., Zhang, Y., Ning, C., Xie, E., 2019. Fracture attributes in reservoir-scale carbonate fault damage zones and implications for damage zone width and growth in the deep subsurface. Journal of Structural Geology 118, 181–193. https://doi.org/10.1016/j.jsg.2018.10.008

Figure Captions

Figure 1- Conceptual model of a normal fault zone illustrating the main architectural elements: protolith (host rock), damage zone, fault core, fracture systems, lineations and kinematic indicators.

Figure 2- Aeromagnetometric map (reduction to the pole) of the intraplate basins, northeastern Brazil, with the regional shear zones and sub- basins of the Araripe Basin highlighted. PASZ = Patos shear zone; EPSZ = East Pernambuco shear zone; WPSZ = West Pernambuco shear zone; AB = Araripe Basin; JB = Jatobá Basin; FB = Fátima Basin; SJBB = São José do Belmonte Basin; CB = Cedro Basin; RPB = Rio do Peixe Basin; MB = Mirandiba Basin; SB = Socorro Basin; BB = Betânea Basin; CPB = Carnaubeira da Penha Basin.

Figure 3- Flowchart of the stages performed during the analysis of topographic lineaments extracted from the digital elevation model.

Figure 4- (A) Aeromagnetometric map (first derivative) of the Araripe Basin region, highlighting the magnetic lineaments on basement and Araripe Basin sectors; (B) Rose diagram of magnetic lineaments illustrating a preferred ENE-WSW trend, showing the ductile deformation, represented by the PASZ; (C) Study area.

Figure 5- (A) Digital elevation model (315Az) of the northern border of Araripe Basin superimposed on the geological map. Red lineaments represent the adjacent basement sector and orange lineaments represent the sedimentary. Each pair of rose diagrams illustrates an illumination direction (0, 45, 90, and 315Az) for each criterion, (Cr) crest; (V) valley; (B)

Rose diagram of the topographic lineaments of the interior of the basin with major trends B1 and B2 and secondary B3; (C) Rose diagram of the adjacent basement illustrating the main trends E1 and E2; and secondary E3.

Figure 6- Rose diagrams for each studied sector, illustrating the directions of the lineaments at an interval of 500m. (A) Basement sector: the lineaments were classified in terms of their length distribution as small (62 to 500 m), medium (500 to 1000 m) and long (1000 to 2975 m); (B) Sedimentary cover sector: the lineaments were classified as small (13 to 500 m), medium (500 to1000 m) and long (1000 to 2223 m). Each rose expresses the preferred trends of lineaments extracted from the DEM. Continuum lines represent the main direction; dashed line represents the secondary direction.

Figure 7- 3D Digital elevation model of the region of the northern border of the Araripe Basin superimposed on the geological map with the location of the six profiles crossing the Triunfo fault: P01- Profile 01; P02- Profile 02; P03- Profile 03; P04- Profile 04; P05- Profile 05 and P06- Profile 06.

Figure 08- Six transversal topographic profiles of the Triunfo Fault. (A) Profile 01; (B) Profile 02; (C) Profile 03; (D) Profile 04; (E) Profile 05; and (F) Profile 06.

Figure 9- Field aspects of the Granjeiro Complex, Cariri Formation and Crato Formation, and examples of fault kinematic indicators. (A) Outcrop of the Granjeiro Complex, composed of mylonitic orthogneiss with well-developed foliation-oriented ENE-WSW, dipping to SE and NW, detail for stereographic projection, n = 79; (B) Mylonitic foliation planes carry an horizontal stretching lineation with attitude 250/06; (C) Shear criteria in mylonitic orthogneiss, dextral δ-type porphyroclast showing the kinematics of the PASZ; (D) Conjugate pair of strike-slip faults of the mylonitic orthogneiss (NW-SE, R, dextral; and N-S, R', sinistral), detail for stereographic projection, n= 48; (E) Sinistral strike-slip fault, R'; (F) Dextral strike-slip fault, R; (G) Strike-slip fault plane with sub-horizontal slickenside filled by

epidote and calcite. Fault plane attitude: 030/85 and slickenside: 300/27; (H) Negative flower structure in the orthogneiss of the Granjeiro Complex, observed along an NNW-SSE oblique fault. Traces in red correspond to the fault planes and in yellow the banding displaced by them;

Figure 9 (cont.) - (I) Triunfo fault plane with well-developed dip-slip slickenlines in mylonitic orthogneiss. Fault plane attitude: 150/65 and slickenside: 150/65; (J) Cariri Formation sandstone fault plane, marking the presence of the Triunfo Fault. Steps indicating the normal direction of movement of the blocks. Fault plane attitude: 142/65 and slickenside: 142/64; (K) Normal fault plane with dip-slip slickenlines in sandstone. Fault plane attitude: 154/35 and slickenside: 136/35 and (L) Tectonic Breccia of the Cariri Formation consisting of numerous deformation bands (singles and clusters) marking the core of the Triunfo Fault; (M) Tilted blocks of the Crato Formation laminites.

Figure 10- Lithostratigraphic units that represent the architectural elements of the Triunfo Fault. (A) Fractured orthogneiss; (A1, n = 1474) and (A2, n = 219) stereographic projections showing density contours of poles and rose diagram to joints and faults, respectively. (Contouring interval C.i.=0,70 % (A1 and A2)).; (B) Cariri Formation: sandstone with single deformation band, stereographic projections with density contours of poles and rose diagram B1 (n= 162), B2 (n= 281) and B3 (n= 6), indicate the trends of the deformation bands, joint and fault, respectively. (Contouring interval C.i.=1,82 (B1); 0,87 (B2) and 8,04% (B3)); (C) Crato Formation: fractured limestone, stereographic projections with density contours of poles and rose diagram C1 (n= 49) and C2 (n= 5) indicate preferred joint (dashed line) and fault directions, respectively. (Contouring interval C.i.=1,97 (C1) and 2,57% (C2)); and (D) Crystalline basement breccia fault, detail for the calcite vein.

Figure 11- (A) Digital outcrop model of the Triunfo Fault's damage zone (crystalline basement). Highlight for the compositional variation of the basement, with mafic and felsic

portions. Red lines indicate the main faults (n = 23) with their respective stereograms (medium plane is showed in red color). (B) Detail of faults F1 and F2 illustrating displacements of a quartz feldspar veins. (C) Schematic drawing of the digital outcrop model; (D) Diagram of frequency and cumulative frequency of brittle structures versus distance of a scanline carried out with a length of 23 m. The graph is divided into two parts. The bars with red lines consist of data referring to felsic facies, 16m. The cumulative frequency consists of the red line and the points listed are the cumulative frequency values along the scanline, which help in the calculation of the density of structures (total cumulative frequency of the facies / distance of scanline performed in each facies). The bars with green lines consist of data referring to mafic facies, 7 m. The cumulative frequency consists of the green line and the points listed are the values of the cumulative frequency along the scanline; (E) Pie chart illustrates the density of fractures per meter for the facies analyzed, the percentage for each one is also illustrated.

Figure 12- Frequency of brittle structures and cumulative frequency diagram of each profile performed from the scanline technique (Fig. 7), highlighting the limits of the damage zone. (A) Profile 01; (B) Profile 02; (C) Profile 03; (D) Profile 04; (E) Profile 05 and (F) Profile 06. The zero in the X-axis represents the fault and positive and negative values indicate distances to the fault. The locations of the outcrops are also indicated (e.g. AR08) in this axis. Y-axis represents frequency data and cumulative frequency of brittle structures.

Figure 13- Fracture density as a function of the core distance from the fault. (A) Footwall of Triunfo Fault; (B) Hangingwall of Triunfo Fault.

Figure 14- Log–log plot of the damage zone width versus displacement from the previous studies (Choi et al, 2016; Mitchell and Faullkner, 2016; Ellingsen, 2017; Mayolle et al, 2019) and this study. Damage zone widths were measured using faults, joints and deformation bands.

Figure 15- Structural map of the northern border of the Araripe Basin, highlighting the shear zones of red color, indicating their development during the Dn phase; blue faults were developed during the Dn + 1 phase; and the green faults that developed during the Dn + 2 phase.

Figure 16- Tectonic evolution model for the northern border of the Araripe Basin. A) Deformational event Dn that occurred during the Neoproterozoic Brasiliano Orogeny; B) Deformational event Dn + 1 of Paleozoic age, under dextral strike-slip, but with ductile-brittle deformation; and C) Deformational event Dn + 2 of Cretaceous age, under oblique rift with giving rise to the Triunfo Fault.

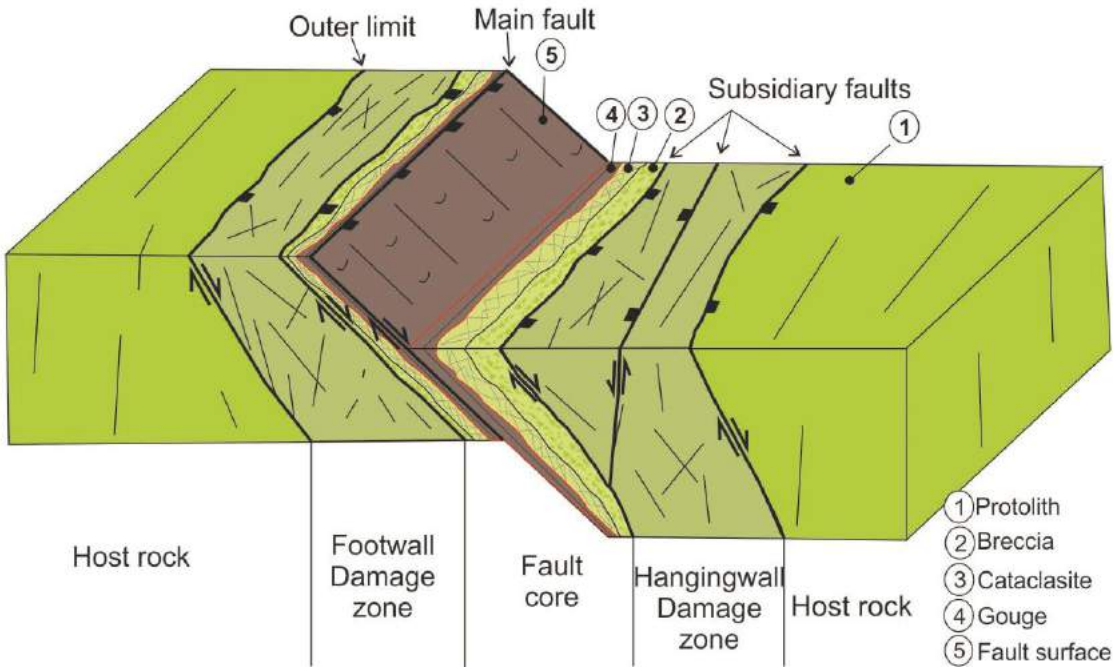

Figure 1

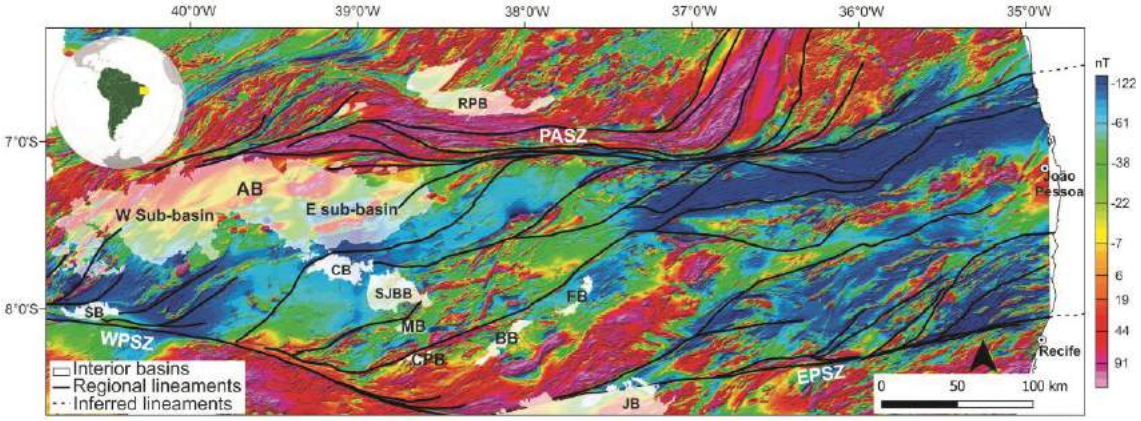
40°0'W
39°0'W
38°0'W
37°0'W
36°0'W
35°0'W
7°0'S
8°0'S
RPB
PASZ
AB
W Sub-basin
E sub-basin
CB
SJBB
FB
SB
MB
BB
WPSZ
CPB
EPSZ
JB
João Pessoa
Recife
nT
-122
-61
-38
-22
-7
6
19
44
91
Interior basins
Regional lineaments
Inferred lineaments
0
50
100 km

Figure 2

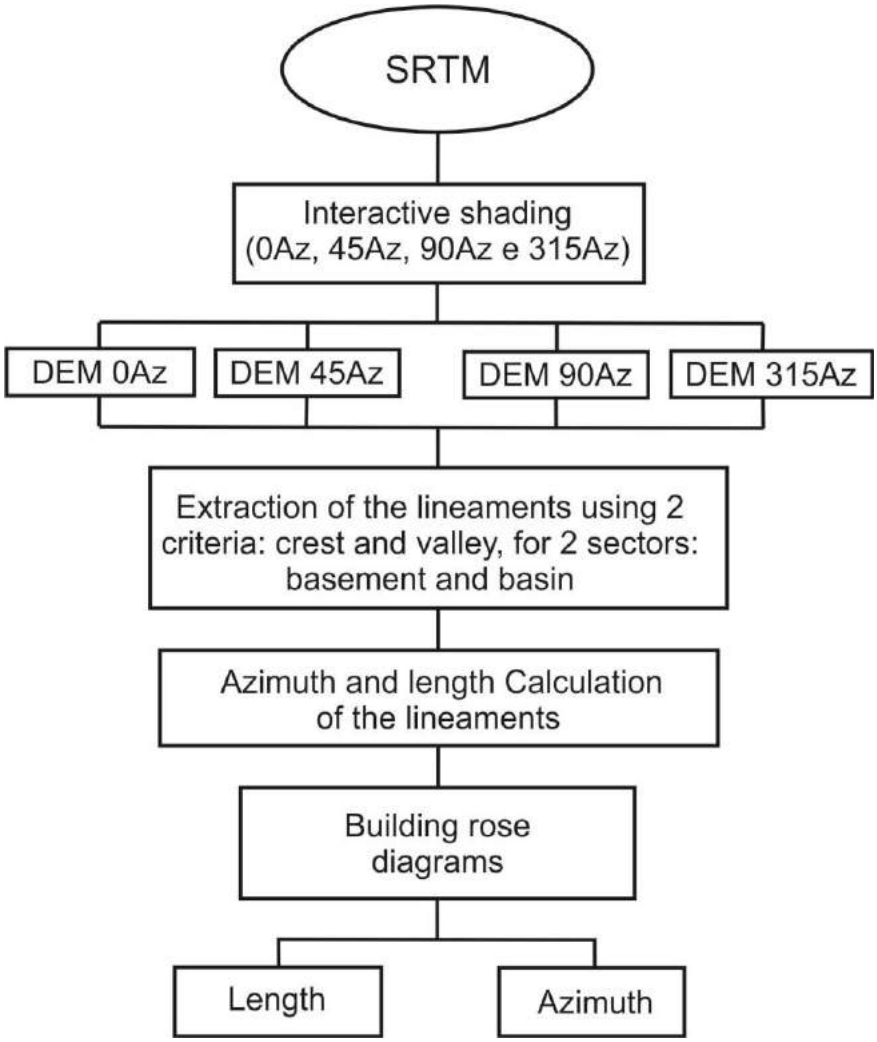
SRTM
Interactive shading
(0Az, 45Az, 90Az e 315Az)
DEM 0Az
DEM 45Az
DEM 90Az
DEM 315Az
Extraction of the lineaments using 2
criteria: crest and valley, for 2 sectors:
basement and basin
Azimuth and length Calculation
of the lineaments
Building rose
diagrams
Length
Azimuth

3

4 Figure 3

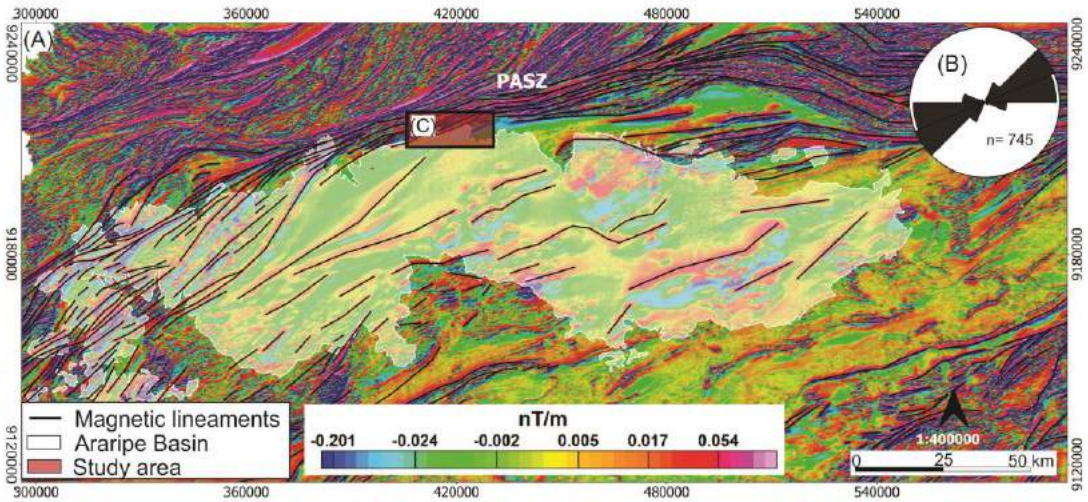
300000
360000
420000
480000
540000
9240000
9180000
9120000
(A)
PASZ
(C)
(B)
n= 745
Magnetic lineaments
Araripe Basin
Study area
nT/m
-0.201
-0.024
-0.002
0.005
0.017
0.054
1:400000
0
25
50 km

Figure 4

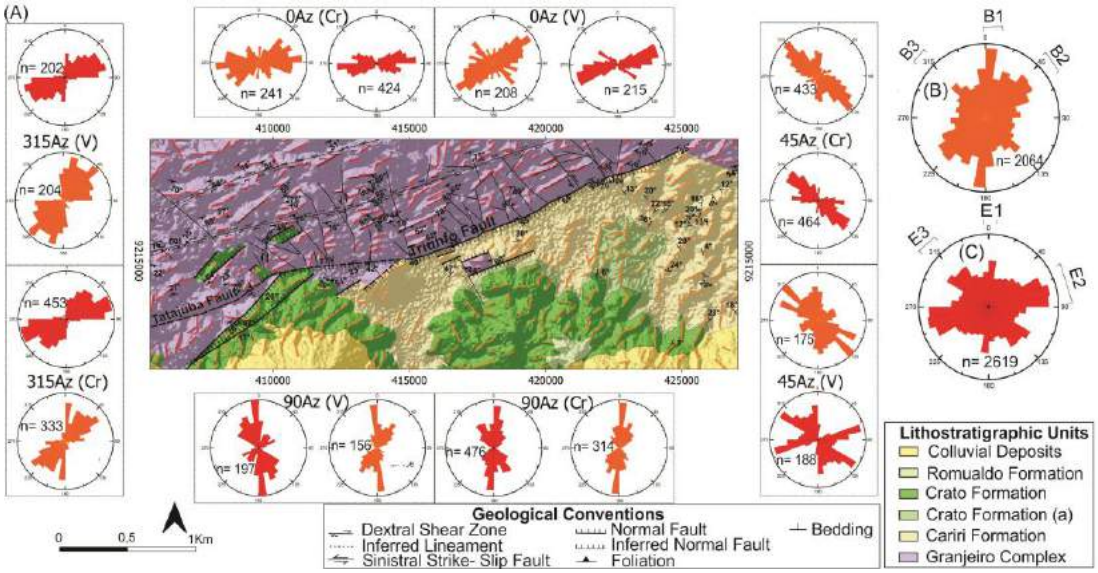
(A)
n= 202
315Az (V)
n= 204
n= 453
315Az (Cr)
n= 333
0Az (Cr)
n= 241
n= 424
0Az (V)
n= 208
n= 215
410000
415000
420000
425000
9215000
9205000
Jatobá Fault
Trinchã Fault
90Az (V)
n= 197
n= 156
90Az (Cr)
n= 476
n= 314
n= 433
45Az (Cr)
n= 464
n= 175
45Az (V)
n= 188
B1
B2
B3
(B)
n= 2064
E1
E2
E3
(C)
n= 2619
0
0.5
1Km
Geological Conventions
Dextral Shear Zone
Inferred Lineament
Sinistral Strike- Slip Fault
Normal Fault
Inferred Normal Fault
Foliation
Bedding
Lithostratigraphic Units
Colluvial Deposits
Romualdo Formation
Crato Formation
Crato Formation (a)
Cariri Formation
Granjeiro Complex

Figure 5

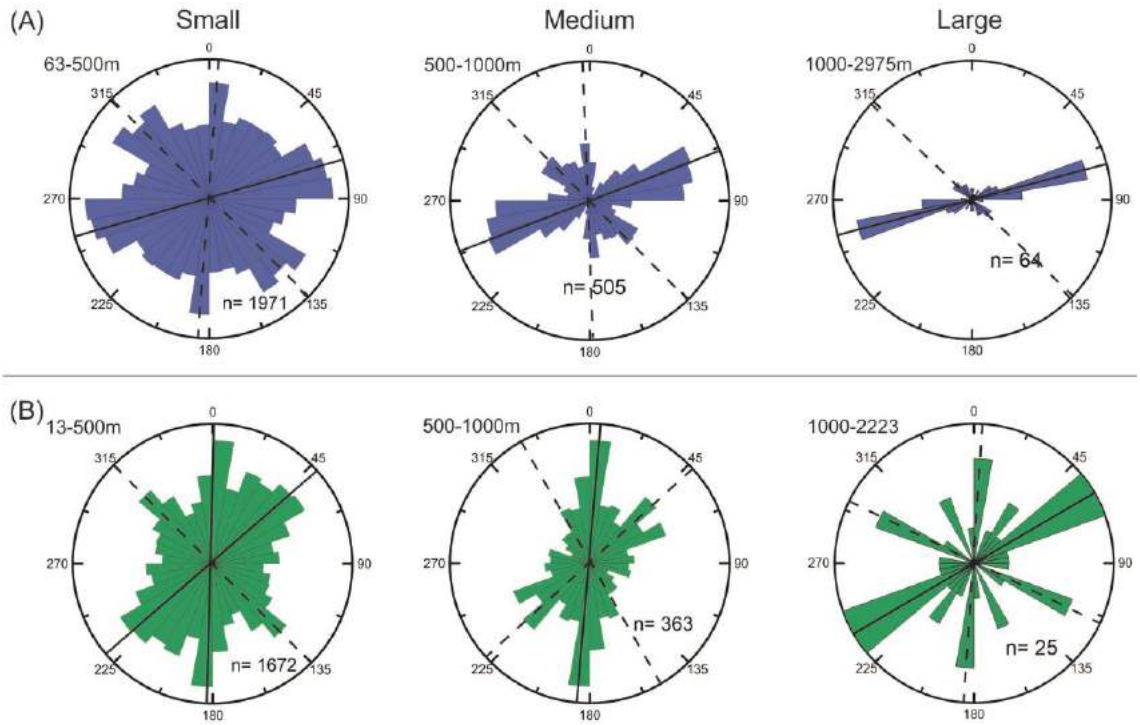
(A)
Small
Medium
Large
63-500m
500-1000m
1000-2975m
n= 1971
n= 505
n= 64
(B)
13-500m
500-1000m
1000-2223
n= 1672
n= 363
n= 25
0
45
90
135
180
225
270
315

Figure 6

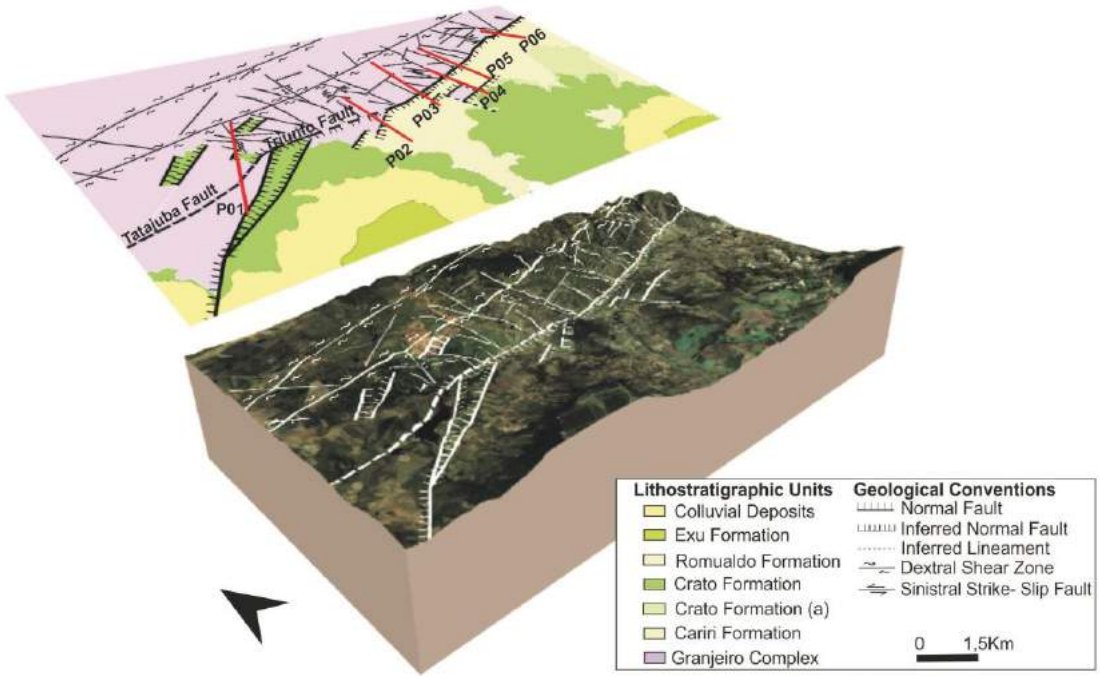

11

12 Figure 7

13

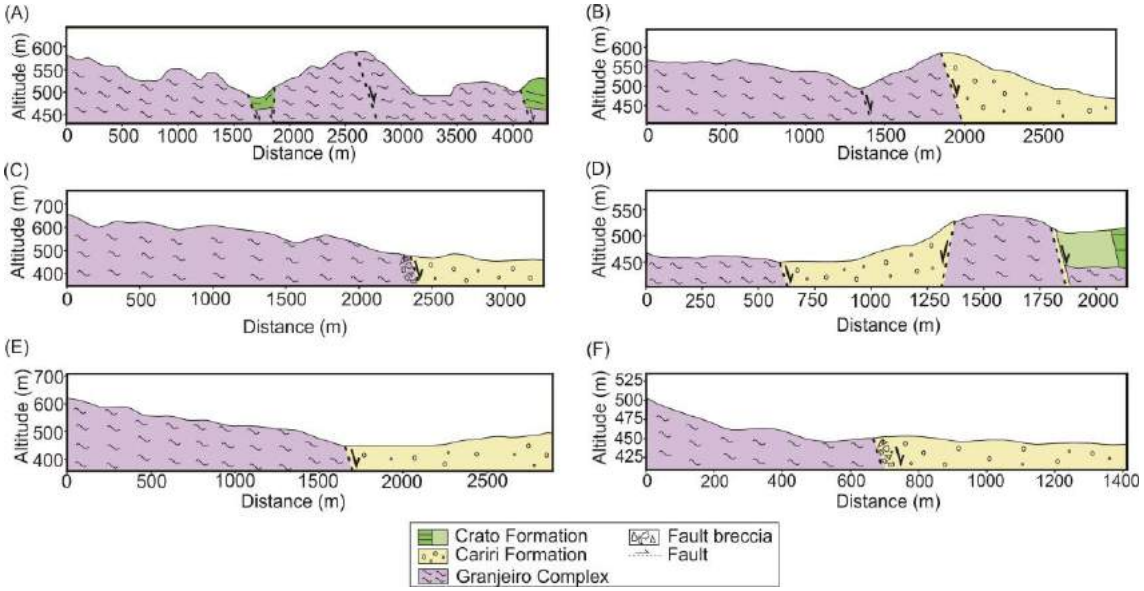

14

15 Figure 8

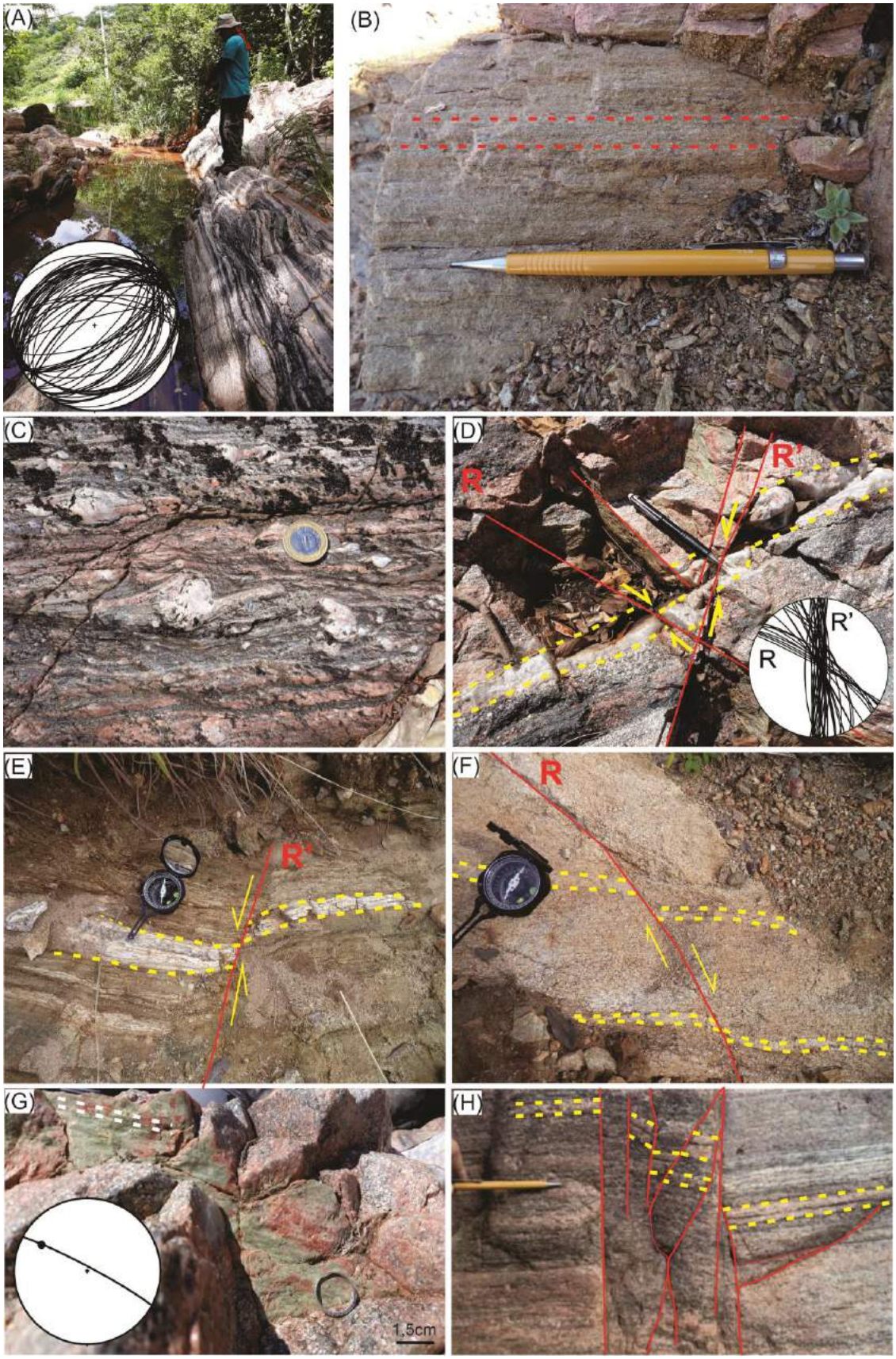

Figure 9

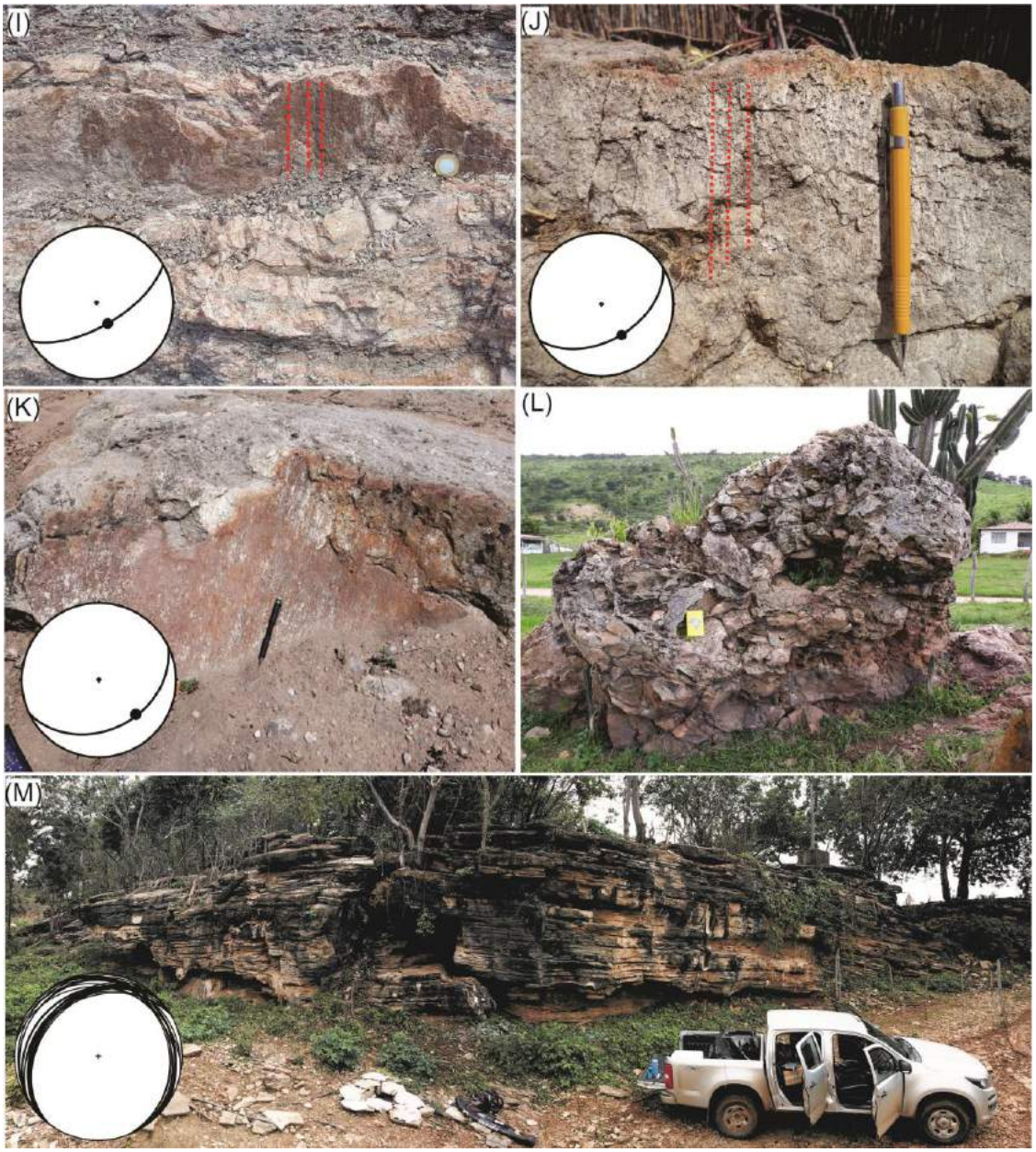

Figure 9 (cont.)

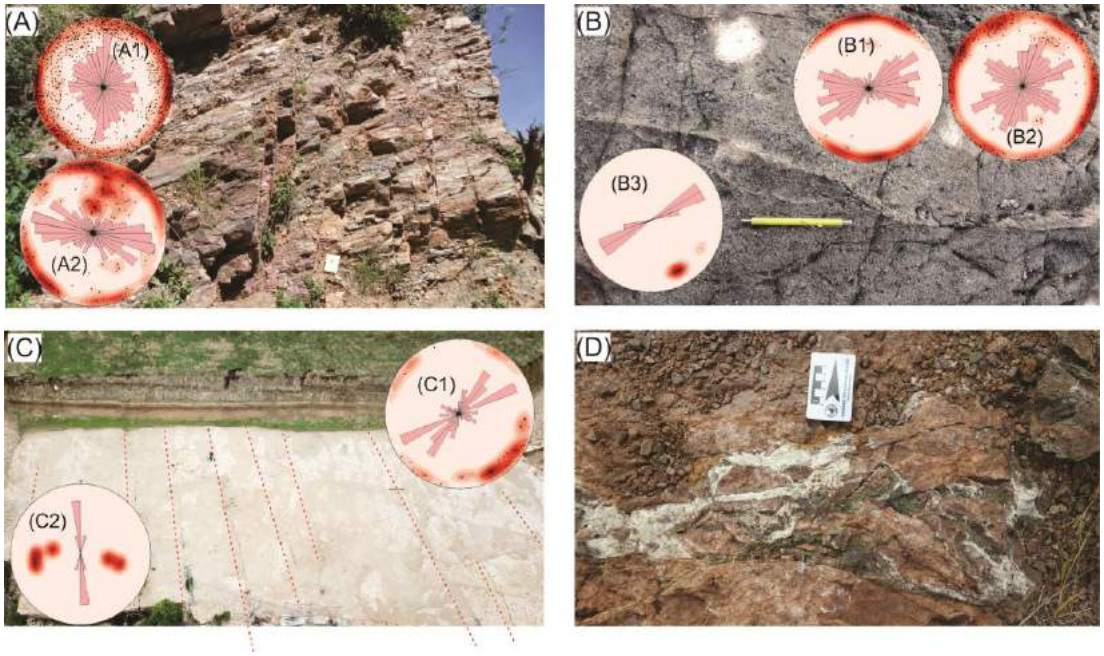

Figure 10

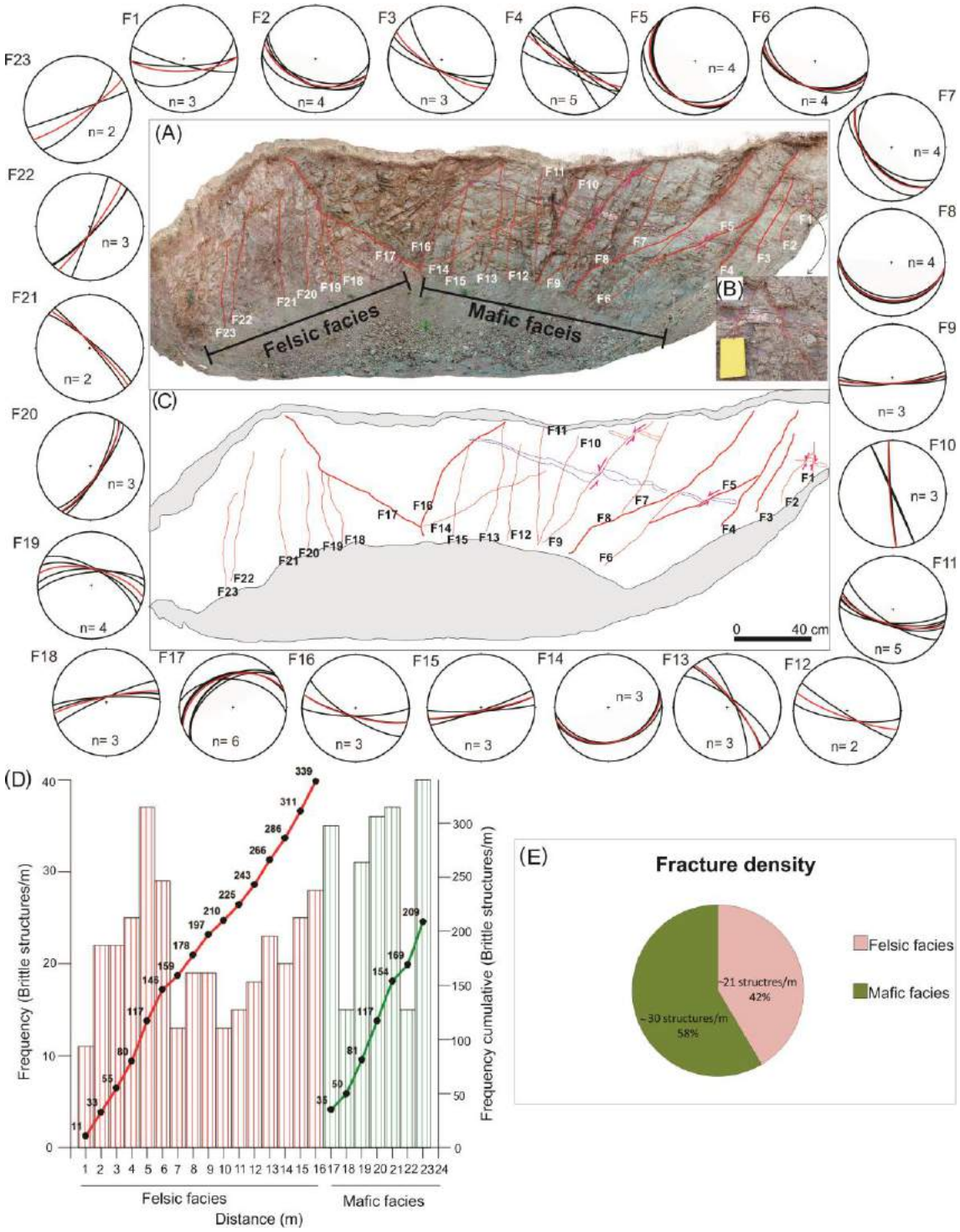
F1
F2
F3
F4
F5
F6
F7
F8
F9
F10
F11
F12
F13
F14
F15
F16
F17
F18
F19
F20
F21
F22
F23
n= 3
n= 4
n= 3
n= 5
n= 4
n= 4
n= 2
n= 3
n= 4
n= 4
n= 2
n= 3
n= 3
n= 4
n= 3
n= 5
n= 3
n= 6
n= 3
n= 3
n= 3
n= 2
(A)
(B)
(C)
Felsic facies
Mafic faceis
0
40 cm
(D)
Frequency (Brittle structures/m)
Frequency cumulative (Brittle structures/m)
Felsic facies
Mafic facies
Distance (m)
(E)
Fracture density
~21 structres/m
42%
~30 structures/m
58%
Felsic facies
Mafic facies

Figure 11

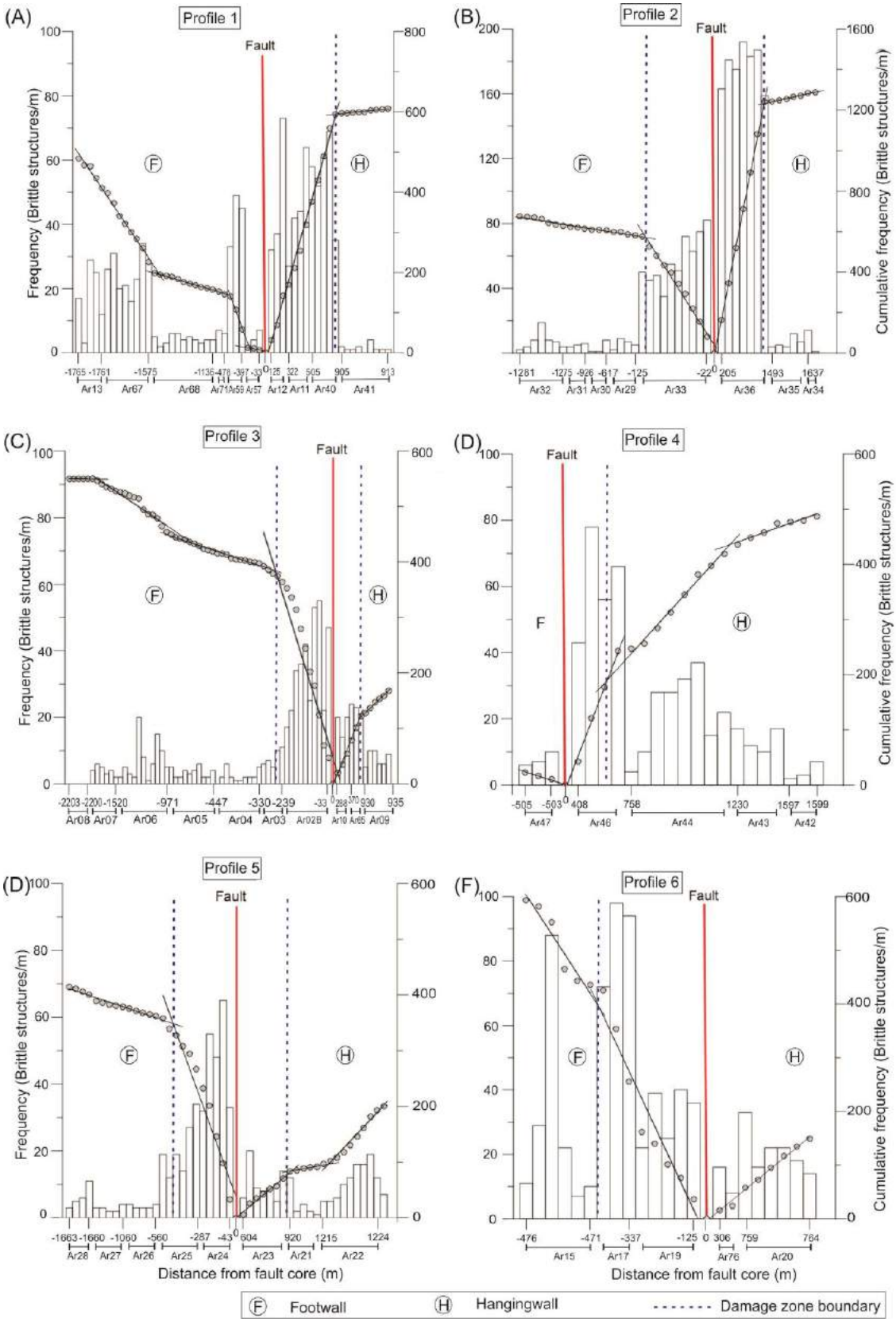
(A)
Profile 1
Fault
Frequency (Brittle structures/m)
Cumulative frequency (Brittle structures/m)
F
H
Ar13 Ar67 Ar68 Ar71 Ar58 Ar57 Ar12 Ar11 Ar40 Ar41
(B)
Profile 2
Fault
Ar32 Ar31 Ar30 Ar29 Ar33 Ar36 Ar35 Ar34
(C)
Profile 3
Fault
Ar08 Ar07 Ar06 Ar05 Ar04 Ar03 Ar02B Ar10 Ar65 Ar09
(D)
Profile 4
Fault
F
H
Ar47 Ar46 Ar44 Ar43 Ar42
(D)
Profile 5
Fault
Ar28 Ar27 Ar26 Ar25 Ar24 Ar23 Ar21 Ar22
Distance from fault core (m)
(F)
Profile 6
Fault
Ar15 Ar17 Ar19 Ar76 Ar20
Distance from fault core (m)
F Footwall
H Hangingwall
Damage zone boundary

Figure 12

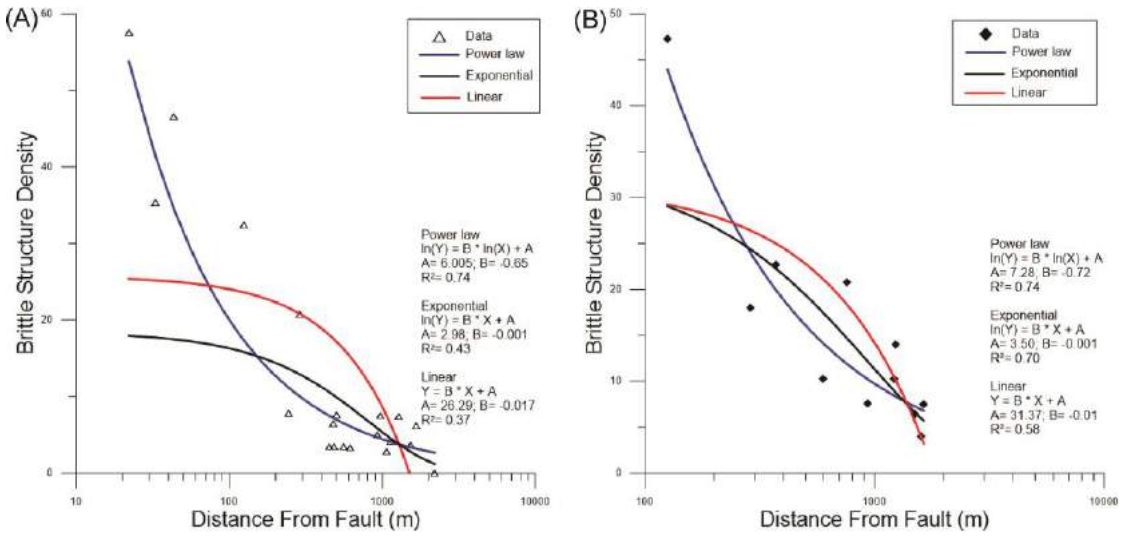

27

28 Figure 13

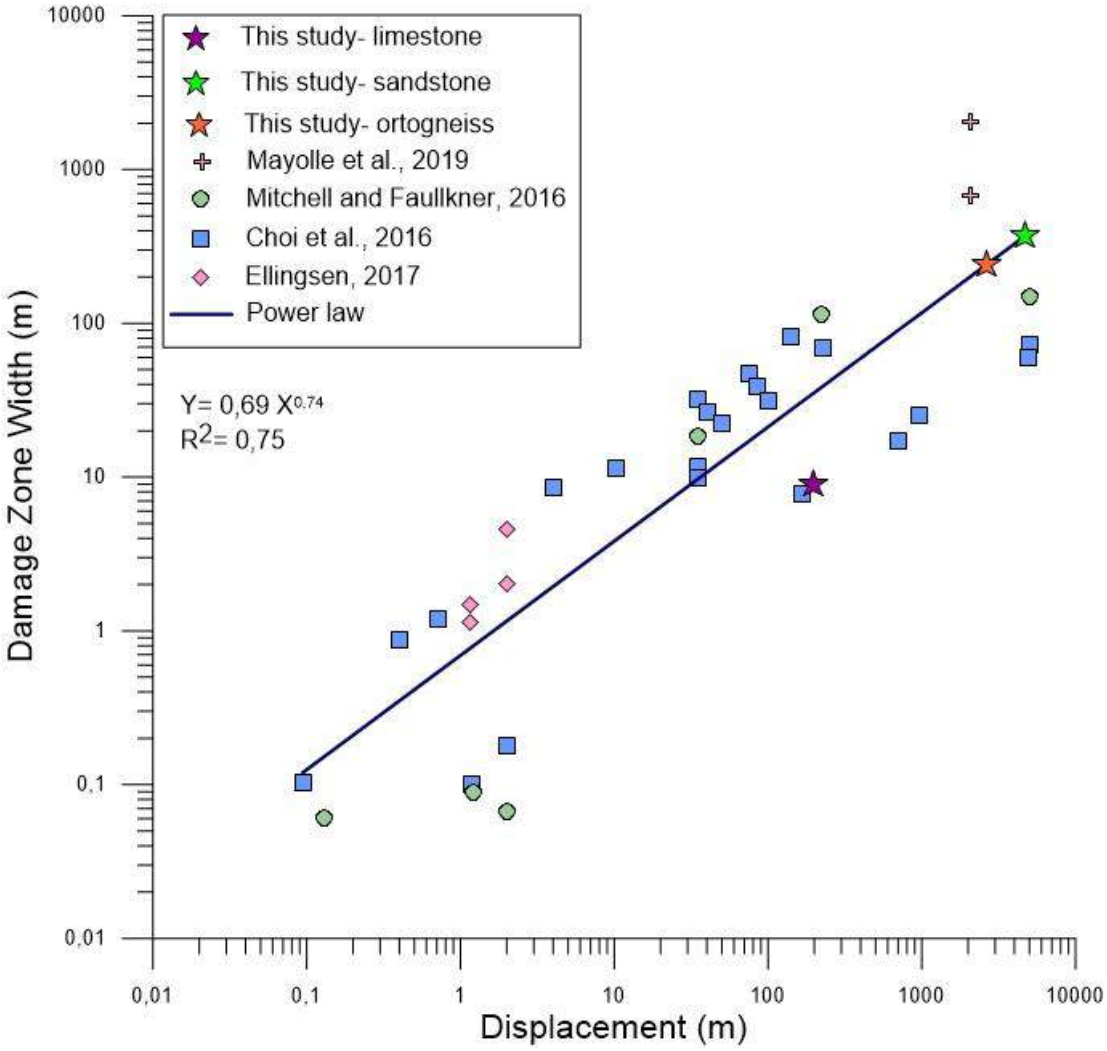
This study- limestone
This study- sandstone
This study- ortogneiss
Mayolle et al., 2019
Mitchell and Faullkner, 2016
Choi et al., 2016
Ellingsen, 2017
Power law
Y= 0,69 X0.74
R2= 0,75
Damage Zone Width (m)
Displacement (m)
10000
1000
100
10
1
0,1
0,01
0,01
0,1
1
10
100
1000
10000

Figure 14

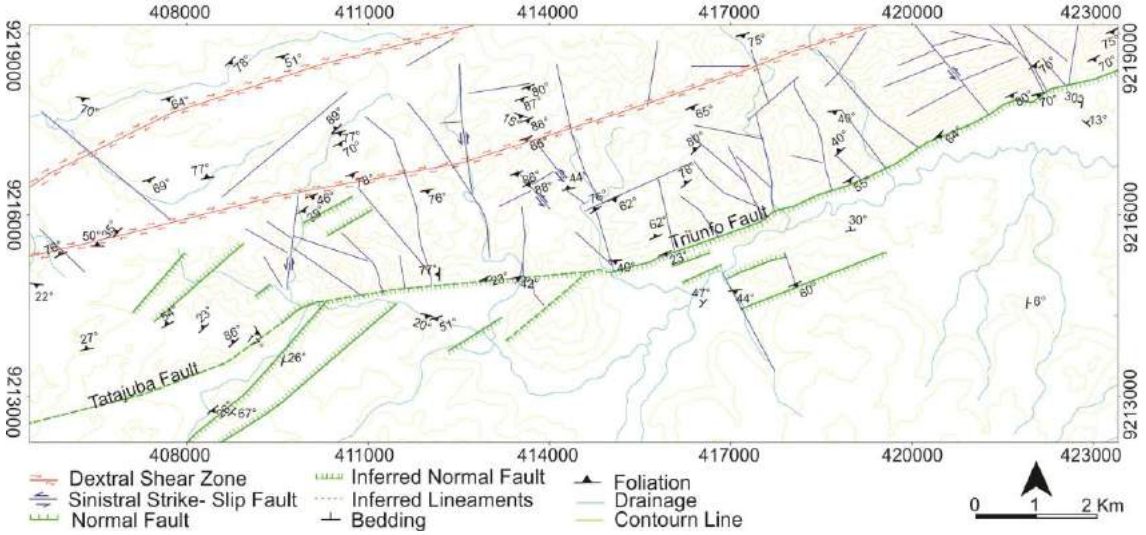
408000
411000
414000
417000
420000
423000
9219000
9216000
9213000
Triunfo Fault
Tatajuba Fault
Dextral Shear Zone
Sinistral Strike- Slip Fault
Normal Fault
Inferred Normal Fault
Inferred Lineaments
Bedding
Foliation
Drainage
Contourn Line
0
1
2 Km

Fig. 15

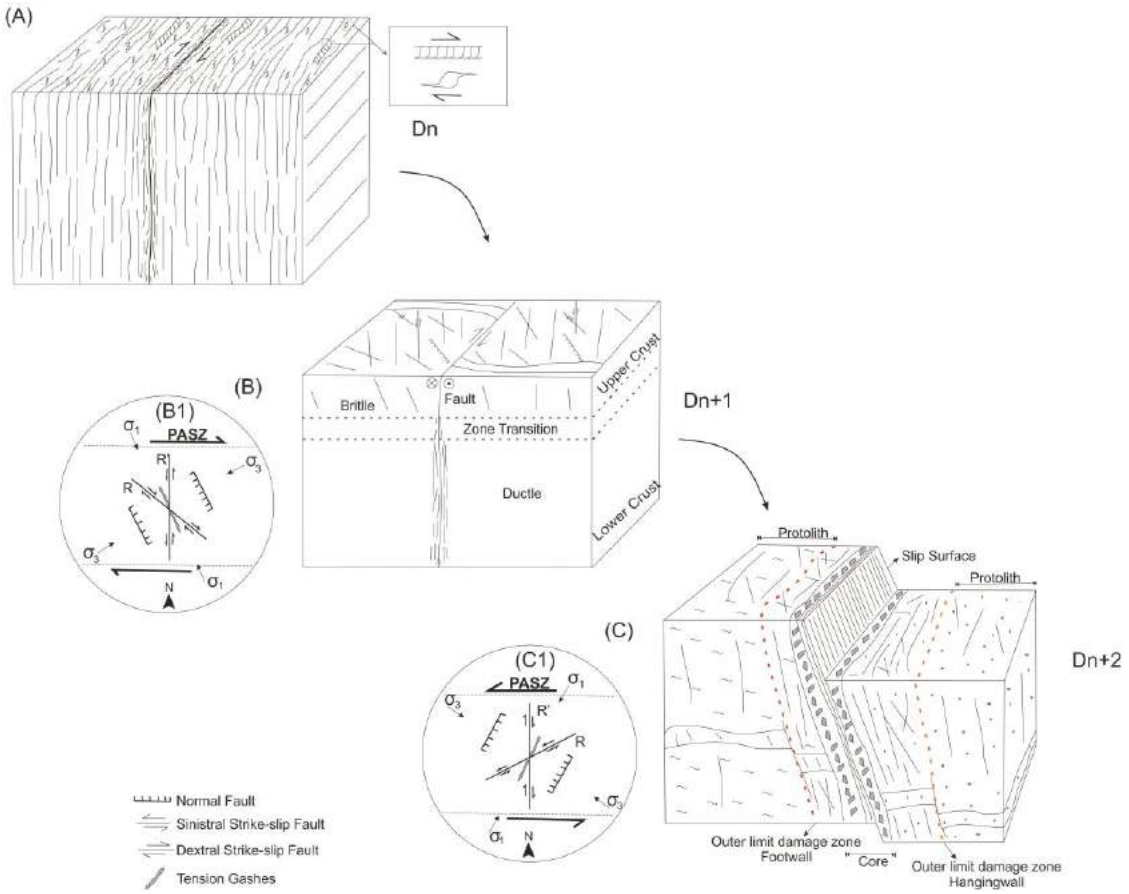
(A)
Dn
(B)
(B1)
PASZ
Brittle
Fault
Upper Crust
Zone Transition
Ductile
Lower Crust
Dn+1
(C)
(C1)
PASZ
Protolith
Slip Surface
Protolith
Dn+2
Outer limit damage zone
Footwall
Core
Outer limit damage zone
Hangingwall
Normal Fault
Sinistral Strike-slip Fault
Dextral Strike-slip Fault
Tension Gashes

Figure 16

3.2 STRUCTURAL CONTROL AND GEOCHRONOLOGY OF CRETACEOUS CARBONATE BRECCIA PIPES, CRATO FORMATION, ARARIPE BASIN, NE BRAZIL

Gmail Alcione Lima <alcionelimma22@gmail.com>

A manuscript number has been assigned: JMPG-D-20-01378
1 mensagem

Marine and Petroleum Geology <eesserver@eesmail.elsevier.com> 20 de outubro de 2020 01:39
Responder a: Marine and Petroleum Geology <jmpg@elsevier.com>
Para: alcionelimma22@gmail.com, alcionelimma@hotmail.com

*** Automated email sent by the system ***

Ms. Ref. No.: JMPG-D-20-01378
Title: Structural control and geochronology of Cretaceous carbonate breccia pipes, Crato Formation, Araripe Basin, NE Brazil
Marine and Petroleum Geology

Dear Miss Celestino,

Your submission "Structural control and geochronology of Cretaceous carbonate breccia pipes, Crato Formation, Araripe Basin, NE Brazil" has been assigned manuscript number JMPG-D-20-01378.

Structural control and geochronology of Cretaceous carbonate breccia pipes, Crato Formation, Araripe Basin, NE Brazil

Maria Alcione Lima CELESTINO[a]* (alcionelimma22@gmail.com)

Tiago Siqueira de MIRANDA[b] (tiago.smiranda@ufpe.br)

Gorki MARIANO[b] (marianogorki@gmail.com)

Marcio Lima ALENCAR[a] (marcio.lima@ufpe.br)

Jim BUCKMAN[c] (j.buckman@hw.ac.uk)

Nick M. W. ROBERTS[d] (nirob@bgs.ac.uk)

José Antonio BARBOSA[b] (jose.antoniob@ufpe.br)

Virginio H. M. L. NEUMANN[b] (virginio.neumann@ufpe.br)

Jorge André Braz SOUZA[e] (jorgeabs@petrobras.com.br)

Eduardo ROEMERS-OLIVEIRA[e] (roemers@petrobras.com.br)

[a]Geosciences Graduate Program, Federal University of Pernambuco, Recife, PE, 50740-530, Brazil

[b]Department of Geology, Federal University of Pernambuco, Recife, PE, 50740-530, Brazil

[c]Institute for GeoEnergy Engineering, Heriot-Watt University, Riccarton, Edinburgh EH14 4AS, UK

[d]Geochronology and Tracers Facility, British Geological Survey, Environmental Science Centre, Nottingham, NG12 5GG, UK

[e]Petrobras Research Center, Av. Horácio de Macedo, 950, Cidade Universitária. Ilha do Fundão, Rio de Janeiro, 21941-915, Brazil.

*Corresponding author; e-mail: alcionelimma22@gmail.com; telephone: +55 81 99636-3490; postal address: Av. da Arquitetura, 953-995 - Cidade Universitária, Recife - PE, 50740-540, Brazil.

Abstract

The laminated limestones of the Crato Formation, Araripe Basin (NE of Brazil) have been investigated, as they are analogous to facies of the carbonate reservoirs of the pre-salt sequence of the Brazilian marginal basins. The Early Cretaceous Crato laminites comprise a complex range of structures that may play an important role in the porosity and permeability distribution in carbonate reservoirs. This work aims to (1) understand the control of a boundary fault zone (the Triunfo Fault, Lower Cretaceous) on the development in carbonate breccia pipes of the Crato Formation, and (2) constrain the timing of brittle deformation, based on field observations, microstructural investigation and U-Pb carbonate geochronology. The breccia pipes are observed surrounding both normal and strike-slip faults. The brittle deformation superimposed on the pipes is characterized by brecciation and veining that show multiples phases of mineralization. Our results propose the circulation of fluid along the pre-existing faults and pipes, these fluids are responsible for polyphasic deformation in the pipes. We report two U-Pb ages from carbonate-vein mineralization of 94.9 ± 3.8 Ma (Cenomanian to Turonian) and 80.2 ± 3.0 Ma (2σ) (Campanian), which provide time constraints on the brittle reactivations of the Triunfo Fault Zone, during the post-rift phase of the Araripe Basin.

Keywords

Breccia Pipe, U-Pb geochronology, Fault reactivation, dolomitization, Araripe Basin

1- Introduction

The identification of different architectural elements of a fault zone, fluid-rock interactions and the absolute timing of deformation affecting sedimentary reservoirs are essential in various research areas, such as the exploration and production of hydrocarbons, radioactive waste management, groundwater and CO_2 storage (Schueller et al., 2013; Rohmer et al., 2015; Dimmen et al., 2017; Peacock et al., 2017; Wu et al., 2019). Constraining the timing of brittle deformation is critical in understanding crustal evolution, especially of sedimentary basins, and fluid flow during successive deformation events, but many regional-scale fault systems lack readily available techniques to provide absolute chronological information. Carbonate mineralization can occur in crustal structures in many geological settings and can be suitable for U-Pb geochronology (e.g., Roberts and Walker, 2016; Nuriel et al., 2017; Hansman et al., 2018; Parrish et al., 2018; MacDonald et al., 2019; Nuriel et al., 2019; Roberts et al., 2020).

Faults zones are complex 4-D structures composed of rocks in variable degrees of deformational states, which strongly influence fluid flow properties, and can trap fluids through time or act as conduits (Wibberley and Shipton, 2010). As fluid interacts with a rock volume, it changes the rock's properties, such as a decrease or increase in porosity and permeability distribution, due to the cementation or dissolution of the rock, (e.g., Salomon et al., 2020). In addition, fluid flow can cause hydrofracking of rock that leads to the formation of breccias, new fractures and reactivation of pre-existing fractures due to an increase in fluid pressure (Phillips, 1972; Jébrak, 1997; Grare et al., 2018). The origin of these fluids can be diverse, including magmatic, meteoric, metamorphic, diagenetic or a combination of these (Ridley and Dimond, 2000); in addition, fluids can be channeled through faults.

Pre-salt carbonates (e.g., Campos Basin, Brazil and Kwanza Basin, Angola) often exhibit post depositional alterations including dolomitization and silification (Lima and De Ros, 2019; Lima et al., 2019), which may be associated with seismic activity, in which tectonics and hydraulic fracturing, control the flow of hydrothermal fluids (Davies, 2004; Davies and Smith Jr., 2006; Poros et al., 2017; Pagel et al., 2018; Rochelle-Bates et al., 2020). These alterations can cause variations in the quality of the reservoirs due to fluid circulation and fluid-rock interactions, changing their permeability and porosity distribution (Lima et al., 2019). Here, we present an integrated dataset of structural field observations, petrography (optical, cathodoluminescence, and Scanning Electron Microscopy Energy-Dispersive X-ray analysis (SEM-EDX)) and geochronological analyses (U-Pb) of carbonate breccias from the Early Cretaceous lacustrine laminites of the Crato Formation, Araripe Basin, NE Brazil. The Crato Formation is renowned in the international scientific community as a Lagerstätten deposit that contains pristine fossils (Martill et al., 2007). The formation is time-equivalent of the Brazilian Pre-Salt reservoir rocks, and has been used as a carbonate reservoir analogue for presenting depositional, geomechanical and structural similarities to the facies of the Barra Velha and Macabu Formations, Santos and Campos Basins, respectively (Catto et al., 2016; Neumann et al., 2003; Miranda et al., 2018). The laminites of the Crato Formation illustrate similar dolomitization processes to those observed in the Pre-Salt successions (e.g., Lima et al., 2019) and are investigated in this work through the observation of breccia pipes associated within the laminites.

The Crato Formation breccia pipes were initially described by Marttil et al., (2008), who classified them as dolomite pipes. These authors also proposed that the dolomite pipe's origin was linked to the entry of fluids arising from the sandstones of

the underlying Cariri Formation, during the initial stages of burial. More recently, Alencar et al., (2020) associated the origin of pipes with processes of liquefaction and brecciation due to seismic activities, while the limestone was unconsolidated. However, some aspects regarding the formation of these pipes, such as the nature of fluids, ages of formation and tectonic reactivations remain uncertain.

In this study we document the fault system of the northern border of the Araripe Basin, and the implications for the structural control on breccia pipes formed within the Aptian laminites of the Crato Formation. Additionally, using the method of in situ U-Pb geochronology (Roberts et al., 2020), we determined the timing of carbonate vein mineralization associated with these carbonate breccia pipes.

This study of breccia pipes will help to understand the fault reactivation processes in the Araripe Basin, as well as carbonate dolomitization processes.

2- Geological Setting

The study area is located on the northern border of the Araripe Basin, one of the intraplate basins of northeastern Brazil. This basin is located in the Central Domain (or Transversal Zone) of the Borborema Province, which is limited to the north by the west termination of the Patos shear zone (PASZ), locally named as Triunfo Fault (Fig. 1) (Celestino et al., 2020). The PASZ is approximately 600 km long and is characterized by high temperature Precambrian mylonitic orthogneisses (Viegas et al., 2014). Crystalline basement rocks of the northern border of the Araripe Basin comprises mylonitic orthogneisses from the Granjeiro Complex (Neo-Archean), and metasediments from the Cachoeirinha Group (Neoproterozoic) (Silva et al. 2002; Medeiros and Jardim de Sá, 2009). The stratigraphy of the Araripe Basin has been traditionally divided into pre-, syn- and post-rift sequences (Fig. 1-e) (Neumann et al.,

2003; Assine, 2007). The pre-rift unit is represented by the Paleozoic (Siluran-Devonian), Cariri Formation and by the Late Jurassic (Oxfordian-Tithonian), Brejo Santo and Missão Velha Formations. The rift sequence comprises the Early Cretaceous (Neocomian) Abaiara Formation. The post-rift sequences (Aptian-Cenomanian) are represented by post-rift 1, the Barbalha, Crato, Ipubi, Romualdo Formations and post-rift 2, Exu Formation, which represents thermal subsidence as a sag basin (Assine et al., 2014; Neumann and Assine, 2015).

The Araripe Basin is commonly divided into two sub-basins: Feitoria, to the West and Cariri, to the East (Rand, 1983; Rand and Manso, 1984; Ponte and Ponte Filho, 1996; Assine, 2007) (Fig. 1). These sub-basins are compartmentalized by a set of horsts and grabens, with the Dom Leme horst being the central structure that separates the two sub-basins. There are several proposals regarding the tectonic evolution of the Araripe Basin (Marques et al., 2014; Miranda et al., 2014; Peulvast and Bétard, 2015; Garcia et al., 2019; Celestino et al., 2020). Celestino et al. (2020) suggested that the basin has evolved through two deformational stages: (1) dextral transtensional tectonics during the Paleozoic, marked by the development of conjugated pairs of brittle-ductile strike-slip faults (NW-SE, N-S); and (2) sinistral transtensional tectonics during the Cretaceous, characterized by the development of normal faults NE-SW (e.g. Triunfo Fault) and conjugated pairs of strike-slip faults (NE-SW, N-S), who comprise the Triunfo Fault Zone (Figs. 1-b and 2) (Fig. 16 of Celestino et al, 2020). The Crato Formation presents evidence of seismic activity which is marked by the development of soft sediment deformation structures (seismites) (e.g., syn-sedimentary shear fractures, microslumps, breccia pipes) and veins of dolomite, calcite and gypsum, joints and faults (Martill et al, 2008, Miranda et al., 2018; Alencar et al., 2020). These deformations would have occurred after the second deformational stage proposed by Celestino et al,

(2020), during the post-rift phase, associated with brittle reactivation of the Patos shear zone (Alencar et al., 2020).

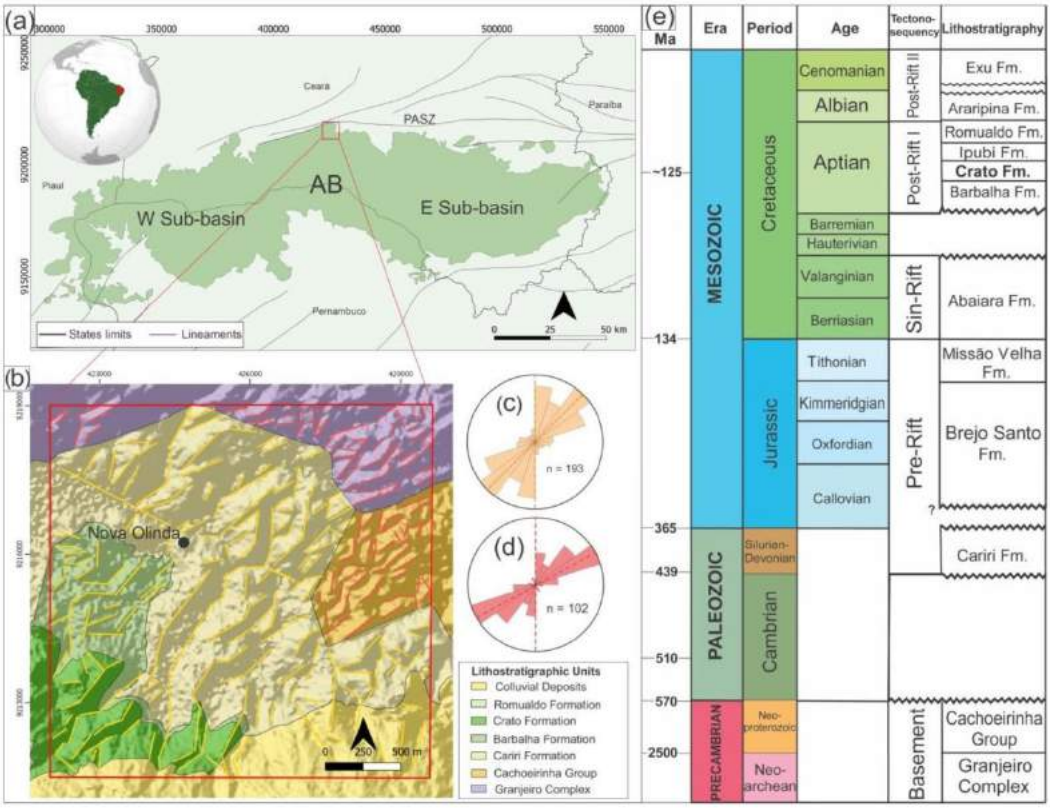

Figure 1. (a) Location of the study area in the northern border of the Araripe Basin (AB); (b) Detailed geological map of the study area showing topographic lineaments of two sectors: basement (red) and basin (yellow). Rose diagrams showing the main directions of (c) basin and d) basement lineaments. Dashed lines correspond to preferred directions; (e) Stratigraphic chart of the Araripe Basin. Modified from: Neumann and Assine (2015); Lúcio et al., 2020.

3- Materials and Methods

3.1- StructuralMap

Firstly, this study carried out a detailed structural mapping which was performed over an area of 57 km^2 (Fig 1-b). Sedimentological and structural observations

(description of lithological types and measurements taken from ductile and brittle structures) were made from field observations and analyses of satellite images (Shuttle Radar Topography Mission imagery, SRTM- https://earthexplorer.usgs.gov). A Digital Elevation Model (DEM) was produced using the interactive shading technique, with the objective of identifying structural lineaments (Fig. 1- b) (Onorati et al., 1992; Salamuni et al., 2004; De Lima and De Sá, 2017; Celestino et al., 2018, Celestino et al., 2020). The interpreted structural lineaments were correlated with the structures observed in the field, aiming to classify the lineaments as faults, joints, deformation bands or foliations.

3.2- Analytical Methods

3.2.1- Optical Microscopy

For optical microscopic observations, polished thin sections of selected samples were analyzed using light (transmitted and reflected) and cathodoluminescence from the Universidade Federal de Pernambuco (UFPE). For the analysis of optical petrography of reflected and transmitted light, we used the Zeiss Scope A2 microscope, which helped to identify mineral contents, textures and temporal relationships. Analysis using cathodoluminescence was performed using a CITL Mk5 Optical Cathodoluminescence Microscope. This technique helped in the identification of carbonate in the rocks, as well as highlights the cutting relationships between the mineral phases.

3.2.2- Energy-Dispersive X-ray

A polished thin section of the brecciated pipe was mapped by energy-dispersive X-ray (EDX) analysis, using a Quanta FEG 650 scanning electron microscope (SEM), operated in low-vacuum mode (0.83 Torr), 20 kV operating voltage, equipped with an Oxford Instruments X-Max^N 150 mm^2 detector and AZtec large area mapping software.

A total of 348 frames (tiles) were taken over a grid 12 tiles wide by 29 tiles deep. At each location, a backscattered (BSE) image was taken, with a field of view of 1.54 mm, and an EDX map for all elements present was generated (1024 x 704 pixels). Each EDX elemental map was constructed from 50 frames, taken with a dwell time of 250 µs, spot size 4.5 and aperture setting 1 (to maximize X-ray flux).

3.2.3- U-Pb Geochronology

A sample was prepared as a thin polished block, mounted in resin with dimensions 5 cm x 3 cm x 1.5 cm. U-Pb geochronology was conducted with Laser Ablation Inductively Coupled Plasma-Mass Spectrometry (LA-ICP-MS) at the Geochronology and Tracers Facility, British Geological Survey, (Nottingham, UK). Analytical procedures are described in Roberts & Walker (2016) and Roberts et al. (2017). The reference materials WC-1 (Roberts et al., 2017) and ASH15 (Nuriel et al., 2020) were used as primary and secondary reference materials, respectively, for normalization of Pb/U ratios. The sample analyzed was from a vein hosted in a carbonate breccia pipe from the Crato Formation (P2B). This sample presented two distinct textures, on the external and internal portion of the vein. These textures possibly indicate the entry of fluids during different periods. Thus, this fact motived to place the geochronology analysis on this sample. Ages are quoted at 2σ, and as $\pm \alpha/\beta$, where α refers to the analytical uncertainty only, and β with propagation of the systematic uncertainties (Horstwood et al., 2016). See supplementary files for full description of the method and the full dataset.

4- Results

4.1- Structuralframework

The study area has a variety of lithological types such as: orthogneisses (Granjeiro Complex), metasedimentary rocks (Cachoeirinha Group), sandstones (Cariri Formation), shales (Barbalha Formation), and limestones (Crato Formation) (Fig. 2).

Crystalline basement rocks display a well-developed mylonitic foliation oriented NE-SW with dip oscillating between a medium to high angle, which represents the PASZ fabric (Fig. 3- a, b). This structure is clearly marked by the topographic lineaments of NE-SW direction (Fig. 1- b). The ductile fabrics are crosscut by a system of brittle-ductile conjugate pair of NW-SE and N-S strike-slip faults, dextral and sinistral, respectively (e.g., Celestino et al., 2020). In addition, the orthogneisses and metasedimentary rocks are dominated by brittle deformations (faults, joints, veins) developed during the brittle reactivation of the PASZ (Celestino et al., 2020). These deformations occur overprinted on the NE-SW direction lineaments, as normal faults, and on the N-S lineaments as strike- slip faults (Figs. 1 and 3- c). The contact between the basement and the basin is marked by the N60E-direction Triunfo Fault Zone (Figs. 2 and 3-d). The damage zones include faults, joints and deformation bands, whereas the core of the Fault Triunfo comprises various breccias and cataclasites (Figs. 8 and 9-d of Celestino et al., 2020).

In the study area, the sedimentary cover is represented by the Cariri, Barbalha and Crato Formations. The Cariri Formation comprises medium to coarse grained sandstones. Deformation bands represent the main brittle structures of the Cariri Formation, besides the occurrence of joints and faults in these rocks (Fig. 3-d, e, f). The deformation bands show a NE-SW main direction, with variable kinematics, sinistral and dextral, which occur either as single bands or as clusters. The Barbalha Formation comprises reddish shales.

Normal and strike-slip faults represent the brittle deformation of the Crato Formation laminites (Fig. 3- g). Vertical and sub-vertical pipe structures only occur in the laminites of the Crato Formation, and are related to the Triunfo Fault Zone (Figs. 2 and 4) (see section 4.2). The topographic lineaments show three main directions (Fig. 1): NE-SW, N-S and ENE-WSW (N70E), which reflect this fault system. Thus, the NE-SW alignments are represented by normal faults, the N-S and ENE-WSW lineaments may represent a conjugate pair of strike- slip faults (e.g., Celestino et al., 2020).

From the structural analysis of the study area, we have identified and named several faults, such as the Nova Olinda, Pedra Branca, Riacho do Caboré and Seu Crato faults (Fig. 2).

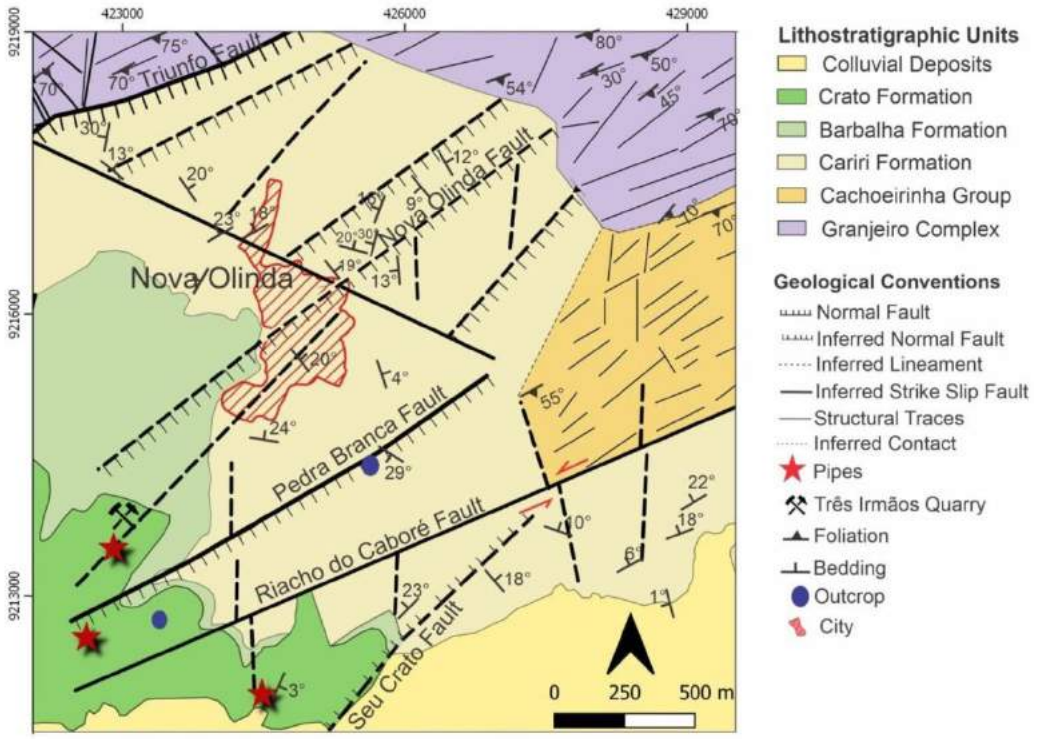

Figure 2. Structural map of the northern border of the Araripe Basin with emphasis on the location of the breccia pipes and key outcrops.

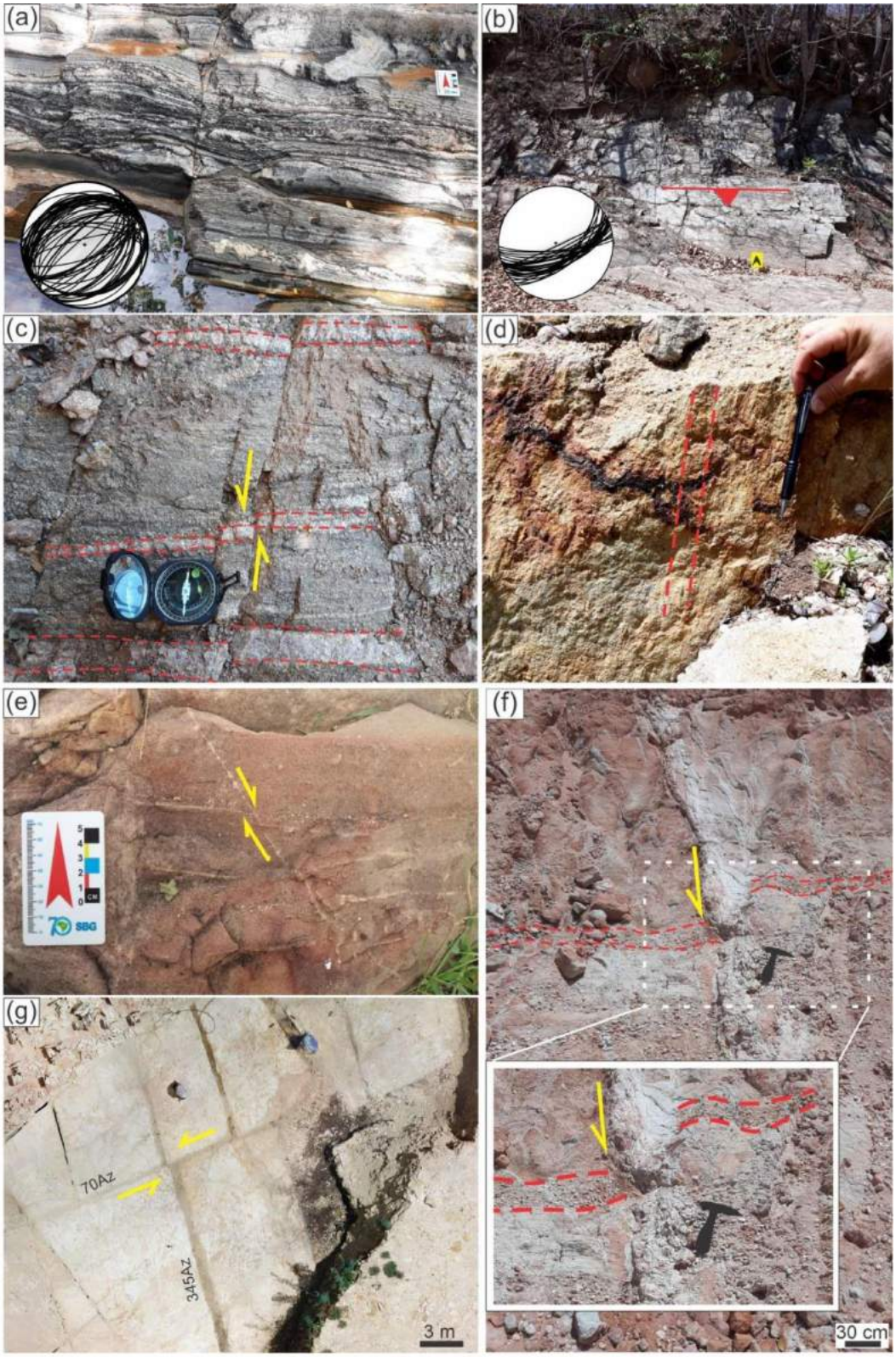

Figure 3. (a) Orthogneiss of the Granjeiro Complex with well-developed foliation striking NE-SW with dipping to SE and NW, detail for stereographic projection, n = 79,

map view; (b) Outcrop of metasedimentary rocks belonging to the Cachoeirinha Group, showing a NE-SW direction foliation with a moderate dip angle to SE, detail for stereographic projection, n = 38, section view (c) Sinistral strike slip fault of N-S direction in orthogneiss of the Granjeiro Complex, map view; (d) N60E direction fault plane in sandstone of the Cariri Formation with down dip slickenside, of the Triunfo Fault and, section view; (e) Cariri Formation sandstone deformation bands, illustrating indicators of sinistral movement, map view; (f) Normal fault with N55E direction in sandstone of the Cariri Formation, section view (g) Aerial photograph of limestone from the Crato Formation, with fractures displaced by a NE-SW sinistral strike slip fault.

4.2- Breccia Pipes

The breccia pipes are observed throughout the laminated limestones and are well-exposed in quarries, mainly at the Três Irmãos Quarry located in the northern border of the Araripe Basin (Fig. 2). These carbonate breccias pipes occur in the surrounding area of the Pedra Branca, Riacho do Caboré and Seu Crato fault zones (Fig. 2). These structures have a vertical to sub-vertical sub-cylindrical geometry (Fig. 4-a), with diameters varying from 1 to 2 m (Fig. 4-b). Nevertheless, the pipes crop out as a topographic high in relation to the host limestone and are discarded by the mining process because they do not preserve the plane-parallel lamination of the limestone (Fig. 4-c).

The carbonate breccia pipes of the Crato Formation show a chaotic texture characterized by angular fragments of the host rock (laminated limestone) and veins filled with calcite and dolomite that crosscut the framework of the rock (Fig. 4- a, b, e, f) (see section 4.2.2- EDX). In general, the pipe color is also a factor that differentiates it from the host rock, due to its top that usually displays gray and brownish colors, due

to dolomitization (Fig. 4- a, b, c). The pipe structure is commonly observed by arching of the layers of laminated limestone adjacent to it (Fig. 4- d).

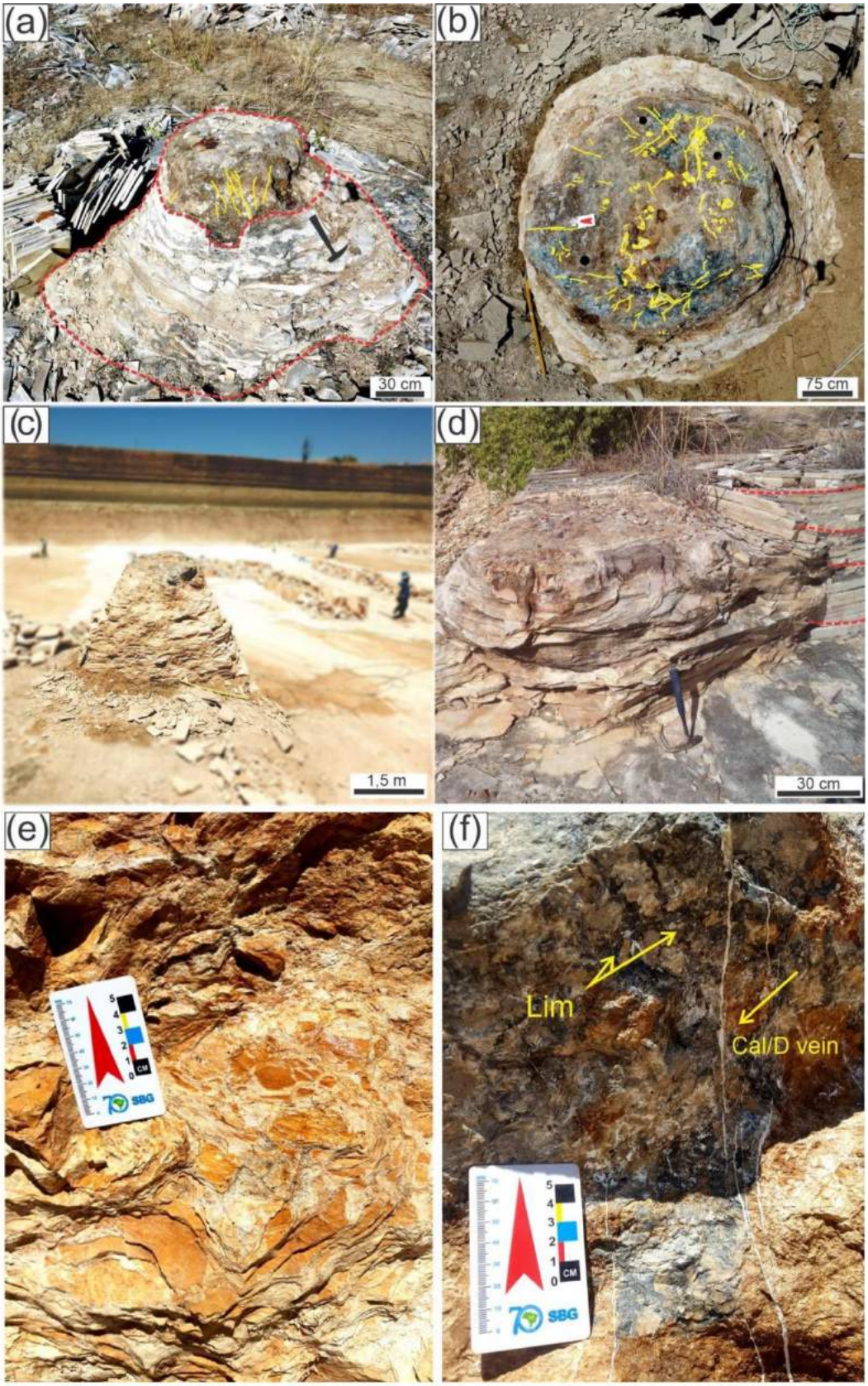

280

Figure 4. Carbonate breccia pipes of Crato Formation. (a) Vertical breccia pipes with their boundaries highlighted (dashed red lines), detail for the top of the breccia pipes of a brownish color, different from the body of the pipes, due to dolomitization. Yellow arrows indicate the presence of veins filled with calcite and dolomite, with dispersed distribution; (b) View of the top of the breccia pipes, gray color and cut by veins filled with calcite and dolomite (yellow lines); (c) Breccia pipes at Três Irmãos Quarry, this structure stands out in relation to the surrounding relief, being discarded when removing laminated limestone; (d) Arched layers of the host limestone by the breccia pipes; Angular fragments of the host limestone present in the (e) body of the breccia pipes; (f) on the head of breccia pipes with limestone fragments of different sizes (Lim) and calcite and/or dolomite veins (yellow arrows).

4.2.1- Petrographical observations

Petrographic observations of structures and calcite and dolomite mineralization in the breccia pipes allowed us to identify and establish its mineral paragenesis. These rocks are constituted by saddle dolomite, dolomite, calcite, gypsum, galena, chalcedony and pyrite (Figs. 5-7). The breccia pipes have a chaotic arrangement of veins and angular fragments of laminated limestone (Fig. 5- a, b').

4.2.1.1- Fragments of laminated limestone

The laminites angular fragments are typically 1 to 30 mm in size (Fig.5-a,b'). These fragments commonly occur dolomitized or partially dolomitized (Fig. 5-a,b) and are associated with pyrite distributed randomly through the fragments (Fig. 6-a) and chalcedony (Fig. 6-d). The space between theses fragments is filled by dolomite and calcite cements (Figs. 5-a,b',c,d). In addition, they are crosscut by veins of calcite

and/or dolomite (Figs. 5,6). In the cathodoluminescence imagery they show luminescence varying from dark orange.

4.2.1.2 Pyrite

The pyrites are of a micrometer scale and are disseminated in the fragments of laminated limestone of the breccia pipes. Under cathodoluminescence they are non-luminescent. Commonly, these minerals are associated with the limestone fragments that are included in the dolomitic cement (Fig. 6-a,b).

4.2.1.3 Chalcedony

Chalcedony occurs in a dispersed form in the breccia pipes mailing fillings pores (micrometric to millimetric scale). Locally, this mineral is crosscut by gypsum veins (Figs. 6 and 7-d). Additionally, we observed that the chalcedony minerals are non-luminescent under cathodoluminescence.

4.2.1.4 Dolomites + Galena

The dolomites observed in the breccia pipes occur as cement between the limestone fragments and filling veins (Figs. 5-7). They are thick crystals (micrometric to millimetric scale) and have zoning patterns. According to the classification of Gregg & Sibley (1984), the analyzed dolomite cements can be classified as idiotopic-S, and idiotopic-C dolomites. In addition, we observed that the dolomite veins, in general, tend to exhibit wavy extinction, pointed ends and curved faces, representing the occurrence of saddle dolomite, which can be classified as xenotopic-C.

The zoned dolomites with up to four filling pulses (four zones) occur as the main cement for the breccia pipes. The zoned dolomitic cement has luminescence varying

between red and non-luminescent zones interspersed in the cathodoluminescence imagery (Figs. 5-7). Angular fragments of dolomite and limestone are also found associated with the filling of calcite as cement (Fig. 5- c, d).

Galena occurs on a micrometric scale as subhedral crystals and with typical triangle pits (Fig.6-a,b,c). Galena inclusions in dolomitic cement are observed and sometimes these include limestone fragments with associated pyrite (Fig. 6- a,b,c).

The saddle dolomite occurs mainly as fringes in veins, and can also appear combined in veins with calcite cores (Figs. 5- e, f and 7). The thickness of the veins varies from micrometers to centimeters, and the luminescence has a zoning ranging from red to brown areas of varying thickness in the cathodoluminescence imagery (Figs. 6 and 7). The veins that crosscut the carbonate breccia pipes have different textures and filling stages (Figs. 6 and 7). One vein with dolomite filling, including an angular fragment of the host limestone, records only one phase of mineral pulse (Figure 7- c). A zoned dolomite vein, which is interpreted as antitaxial is also observed (Fig. 6 - e,f). However, it is commonly observed in other veins, are mineralization comprising more than one mineral phase, with gypsum edges and a core comprised by zoned dolomite (Fig. 6 g,h). The mosaic in Figure 7 - a illustrates that the main vein, which crosscuts the carbonate breccia pipe, is filled with zoned saddle dolomite on its edges, forming a fringe, with the center being filled with thick calcite. This is the vein that has been dated (see section 4.2.3).

4.2.1.5 Gypsum

Gypsum occurs as antitaxial fine veins of micrometric scale, in cathodoluminescence imagery are non-luminescent. This mineral usually occurs at the edges of other veins filled with dolomite and / or calcite (Figs. 6- g,h and 7). Commonly

seen by crosscutting chalcedony included in limestone fragments (Figs. 6-d and 7-d). Inclusions in the core gypsum veins are also observed, fine calcite (Fig. 7-e) and saddle dolomite (Fig. 7- h,i).

4.2.1.6 Calcite

Calcite occurs mainly by filling veins and commonly occurs by cross-cutting the veins filled with dolomite (Fig. 5- g,h). Locally it is also observed as cement involving angular fragments of limestone and dolomite (Fig. 5-c,d). In the cathodoluminescence imagery they have an orange or non-luminescent color without zoning (figs. 5-7). Calcite veins occur as two types - fine veins filled only with calcite, orange or non-luminescent, (Figs. 6-g,h and 7-g,i), and veins with a core filled with calcite, orange luminescence, and with edges filled with dolomite (Fig. 7-g,i).

The fine calcite-filled vein (Fe-rich, non-luminescent in cathodoluminescence) occurrence crosscuts across the saddle dolomite fringe of the main vein (Fig. 7- d, f, g), it also percolates along the antitaxial vein filled with gypsum (Fig. 7- e), which occurs on the outer margins of the main vein (Fig. 7- a). In figure 7, we also observe the occurrence of calcite that occurs filling the core of a vein with multiple fills, they are subhedral crystals, centimeter scale; the luminescence is orange in cathodoluminescence. This same type of calcite is observed to fill veins that crosscut veins of zoned dolomite (Fig.5-g,h).

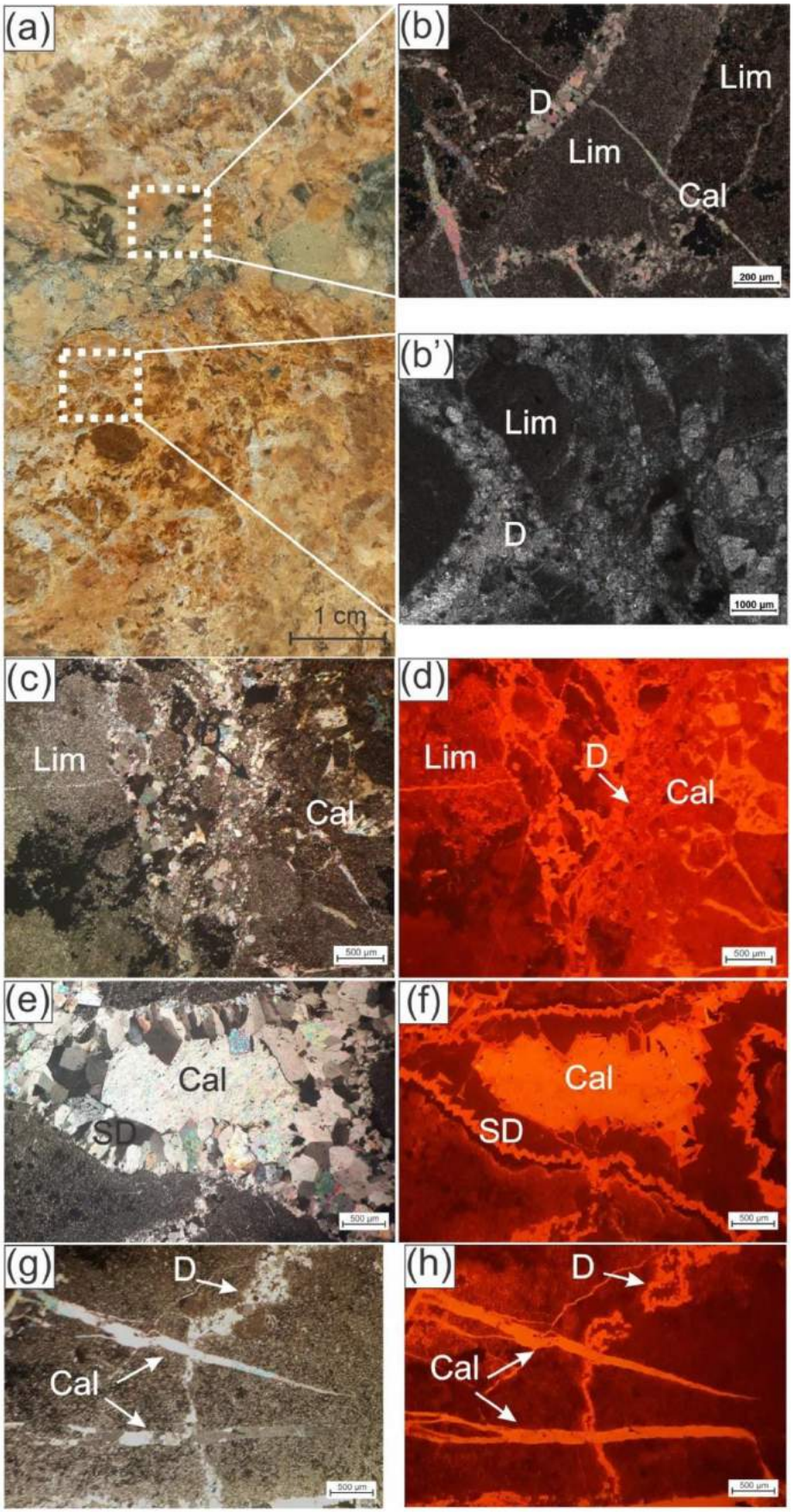
(a)
1 cm
(b)
Lim
D
Lim
Cal
200 µm
(b')
Lim
D
1000 µm
(c)
Lim
Cal
500 µm
(d)
Lim
D
Cal
500 µm
(e)
Cal
SD
500 µm
(f)
Cal
SD
500 µm
(g)
D
Cal
500 µm
(h)
D
Cal
500 µm

377

Figure 5. Photomicrographs highlighting main features of the carbonate breccia pipes from the Crato Formation. (a) Photograph of breccia pipe samples, detail for the central portion of the sample (gray color) partially dolomitized, extremity portions with dolomitized limestone and carbonate filling between the limestone fragments; (b) Detail figure (a), dolomite and partially dolomite limestone crosscut by calcite and dolomite veins; (b') Detail figure (a), Limestone fragments of varying sizes with dolomite between the fragments; Angular fragments of limestone and dolomite with associated calcite, in polarized light (c) and cathodoluminescence (d); Zoned saddle dolomite fringe with thick calcite in the core, in polarized light (e) and cathodoluminescence (f); Dolomite filled vein crosscut by calcite filled vein, indicating the later formation of the calcite filled veins, in polarized light (g) and cathodoluminescence (h) Lim, Limestone; D, Dolomite; Cal, Calcite; SD, Saddle dolomite.

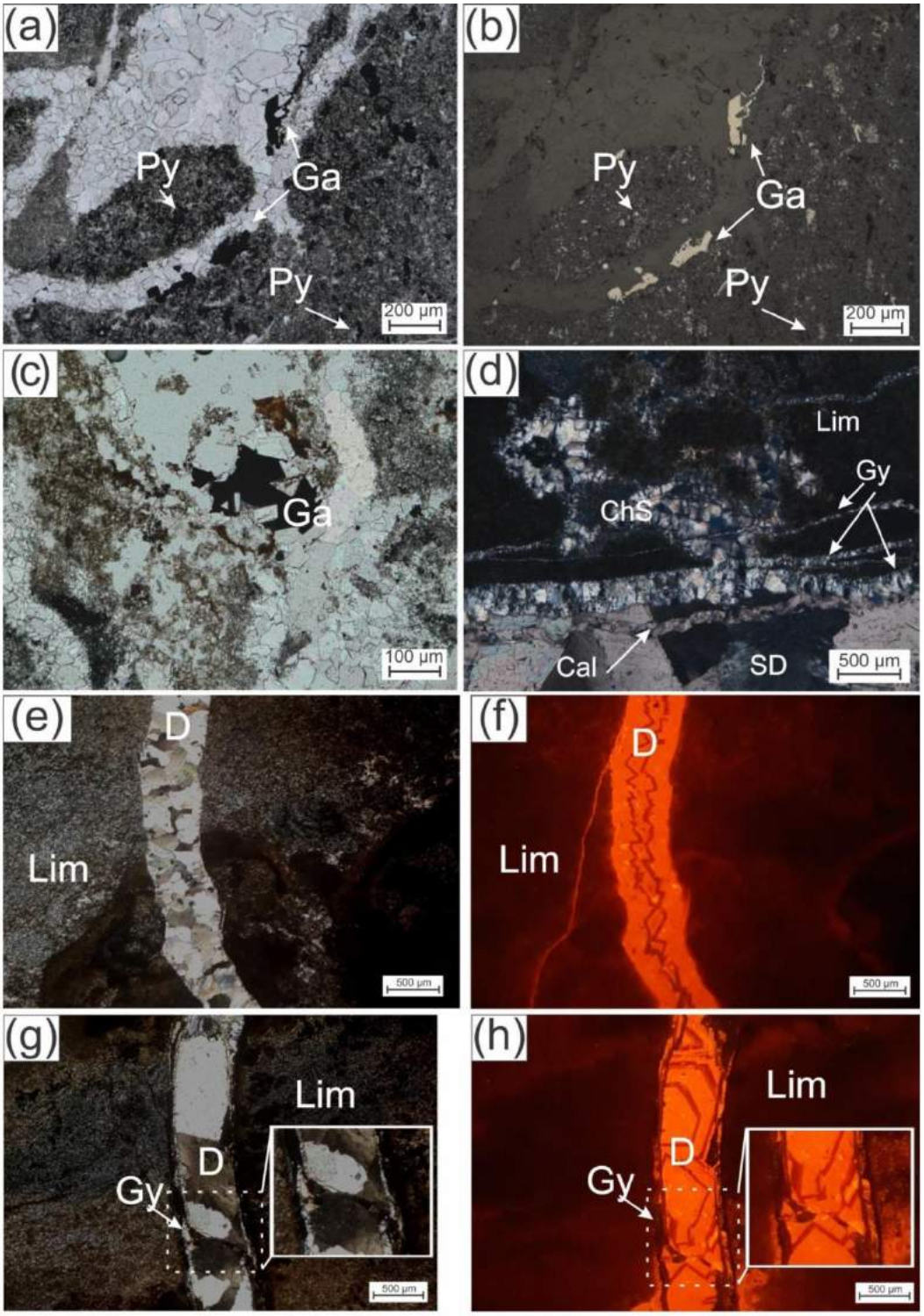

Figure 6. (a) Galena in parallel polarized light under transmitted light, associated with carbonate material, detail for the limestone fragment that occurs with inclusions of pyrite also present in the host rock (b) Galena in parallel polarized light under reflected

light; (c) Galena in parallel polarized light under transmitted light with typical triangle pits included in dolomite that occurs filling voids; (d) Detail of gypsum vein cutting chalcedony and Fe- rich calcite vein cutting dolomite, in polarized light; Another mode of occurrence of veins in carbonate breccia pipes, registering only one filling characterized by zoned dolomite, in polarized light (e) and cathodoluminescence (f); Dolomite vein with gypsum fringe, in polarized light (g) and cathodoluminescence (h). Lim, Limestone; D, Dolomite; Ga, Galena, Gy, Gypsum.

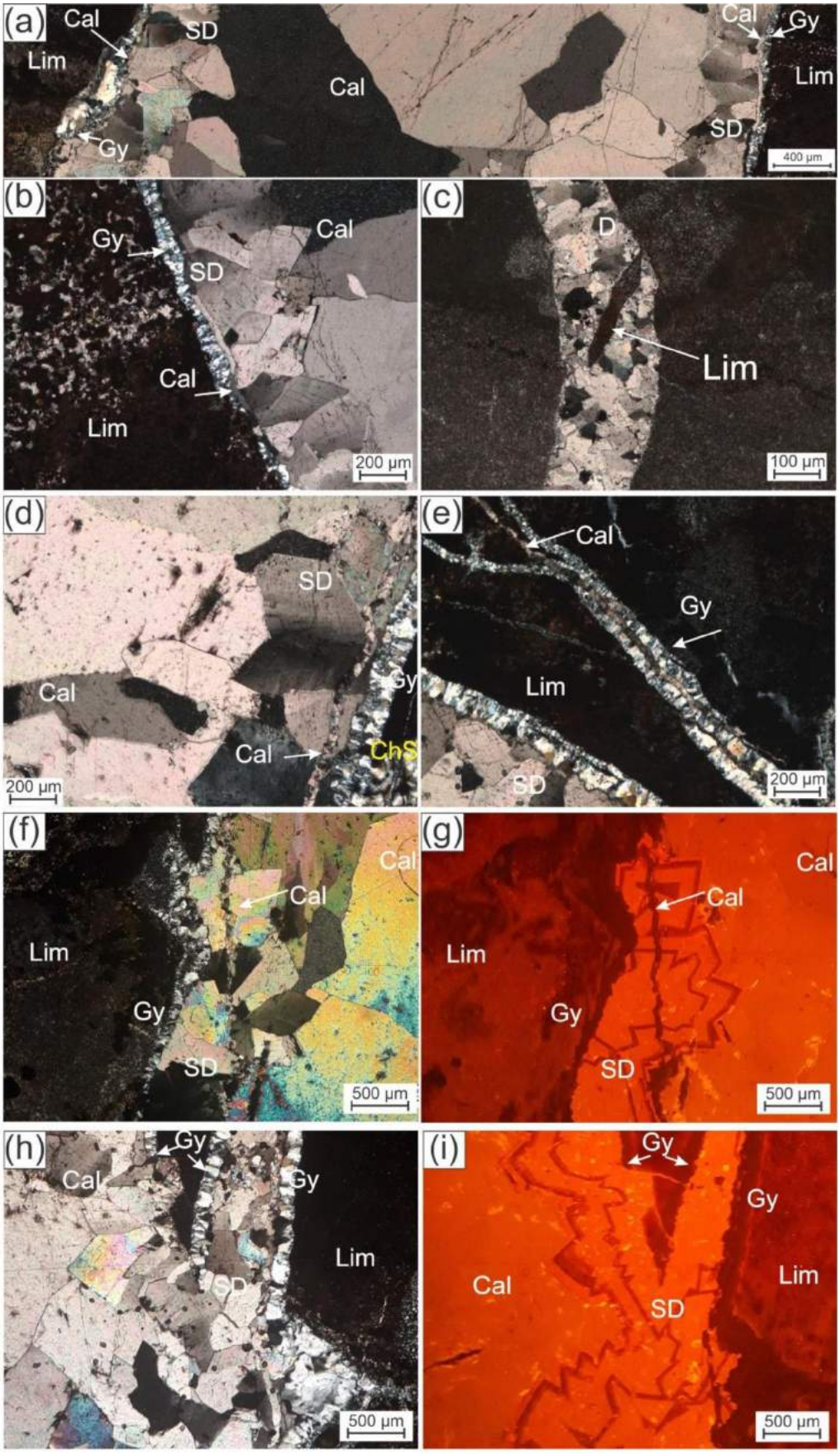
(a)
Cal
SD
Lim
Cal
Gy
Cal
Gy
Lim
SD
400 µm
(b)
Gy
Cal
SD
Cal
Lim
200 µm
(c)
D
Lim
100 µm
(d)
SD
Cal
Gy
Cal
ChS
200 µm
(e)
Cal
Gy
Lim
SD
200 µm
(f)
Cal
Cal
Lim
Gy
SD
500 µm
(g)
Cal
Cal
Lim
Gy
SD
500 µm
(h)
Gy
Cal
Gy
Lim
SD
500 µm
(i)
Gy
Gy
Cal
Lim
SD
500 µm

401

Figure 7. Petrographical observations of the carbonate breccia pipe veins. (a) Mosaic of the veins in carbonate breccia pipes illustrating more than one generation of mineral fill; (b) Detail of the mosaic illustrating the occurrence of saddle dolomite as a fringe on the vein, thick calcite in the center of the vein, and thin veins filled with gypsum and calcite, in polarized light; (c) Vein in the breccia pipes, filled with dolomite, detail for the angular fragment of limestone included; (d) Thin calcite vein cutting through the saddle dolomite indicating that it was formed later, detail for the fine gypsum vein that cuts the chalcedony; (e) Thin calcite vein included within the antitaxial gypsum vein; Calcite-filled vein cutting through the dolomite, in polarized light (f) and in cathodoluminescence (g); Another mode of occurrence of the gypsum-filled vein associated with the dolomite-filled vein, in polarized light (h) and in cathodoluminescence (i). Lim, Limestone; D, Dolomite; Cal, Calcite; SD, Saddle dolomite; Gy, Gypsum; ChS, chalcedony.

4.2.2- EDX

Energy-dispersive X-ray (EDX) maps for Ca and Mg (Fig. 8- a, c) when plotted as part of a composite elemental map (Fig. 9- a) can be used to indicate the distribution of calcite, low Mg-calcite and dolomite, within the matrix material, surrounding breccia clasts as a cement and as veins that fill newly developed fractures. Areas of brecciated clasts within Fig.9- a, that are orange to pale orange in colour represent partially dolomitized material with minor amounts of Fe and sometimes also Mn (Table 1), while pale green areas are similar but with higher concentrations of Mg. Pale blue (teal coloured) areas occur in the spaces around the brecciated material, with the highest recorded values for Mg, and lower Fe (Table 1), which represents the formation of dolomite cement in the voids surrounding brecciated material (dolomite anastomosing

vein network). In addition, two compositionally distinct sets of mineral filled fractures are clearly observed (Fig. 9- a-c). Blue (teal) fractures (Fig. 9), comprise dolomite, with a similar Ca to Mg ratio as recorded from other dolomitic cemented areas (Table 1), and have up to 0.2 atiomc % Fe. These appear to mainly be oriented parallel to the length of the area scanned (see Figure 8- c). In addition, other fracture fills (Red in Figs. 8- a and 9- a) are composed of low Mg-calcite (Table 1), are generally relatively short and have a more varied range of orientations. The occurrence of pyrite is indicated by the Fe and S EDX maps (Fig. 8- b, d), where the two elements occur together. The distribution of pyrite is clearly observed to be patchy (Figure 9- a), lining distinct voids, fracture surfaces and randomly distributed though the matrix. The identification was confirmed by the atomic% ratio of Fe:S (approximately 1:2), although some arears appear depleted in S (approximately 1:1) ratio, which may represent the effect of localized weathering (oxidation) (Fig. 10). The rare occurrence of barite, as infills, is marked where S and Ba occur together (Figs. 8- d, f and 9-a) and is confirmed from the spectrum in Fig. 8-g. Other phases such as gypsum and galena (section 4.2.1) were not observed by SEM-EDX mapping, possibly reflecting the limited area examined, or the resolution used to scan the sample.

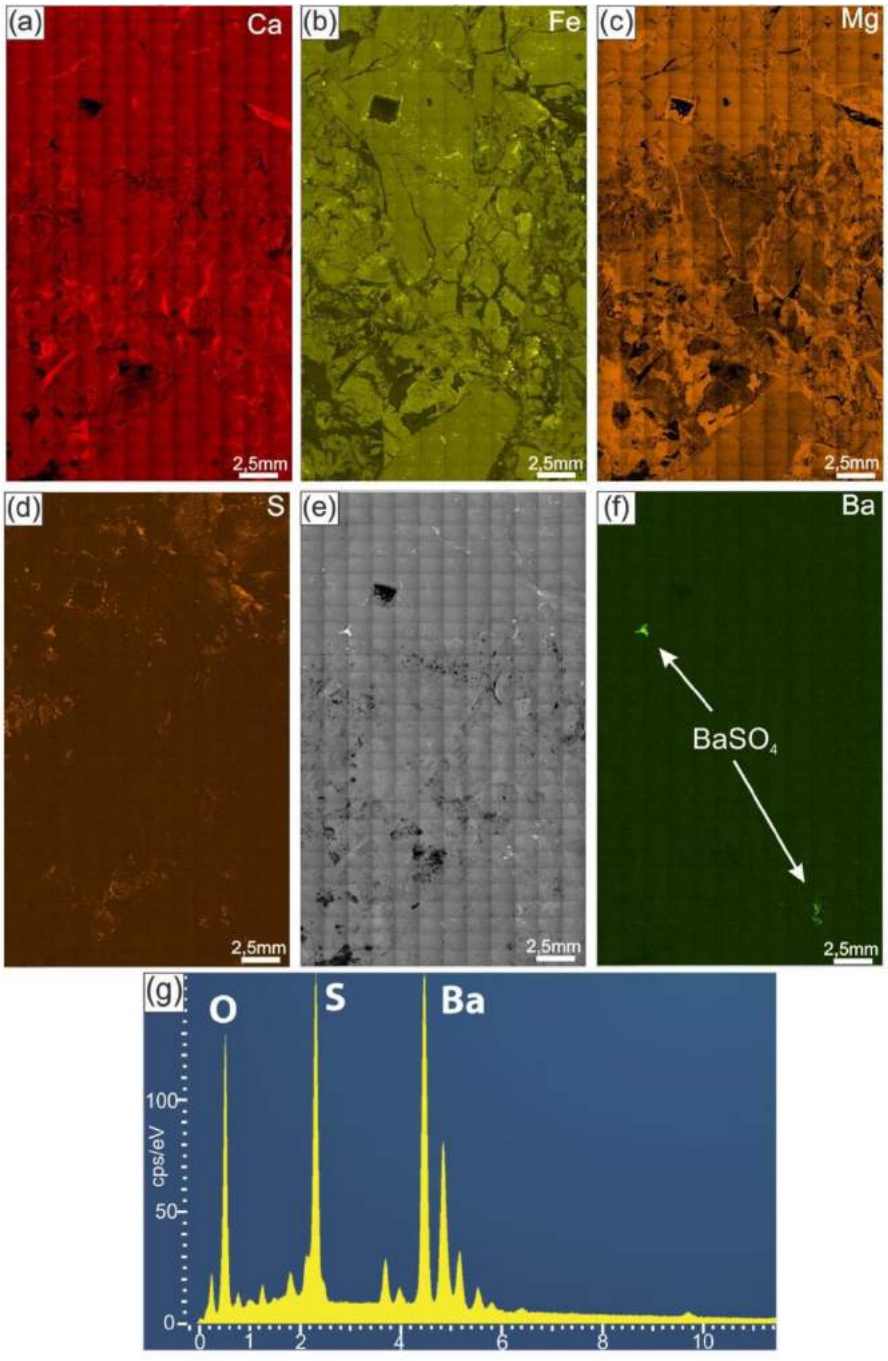

Figure 8. EDX maps of the breccia pipes from the Crato Formation, (a)– (d) and (f) Individual element maps for calcium, iron, magnesium, sulphur and barium (white arrow indicating the places of occurrence of barite), respectively; (e) BSE image of the same area as in (a) – (d) and (f); (g) EDX spectrum of area recording Ba, with the

occurrence of Ba, S and O indicating the formation of barite. Note that in (a) - (e) black areas represent voids.

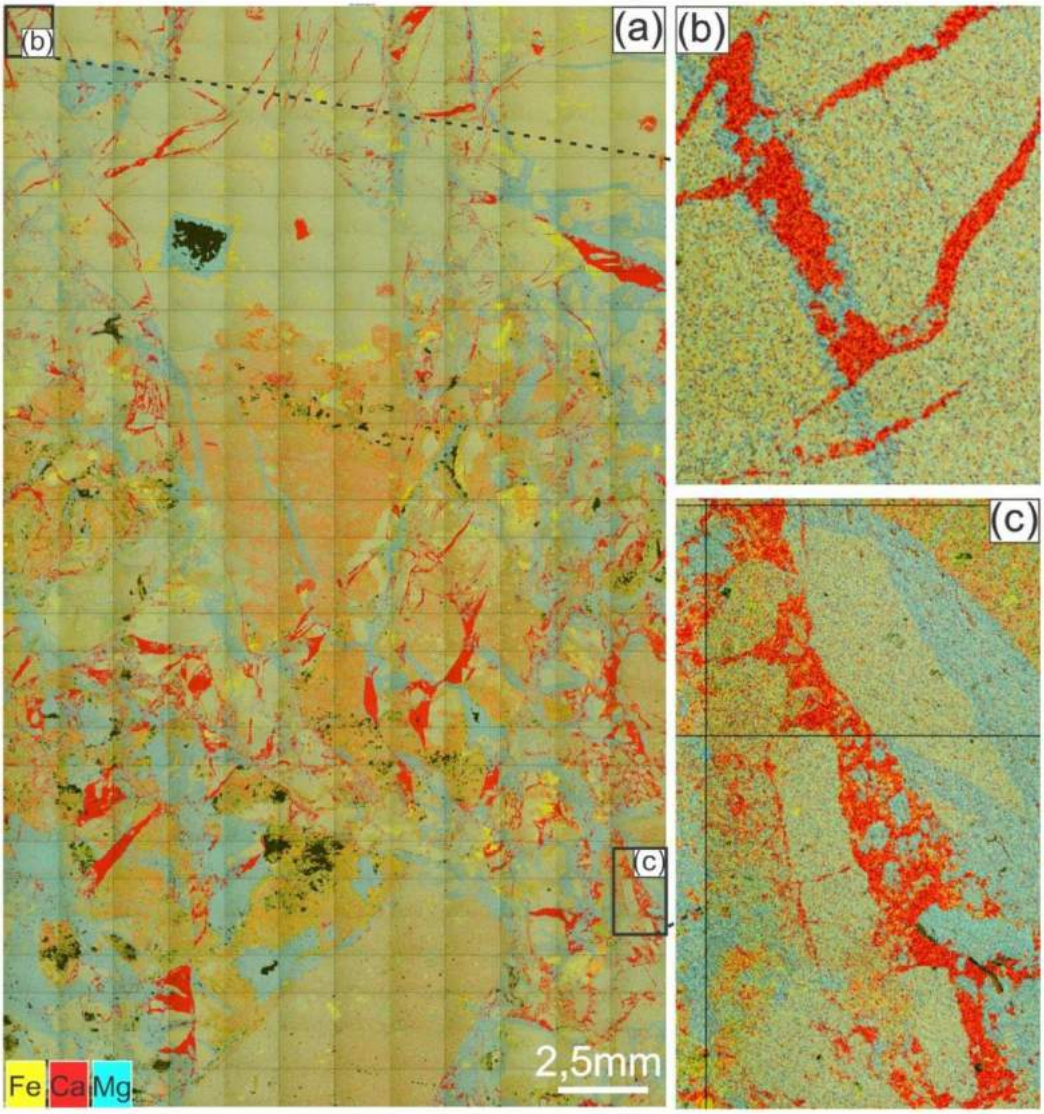

Figure 9. Composite EDX map for the elements in Fig. 8. (a) to (c), illustrating the distribution of dolomite (light blue), calcite (red), iron-rich areas (yellow). Note that the color scheme for Mg in the composite map has been changed from that in (c) to highlight the occurrence of dolomite; (b) Calcite filled veins are observed to crosscut the dolomite filled veins, indicating the later formation of the calcite filled fractures; (c)

Calcite involving angular fragments of dolomite and limestone. Note that black areas represent voids, or areas that do not contain Fe, Ca or Mg.

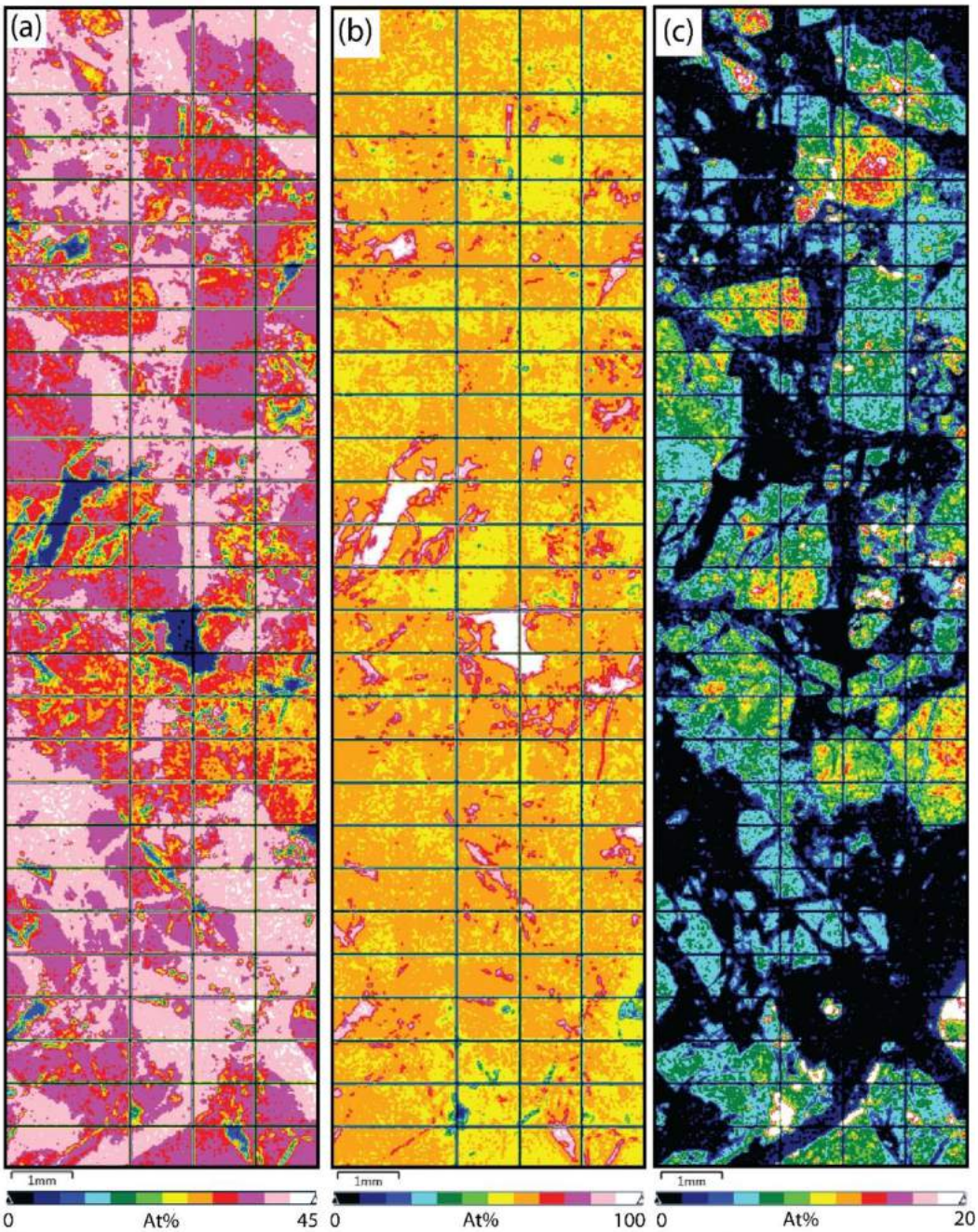

Figure 10. Quantitative energy dispersive X-ray (EDX) atomic % maps for (a) Mg, (b) Ca and (c) Fe, from the same sample and similar area as in figure 9. Note pixels binned by a factor of 16, which has the effect of introducing an artifact suggesting the

occurrence of gradational boundaries. In (a) note that most areas have greater than 20% Mg indicating the occurrence of dolomite, or dolomitized carbonates rather than Mg-calcite (low and high Mg calcite). Also, white and pink areas represent dolomite veins through original brecciated carbonate, or cementing breccia; In (b) white and pink areas represent low Mg calcite veins, which correspond to dark areas (black, dark purple, dark blue) in (a); In (c) dolomite and calcite veins, and dolomite cement are dark (no Fe content), while the brecciated carbonate shows a variable Fe content, although generally less than 10%. Also note that white areas (20% Fe) correspond to areas low in Ca in (b), and likely represent patches of pyrite or Fe-oxide (hydroxide).

	Clasts	Veins	
	Dolomitized limestone	Calcite	Dolomite
Ca	8.9 – 9.7	13.6 – 15.8	9.0 – 9.5
Mg	2.3 – 5.6	0.3 – 1.9	6.9 – 7.1
Fe	0.8 - 1.2		0 - 0,2
Mn	0 - 0.2		

Table 1 – EDX compositional data (atomic%) from selected features of interest. Colors refer to those in the composite EDX map (Figure 9-e); Orange 1 = dark orange, orange 2 = lighter orange.

4.23- U-Pb Geochronology

To put some constraints on the timing of the cement precipitation of the carbonate breccia pipes we dated one example of a carbonate vein using U-Pb geochronology (Fig. 11 and 12). The dated sample (P2B) has two distinct textures visible to at macroscopic scale, represented by a fringe on both internal walls of the vein, and a thick textured core (Fig. 11-c-e). The sample was also analyzed for petrographic analysis (optics and cathodoluminescence) and we observed that the dated fills correspond to dolomite (fringe, red) and calcite (core, blue), (Fig. 7 and 11c-e).

These two regions across the sample were dated, one on the fringe of the vein and one in the central region of the vein. Two ages were obtained 94.9 ± 2.1/3.8 Ma (red) (Cenomanian to Turonian) for fringe of the vein and 80.2 ± 1.4/3.0 Ma (blue) (Campanian) in the central portion of the vein (Fig. 12).

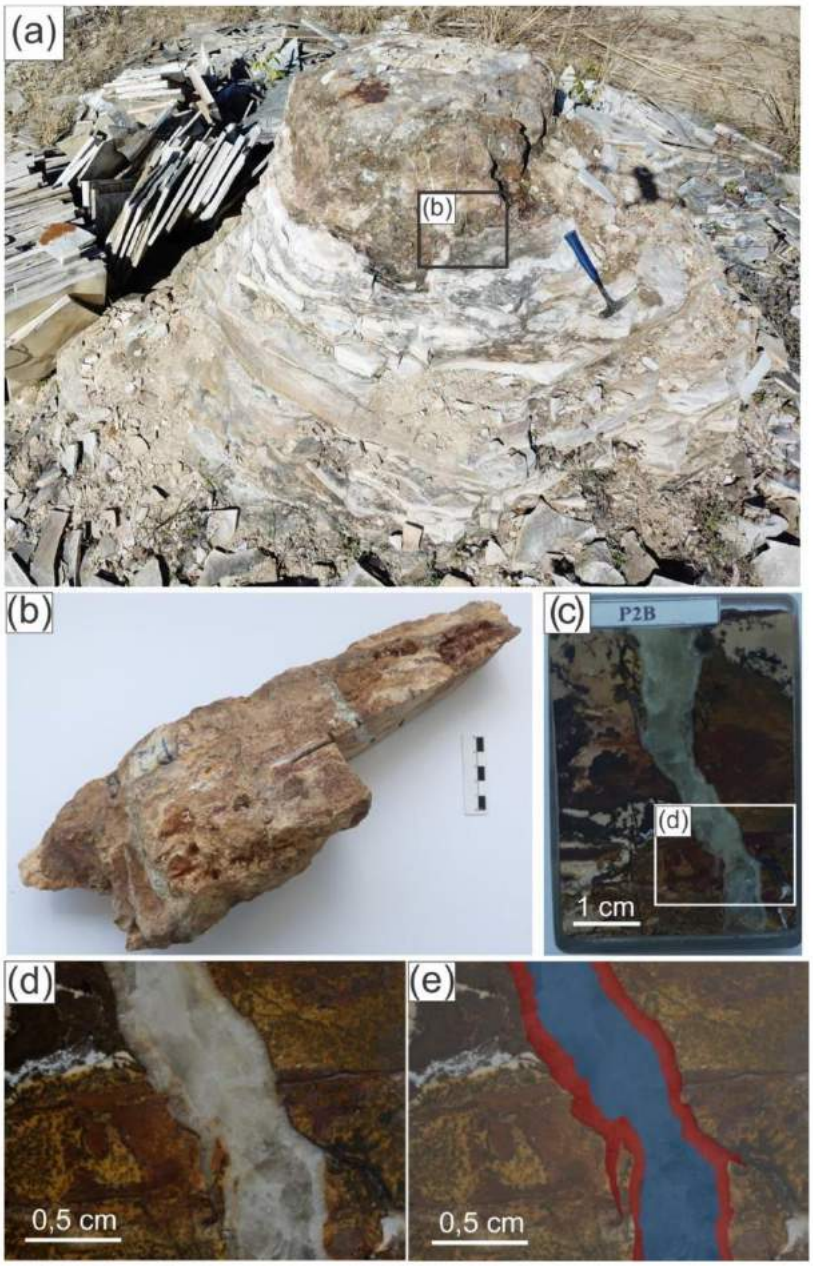

Figure 11. (a) General view of the outcrop of breccia pipes, with details for the place where the dated sample was collected; (b) Sample collected for U-Pb dating (P2B); (c)

Sample block mounted in resin, detail for the vein that was the dating object; (d) Vein with carbonate filling, described in figure 7, it is evident the presence of two distinct mineral stages in this vein, a fringe of dolomitic content (red) and the core filled with calcite (blue), interpretation in (e).

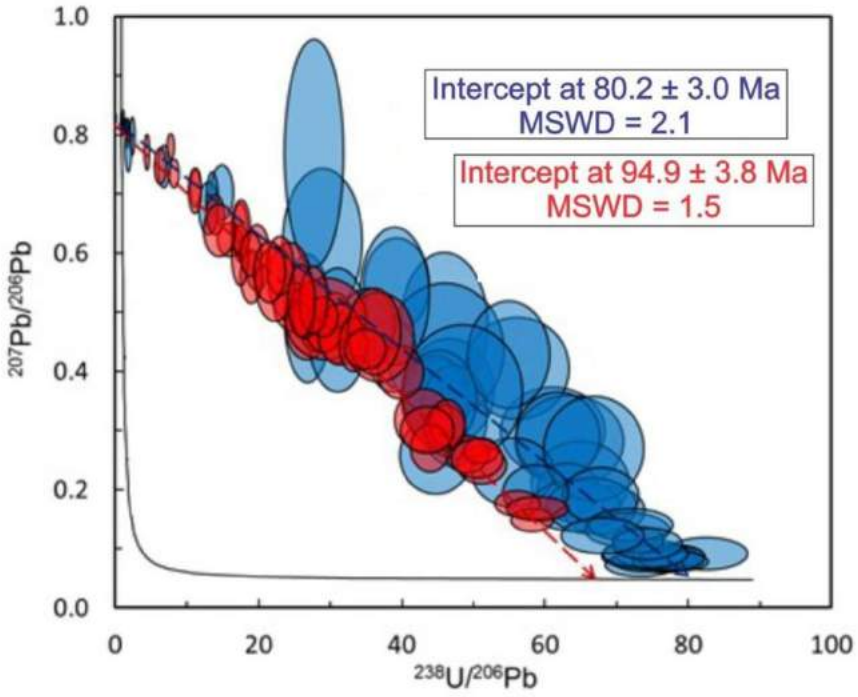

Figure 12. Tera-Wasserburg concordia plot showing U-Pb dates for the vein of the P2B sample from a breccia pipe of the Crato Formation. Two obtained ages: 94.9 ± 2.1/3.8 Ma (red) and 80.2 ± 1.4/3.0 Ma (blue), for dolomite and calcite, respectively, illustrating multiple phases of fluid-flow with different compositions during reactivation of the Triunfo Fault Zone.

5- Discussion

The integration of petrographic data (optical and cathodoluminescence), EDX and U-Pb geochronology allowed us to identify successive deformations in the breccia

pipes that are characterized by mineral paragenesis and fracturing. This is summarized in figure 13 and is discussed in the following sections.

5.1- Paragenetic Sequence

The carbonate breccia pipes of the Crato Formation have a paragenetic sequence composed of: pyrite, chalcedony dolomite + galena, gypsum, saddle dolomite and calcite. In figure 13, the diagenetic processes and deformational events that occurred in the studied area are summarized.

We observe that the limestone angular fragments of the breccia pipes are dolomitized and/or partially dolomitized (Figs. 5 and 9). This dolomitization can be associated with the initial processes of the pipe formation, which occurred during the Early Albian, post-rift phase of the Araripe Basin (e.g., Alencar et al., 2020). Additionally, these fragments commonly have pyrite and chalcedony, which are commonly observed in the host rock (Fig. 6-a,b,d) (e.g., Cabral et al., 2019; Catto et al., 2016). Particularly, pyrite occurs included in the limestone fragments that were encompassed by the dolomitic cement of the rock. Nevertheless, pyrite crystals associated with dolomite were not observed in this work. In addition, chalcedony occurs by filling pores in the rock and is usually cut by carbonate veins (Fig. 7-d). Thus, these observations indicate that the pyrite and chalcedony are possibly related to the deposition of the laminite limestone, prior to the brecciation event.

The cementation of breccia pipes is essentially composed of dolomite, thought is also possible to observe calcite occurring locally as cement (Fig. 5-a-d). Dolomitic cement occurs associated with some subhedral galena crystals, which are not observed included in the limestone fragments (Fig. 6-a-c). This fact suggests that the brecciation process is connected to the entry of a dolomitic fluid accompanied by Pb. We observed

that the dolomites of the idiotopic-S, and idiotopic-C types (e.g., Gregg & Sibley, 1984) occur mainly by filling the spaces between the limestone angular fragments. They have four zonations that could be differentiated in the cathodoluminescence (red and brown luminescence) (Fig. 5). The saddle dolomite (xenotopic-C) occurs mainly cementing the fractures, with four zonations (red and brown luminescence) (Fig. 7). Thus, these dolomite zonations can be associated with multiple growth phases and the entry of fluids with different compositions (e.g., Lukoczki et al., 2018).

The breccia pipes are crosscut by a system of veins with single or multiple mineral fills (Fig. 7), that would be associated with the stages of deformation of the breccia pipes. Using cathodoluminescence we observed two periods of carbonate cement formation which are, associated with the development of fractures; a) dolomite and b) low Mg-calcite. The calcite filled veins are occasionally observed to crosscut the dolomite filled veins, indicating the later formation of the calcite filled fractures (Fig. 5-g, h and Fig. 9- b, c). Therefore, a clear change in fluid chemistry is indicated: Mg-rich with minor Fe within newly formed fracture systems, and finally, low Mg-calcite (no Fe) associated with a later stage of more randomly oriented fractures.

In summary, the results indicate that this vein system records recurrent fracture episodes, probably due to reactivations of the Triunfo fault zone, accompanied by fluid migrations (e.g., Menezes et al., 2019). In Figure 7, we observed multiple veins fills that record the entry of fluids of different chemical composition during distinct fault reactivation episodes. The general schematic model of vein filling (Fig. 14- c) illustrates an initial fracturing phase that led to the formation of antitaxial gypsum veins (e.g., McKinnon, 2017). The second phase of deformation is represented by new fluid percolation in the system that trigged the formation of a new vein composed of saddle dolomite rim (fringes) (Figs. 14-d and 7). A fluid rich in calcium carbonate and low in

Mg would enter the system and fill the remaining pores of the vein. The last recorded phase consists of the formation of fine Fe-rich calcite veins that take advantage of the weakness planes of the antitaxial veins of the gypsum and commonly crosscut the saddle dolomite rim (Fig.14).

These multiple filling veins of varying compositions reflect the fracturing episodes with the entry of different fluids in the breccia pipes. The two ages obtained from the U-Pb dating of the came from breccia pipes, reflect different episodes of deformation. The age of 94.9 ± 2.1 / 3.8 Ma (Cenomanian to Turonian) was obtained on the vein with saddle dolomite (Fig.7 and 12), which is associated with the dolomitic cementation of the breccia pipes during its initial stages of formation. The second age obtained from 80.2 ± 1.4 / 3.0 Ma (Campanian) was measured in the central portion of the vein that is filled by calcite. This deformation phase reflects the fracturing process after the formation of the breccia pipes (Fig.13).

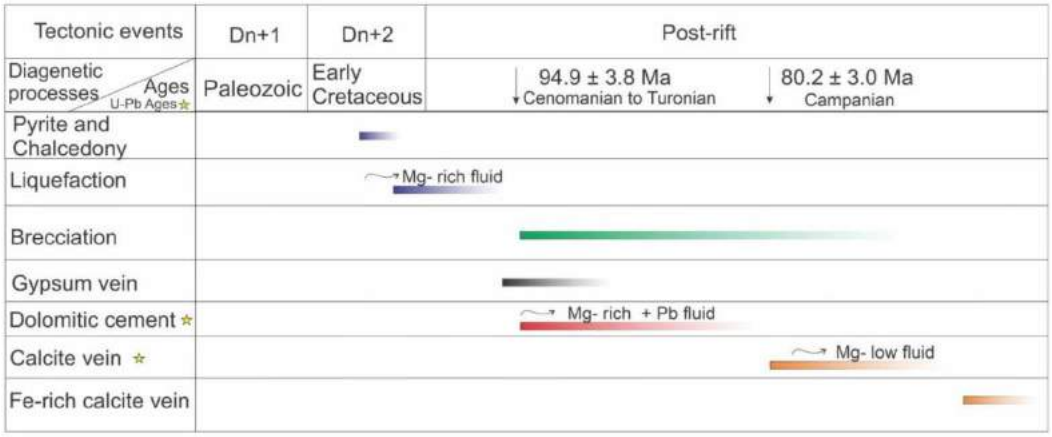

Figure 13. Diagenetic processes evolution of the breccia pipes, including U-Pb ages of the polyphasic deformations that the breccia pipes were subjected. The events Dn+1 and Dn + 2 refer to the deformational events in the Araripe Basin proposed by Celestino et al., 2020.

5.2- Pipe Formation

The formation of the carbonate pipe of the Crato Formation was discussed initially by Martill et al., (2008) who observed the occurrence of pipe-like structures with a high concentration of dolomite, calcite, and goethite. These structures were classified by Martill et al., (2008) as dolomite pipes. These authors suggested that the formation of the pipes was due to the rise of fluids through the laminated limestones, destroying the original framework of the rock. The fluid would have come from paleo-aquifers possibly belonging to the sandstones of the Cariri Formation, underlying the Crato Formation, during the initial stages of limestone compaction.

According to Shukla and Sharma (2018), breccia pipes can originate through hydrofracturing of partially consolidated layer from the entrance of high-pressure hydrothermal fluids or liquefaction processes due earthquake. Alencar et al., (2020) classified the pipes of the Crato Formation as seismic breccia pipes, formed by hydrofracturing processes from paleoseismic activity. According to them, the entry of fluids during seismic events would have caused liquefaction and brecciation of limestone not yet consolidated. The ages obtained in our work reinforce this idea proposed by Alencar et al., (2020). The pipe's brecciation and cementation events occurred at ca. 95 Ma (Cenomanian to Turonian), about 30 to 40 Ma after the deposition of the Crato Formation.

Here, we demonstrated that the formation of the carbonate breccia pipes occurred in more than one deformational phase (polyphase deformation), similar to that discussed by Alencar et al., (2020). Initially, the formation of pipes would have occurred through liquefaction processes with the entry of dolomitic fluid from seismic events at the Early Albian (e.g. Alencar et al., 2020) (Figs. 13 and 14-a). The subsequent phases occurred while the limestone was already consolidated during the

Turonian – Campanian according to ours U-Pb ages. The fault reactivation would lead to the brecciation of the pipe with the entry of new fluids and precipitation of dolomitic cement between the limestone fragments and cementing fractures during the Cenomanian to the Turonian (94.9 ± 3.8 Ma) (Figs. 13 and 14-b). The activation of the faults occurred recurrently, new fracturing episodes that are overprinted as veins filled with calcite and dolomite, which indicate more than one carbonate filling pulse on the same vein during the Campanian (80.2 ± 3.0 Ma) (Figs. 7, 9, 11, 14-c).

The occurrence of dolomite and dolomitized limestone as micrometric fragments with calcite between the fragments reinforces the idea that more than one episode of brecciation and mineralization has occurred during the Campanian (Figs. 5-c,d and 9-c), in addition to the occurrence of gypsum veins. The dolomitization of the breccia pipes could have occurred due to these continuous entries of fluids, possibly before the brecciation of the pipes (Figs. 9 and 13).

In summary, we propose that breccia pipes had their initial stage of formation through the liquefaction processes as discussed by Alencar et al., (2020). Then, the laminated limestone was dolomitized and / or partially dolomitized due to the entry of dolomitic fluids. Subsequently there was the brecciation of the rock and cementation by dolomite associated with galena during the Cenomanian - Turonian. Fractures occurred recurrently due to fault reactivations which led to the formation of new fractures and the entry of new carbonate fluids during the Campanian. This process of forming the breccia pipes of the Crato Formation is similar to the hydrofracturing and brecciation model proposed by Phillips (1972). According to Phillips (1972), initial dolomitization of the rock is followed by brecciation and cementation by dolomite saddle, and episodes of reactivation of faults occur recurrently after the formation of the breccia.

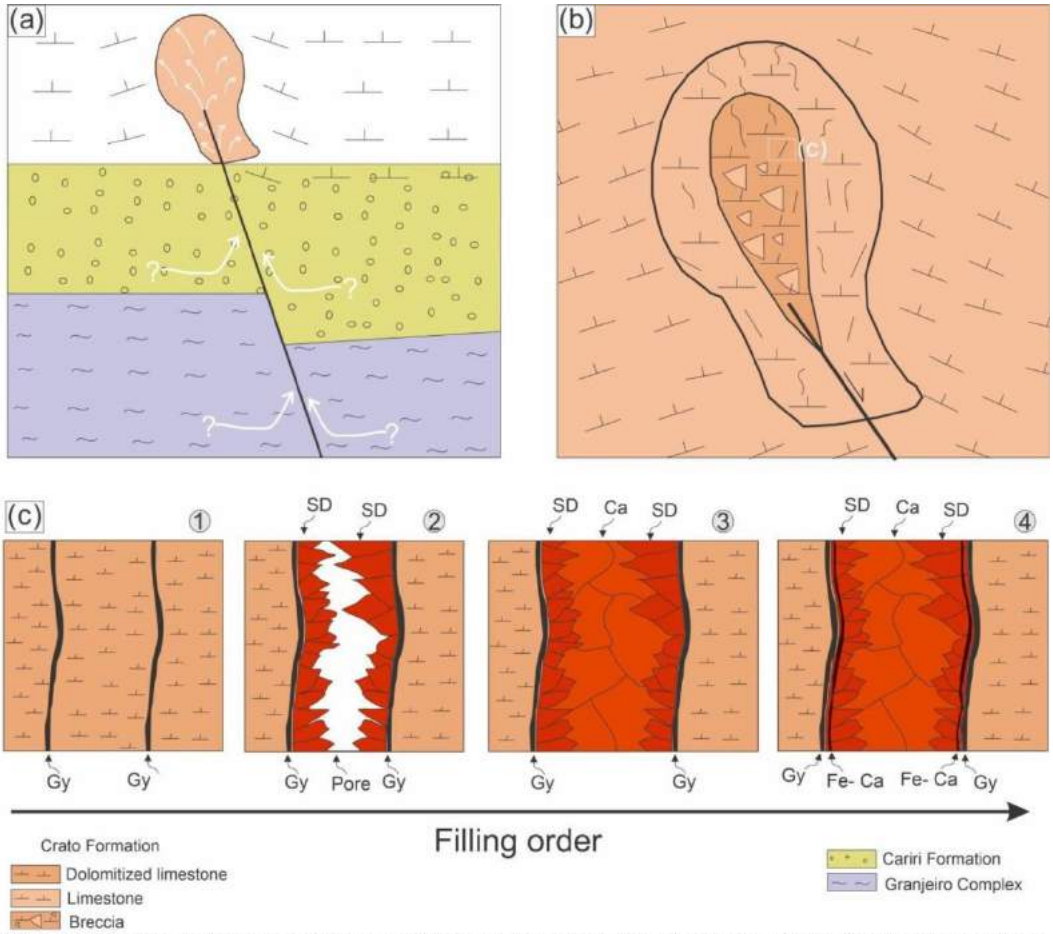

627 Figure 14. Evolutionary process of the carbonate pipes breccia of the Crato Formation.
628 (a) Liquefaction process with Mg-rich dolomite fluids; (b) brecciation of the pipes with
629 dolomitic cimentation; (c) Order of filling the veins observed in breccia pipes, detailed
630 in figure a, and Figures 7, 11. Numbers 1, 2, 3, 4, represent the sequential filling stages,
631 and vein colors correspond to the colors seen in the cathodoluminescence. SD, Saddle
632 dolomite; Gy, gypsum; Ca, calcite.
633
634

635 **5.3- Structural Control and Geodynamic Evolution**

636 During the opening of the South Atlantic Ocean, in the Cretaceous, the
637 continental-scale shear zone systems of the Central Domain of the Borborema Province,
638 were reactivated as brittle fault zones (Miranda et al., 2020; Matos et al., 2021). These
639 shear zone systems control the structural evolution of the intraplate basins of NE Brazil

(e.g., Araripe, Rio do Peixe, Jatobá basins) (Françolin et al., 1996; Araujo et al., 2018; Cabral et al., 2019; Celestino et al., 2020; Alencar et al., 2020; Miranda et al., 2020; Matos et al., 2021). In a recent contribution, Matos et al. (2021) showed that the Pre-Cambrian fabric of the Borborema and Benin-Nigeria Provinces played an important role in the tectonic evolution of the South Atlantic Cretaceous Rift system (SACRS). These authors recognized five chronological rift stages from the Late Jurassic/Early Cretaceous (Tithonian-Berriasian) to Early Cretaceous (Albian).

According to Celestino et al. (2020) the tectonic evolution of the northern border of the Araripe Basin is controlled by the Triunfo fault zone which represents the brittle deformation of a segment of the Patos shear zone. In this study we observed the occurrence of carbonate breccia pipes in the Crato Formation in the vicinity of this fault zone (Figs. 2). Thus, we infer that the Triunfo fault zone faults play an important role in the control of deformation in the laminated limestones of the Crato Formation and the sandstones of the Cariri Formation, which are more deformed in these regions. Additionally, Alencar et al. (2020) described soft sediment deformation structures (e.g., syn-sedimentary shear fractures, microslumps, including breccia pipes) that are related to a process of liquefaction associated with the paleo-earthquakes. This fact also corroborates with the idea that this region was tectonically active during the Aptian even during a post rift tectono-sequence.

Two U-Pb ages were obtained in this contribution (94.9 ± 3.8 Ma (Cenomanian) Ma and 80.2 ± 3.0 Ma (Campanian)), reflecting the entry of two pulses of fluids during reactivations in the Triunfo fault zone, and fluids of different chemical compositions, during the post-rift phase in the Araripe Basin.

According to Matos et al. (2021) at the end of Albian/early Cenomanian, South America was completely separated from its conjugate margin in Africa. Although, plate

dynamics and crustal adjustments remain in the Borborema Province during the Early Cretaceous and Cenozoic. Therefore, Late Cretaceous and Cenozoic magmatic events in the Borborema Province reflect mantle thermal anomalies yet associated with the SACRS (Souza et al., 2003; Matos et al., 2021).

For instance, during the Cenomanian to Campanian the Cuó basaltic flows took place in the Borborema Province (Sial et al., 1981; Araújo et al., 2001; Mizusaki et al., 2002). This magmatic event yields K-Ar ages between 99 and 80 Ma (Mizusaki et al., 2002) placing this magmatism temporally very close to the fluid circulation found in the breccia pipes of the Crato Formation.

5.4- Fluid Circulation

The dolomitic cement that occurs between the fragments of laminated limestone and filling fractures, in addition to the calcite veins developed during the reactivation episodes of the Triunfo Fault zone register as fluid circulation system during the post-rift phase of the Araripe Basin (Fig. 14). During an interval of about 14Ma (Cenomanian - Campanian) the chemical composition of this carbonate fluid varied, becoming poorer in Mg. However, the origin of the fluid that involved the formation of breccia pipes is still a source for much discussion (Fig. 14-a). These fluids could have come from paleo-aquifers possibly belonging to the sandstones of the Cariri Formation, underlying the Crato Formation, through fault systems, as initially proposed by Martill et al., (2008). However, another possible source for these fluids is the crystalline basement, underlying the Cariri Formation, which flowed upwards through faults causing the hydrofracturing of the rocks. These regions would function as reservoirs of fluids and supply the faults that act as conduits for fluids (Sibson, 1990; Lavoie and Chi, 2001; Packard et al., 2001; Al-Aasm et al., 2002; Davies and Smith, 2006; Hollis et al.,

2017; Grare et al., 2018; Koeshidayatullah et al., 2020). Within the study area in the region of the crystalline basement, tectonic breccias with calcite cement and calcite-filled veins are found (Celestino et al., 2020). This suggests the basement has the potential to supply the overlying fault systems during episodes of fault reactivation; however, in the portion of the studied area we cannot rule out a contribution from the paleo-aquifer Cariri Formation. A geochemical study is necessary to confirm the origin of these fluids. In addition, to the pre-existing faults and fractures that possibly served as conduits for the fluids, it is important to take into account that before the breccia formed, the pipes had already been formed, as previously discussed, and this region may have functioned as a preferred channel for transporting new fluids. The proximity of the breccia pipes to faults is an important factor for the circulation of these fluids (Fig. 2).

According to Davies and Smith, (2006), argillites and evaporitic rocks act as seals for underlying rocks and contribute to the location of dolomitization. The Crato Formation presents levels with layers of argillites and shales, and overlying this formation there are evaporites from the Ipubi Formation. The salt of the Ipubi Formation could act as barriers for the percolation of fluids in the overlying layers. These fluids that may have been channeled through pipes and blocked by the evaporative layers. This would have caused the concentration of fluids only in the Crato Formation and, concentrating the formation of breccias pipes in places where the absence of these lithologies occurred.

The dolomitic fluids accompanied by Pb during the Cenomanian to the Turonian ascended along the faults and / or by means of the pipes that already existed. After later fault reactivations in the Campanian the carbonate fluid poor in Mg migrated along the available structural conduits, causing new brecciation in the breccia pipes (Figs. 13 and

14), widening of pre-existing fractures and cementation within them (Figs.7 and 14). The hydrothermal origin for theses fluids that acted on the laminated limestones is still unclear, but some characteristics point to this possible hydrothermal source for the formation and the brecciation of the breccia pipes. The observed mineral association of saddle dolomite, dolomite, calcite, galena, pyrite and barite (Figs. 5- 7), is commonly found in hydrothermal environments (e.g., Davies and Smith, 2006; Lima and De Ros, 2019; Lima et al., 2019). However, the occurrence of barite was observed in the contact between the Crato and Ipubi formations by Cabral et al., (2019). These authors associated this occurrence with a sulfation process in the laminated limestone. On the other hand, barite can also be precipitated in environments with hydrothermal fluids (Griffith and Paytan, 2012; Okubo et al., 2020). For a fluid to be considered hydrothermal it must have a higher temperature in relation to the embedding rock (Davies and Smith, 2006). But in all cases, an isotopic and geochemical study is necessary to define whether the mineral phases found are hydrothermal.

5.5- Impact on Reservoir Properties

In fault zone regions, the permeability of rocks can be increased due to the greater density of fracturing (Blundell et al., 2003; Kolb et al., 2004) and/or decreased later due to the filling of the fractures. Brecciated intervals (fault core) and permeable facies of the rock can also be factors that contribute to the fluid flow or act as a hydraulic barrier (Phillips, 1972; Sibson, 1987; Sibson, 1990; Knipe, 1993; Knipe et al., 1998; Billi et al., 2003; Fossen et al., 2005; Tarasewicz et al., 2005; Davies and Smith, 2006; Grare et al., 2018). In this study we investigated the role of the crystalline basement structures (Triunfo fault zone) on the formation and evolution of breccia pipes in a carbonate reservoir analogue (Crato Formation). Our results indicate that the

breccia pipe's formation is directly associated with the circulation of fluids along fault planes. Nevertheless, these heterogeneities show complex structural diagenesis, which may represent significant variations in the reservoir quality (porosity and permeability distribution) (e.g., Laubach et al., 2010; Lima et al., 2020). For example, Lima et al. (2020) show clear evidence of diagenesis that is related to an intense hydrothermal alteration in the Pre-Salt reservoirs from the Campos Basin, SE Brazil. These authors suggested that the hydrothermal fluid circulations along fault planes have a strong impact on the perm-porosity distribution of the Pre-Salt reservoirs. This study shows that the investigation of rock faults (e.g., breccia) together with the associated fracturing in analogue reservoirs still has huge importance in delivering insights on the structural diagenesis of real carbonate reservoirs.

6- Conclusions

Based on our study of the laminated limestones of the Crato Formation, we suggest the following conclusions:

(1) During the post-rift phase of the Araripe Basin, even after the opening of the South Atlantic, tectonic reactivations continued to occur. The proximity of the carbonate breccia pipes to the Triunfo Fault zone show a clear structural control associated with the development of the breccia pipes. These structures acted as conduits for the carbonate fluids, as well as the pipes themselves.

(2) The analysis of data obtained from the analysis of EDX, optical microscopy and cathodoluminescence made it possible to identify two generations of fluid entering the system, recorded as dolomite cement between fragments of limestone and in fractures, in addition to the calcite that occurs essentially filling veins. Other vein fillings were identified as gypsum and calcite rich in Fe.

(3) Two U-Pb ages of carbonate-vein mineralization, Late Cretaceous of 94.9 ± 3.8 Ma (Cenomanian to Turonian) and 80.2 ± 3.0 Ma (Campanian), provide constraints on two brittle reactivation episodes of the Triunfo Fault Zone, and the entry of fluids from different compositions during post- rift deformation of the Araripe Basin.

(4) The circulation of fluids along the pre-existing faults and pipes were responsible for the polyphase deformation in the breccia pipes that occurred between the Cenomanian to Campanian.

Acknowledgment

We thank the Editor Nicolas E. Beaudoin, the reviewer Geoffrey Motte and the three anonymous reviewers for their suggestions, which improved the early version of this manuscript. We thank Petrobras, the National Petroleum Agency, Natural Gas and Biofuels of Brazil (ANP), which financed the Pseudopoços Project - Petrobras/Federal University of Pernambuco (UFPE). We are grateful to the Department of Geology UFPE and Geolab who prepared all the samples that served as the basis for this research. We thank the Institute for GeoEnergy Engineering, Heriot-Watt University and the Geochronology and Tracers Facility, British Geological Survey for their assistance in the analyzes carried out. We thank Casa da Pedra – UFRJ, located in Satana do Cariri, CE, which provided crucial logistic support to fieldwork. This work is part of a MSc of Maria Alcione under the postgraduate program in Geosciences of the Federal University of Pernambuco (PPGEOC- UFPE) and represents the contribution N. 03 of the Laboratório de Modelagem de Bacias (ModLad-UFPE).

References

Alencar, M.L., Correia Filho, O.J., Miranda, T.S., Barbosa J.A., Celestino, M.A.L, Ramos, G.M.S, Araújo, A.F.L, Neumann, V.L., Topan, J.G.O. 2020. Soft-Sediment Deformation Structures In Aptian Lacustrine Laminites: Evidence Of Post-Rift Paleoseismicity In The Araripe Basin, Ne Brazil. Journal of South American Earth Sciences. doi: 10.1016/j.jsames.2020.102955.

Al-Aasm, I.S., Lonnee, J. and Clarke, J. (2002) Multiple fluid flow events and the formation of saddle dolomite: case studies from the Middle Devonian of the Western Canada Sedimentary Basin. Mar. Pet. Geol., 19, 209–217.

Araújo, M.G.S.; Brito Neves, B.B.; Archanjo, C.J., 2001. Idades 40Ar/39Ar do magmatismo básico Meso-Cenozóico da Província Borborema Oriental, nordeste do Brasil. Simp. Geol. do NE, 19, Natal, Resumos, p. 260-261.

Araujo, R.E.B., Bezerra, F.H.R., Nogueira, F.C.C., Balsamo, F., Carvalho, B.R.B.M., Souza, J.A.B., Sanglard, J.C.D., de Castro, D.L., Melo, A.C.C., 2018. Basement control on fault formation and deformation band damage zone evolution in the Rio do Peixe Basin, Brazil. Tectonophysics 745, 117–131. https://doi.org/10.1016/j.tecto.2018.08.011.

Assine, M.L., 2007. Bacia do Araripe. Bol. de Geociencias da Petrobras 15, 371-389.

Assine, M.L., Perinotto, J. A. J., Custódio, M. A., Neumann, V. H., Varejão, F. G., Mescolotti, P. C., 2014. Sequências Deposicionais do Andar Alagoas da Bacia do Araripe, Nordeste do Brasil. Bol. de Geociências da Petrobras, Rio de Janeiro, 22:3-28.

Billi, A.F., Solvini, F., Storti, F., 2003. The damage zone-fault core transition in carbonate rocks: Implication for fault growth, structure and permeability. Journal of Structural Geology, v. 25, p. 1779– 1794.

Blundell, D.J.; Karnkowski, P.H.; Alderton, D.H.M.; Oszczepalski, S.; Kucha, H., 2003. Copper mineralization of the polish Kupferschierfer: A proposed basement fault-fracture system of fluid flow. Econ. Geol., 98, 1487–1495.

Cabral, F.A.D.A., Silveira, A.C.D., Ramos, G.M.S., Miranda, T.S.D., Barbosa, J.A., Neumann, V.H.D.M.L., 2019. Microfacies and diagenetic evolution of the limestones of the upper part of the Crato Formation, Araripe Basin, northeastern Brazil. Brazilian Journal of Geology,49(1).

Catto, B., Jahnert, R.J., Warren, L.V., Varejao, F.G. and Assine, M.L., 2016. The microbial nature of laminated limestones: lessons from the Upper Aptian, Araripe Basin, Brazil. Sedimentary geology, 341, pp.304-315.

Celestino, M., Miranda, T., Correia Filho, O., Barbosa, J., 2018. Aspectos Tectônicos Da Borda Ne Da Bacia De Fátima, Província Borborema- Ne Do Brasil. Estudos Geológicos 27, 3– 19. https://doi.org/10.18190/1980-8208/estudosgeologicos.v27n2p3-19.

Celestino, M.A.L., Miranda, T.S., Mariano, G., Alencar, M.L., Carvalho, B.R.B.M., Falcão, T.C., Topan, J.G., Barbosa, J.A., Gomes, I.F., 2020. Fault damage zones width: implications for the tectonic evolution of the Araripe Basin, Brazil. Journal of Structural Geology. 138, 104–116. https://doi.org/10.1016/j.jsg.2020.104116.

Davies, G.R., 2004. Hydrothermal (thermobaric) dolomitization: rock fabrics and organic petrology. In: McAuley, R. (Ed.), Dolomites - The Spectrum: Mechanisms, Models, Reservoir Development. Canadian Society of Petroleum Geologists, Seminar and ore Conference. Calgary, Alberta, Canada, p. 17.

Davies, G. R., Smith Jr, L. B., 2006. Structurally controlled hydrothermal dolomite reservoir facies: An overview. AAPG bulletin, 90(11), 1641-1690.

De Lima, F.G.F., De Sá, E.F.J., 2017. Controle estrutural da borda sudeste da Bacia do Parnaíba, Nordeste do Brasil: relação com eventos geodinâmicos no Gondwana. Geologia USP - Serie Cientifica 17, 3–21. https://doi.org/10.11606/issn.2316-9095.v17-125909.

Dimmen, V., Rotevatn, A., Peacock, D.C.P., Nixon, C.W., Nærland, K., 2017. Quantifying structural controls on fluid flow: Insights from carbonate-hosted fault damage zones on the Maltese Islands. Journal of Structural Geology 101, 43–57. https://doi.org/10.1016/j.jsg.2017.05.012.

Fossen, H., T. Erland, T.E.S. Johansen, J., Hesthammer, Rotevatn, A., 2005. Fault interaction in porous sandstone and implications for reservoir management, examples from southern Utah. AAPG Bulletin, v. 89, no. 12, p. 1593 – 1606.

Françolin, J.B.L.; Cobbold, P.R.; Szatmari, P., 1994. Faulting in the early Cretaceous Rio do Peixe basin (NE Brazil) and its significance for the opening of the Atlantic. J. Struct. Geol., 16, 647–661.

Garcia, X., Julià, J., Nemocón, A.M., Neukirch, M., 2019. Lithospheric thinning under the Araripe Basin (NE Brazil) from a long-period magnetotelluric survey: constraints for tectonic inversion. Gondwana Res. 68, 174–184. https://doi.org/10.1016/j.gr.2018.11.013.

Grare, A., Lacombe, O., Mercadier, J., Benedicto, A., Guilcher, M., Trave, A., Ledru, P., Robbins, J., 2018. Fault zone evolution and development of a structural and hydrological barrier: The quartz breccia in the kiggavik area (nunavut, Canada) and its control on uranium mineralization. Minerals, 8, 1–28.

Gregg, J. M., and Sibley, D. F., 1984, Epigenetic dolomitization and the origin of xenotopic dolomite texture: Jour. Sed. Petrology, v. 5, p. 908-93 I.

Griffith, E.M., Paytan, A., 2012. Barite in the ocean — occurrence, geochemistry and palaeoceanographic applications. Sedimentology 59, 1817–1835.

Hansman, R.J., Albert, R., Gerdes A., Ring U., 2018. Absolute ages of multiple generations of brittle structures by U-Pb dating of calcite. Geology 46(3):207–210

Hollis, C., Bastesen, E., Boyce, A., Corlett, H., Gawthorpe, R., Hirani, J., Rotevatn, A. and Whitaker, F., 2017. Faultcontrolled dolomitization in a rift basin. Geology, 45, 219–222.

Horstwood, M.S.A., Košler, J., Gehrels, G., Jackson, S.E., McLean, N.M., Paton, C., Pearson, N.J., Sircombe, K., Sylvester, P., Vermeesch, P., Bowring, J.F. 2016. Communityderived standards for LA-ICP-MS U-(Th-) Pb geochronology–Uncertainty propagation, age interpretation and data reporting, Geostand. Geoanal. Res., 40, 311–332.

Jébrak, M., 1997. Hydrothermal breccias in vein-type ore deposits: A review of mechanisms, morphology and size distribution. Ore Geology Reviews, 12, 111-134.

Koeshidayatullah, A., Corlett, H., Stacey, J., Swart, P.K., Boyce, A., Robertson, H., Whitaker, F., Hollis, C., 2020. Evaluating new fault- controlled hydrothermal dolomitisation models: Insights from the Cambrian Dolomite, Western Canadian Sedimentary Basin. Sedimentology.doi:10.1111/sed.12729.

Kolb, J.; Rogers, A.; Meyer, F.M.; Vennemann, T.W., 2004. Development of fluid conduits in the auriferous shear zones of the Hutti Gold Mine, India: Evidence for spatially and temporally heterogeneous fluid flow. Tectonophysics, 378, 65 –84.

Knipe, R.J., 1993. The influence of fault zone processes and diagenesis on fluid flow, in Horbury, A. D. and Robinson, A. G., eds., Diagenesis and basin development. AAPG Studies in Geology 36, chapter 10, p. 135– 151.

Knipe, R.J., Jones, G., Fisher, Q.J., 1998. Faulting, fault sealing and fluid flow in hydrocarbon reservoirs: An introduction, in G. Jones, Q. J. Fisher, and R. J. Knipe, eds., Faulting, fault sealing and fluid flow in hydrocarbon reservoirs: Geological Society (London) Special Publication 147, p. vii– xxi.

Laubach, S. E., Eichhubl, P., Hilgers, C., Lander, R. H., 2010. Structural diagenesis. Journal of Structural Geology, 32(12), 1866-1872.

Lavoie, D., and Chi, G., 2001. The Lower Silurian Sayabec Formation in northern Gaspé: Carbonate diagenesis and reservoir potential. Bulletin of Canadian Petroleum Geology, v. 49, p. 282– 298.

Lima, B. E. M., and Ros., 2019. Deposition, diagenetic and hydrothermal processes in the Aptian Pre-Salt lacustrine carbonate reservoirs of the northern Campos Basin, offshore Brazil. Sedimentary Geology. doi:10.1016/j.sedgeo.2019.01.006.

Lima, B.E.M., Tedeschi, L.R., Pestilho, A.L.S., Santos, R.V., Vazquez, J.C., Guzzo, J.V.P., De Ros, L. F., 2019. Deep -burial hydrothermal alteration of the Pre-Salt carbonate reservoirs from northern Campos Basin, offshore Brazil: Evidence from petrography, fluid inclusions, Sr, C and O isotopes. Marine and Petroleum Geology, 104143. doi:10.1016/j.marpetgeo.2019.104143.

Lúcio, T., Neto, J.A.S., Selby, D. 2020. Late Barremian/Early Aptian Re–Os age of the Ipubi Formation black shales: Stratigraphic and paleoenvironmental implications for Araripe Basin, northeastern Brazil. Journal of South American Earth Sciences, 102, 102699.

Lukoczki, G., Haas, J., Gregg, J.M., Machel, H.G., Kele, S., John, C.M., 2018. Multi-phase dolomitization and recrystallization of Middle Triassic shallow marine–peritidal carbonates from the Mecsek Mts. (SW Hungary), as inferred from

petrography, carbon, oxygen, strontium and clumped isotope data. Mar. Pet. Geol. https://doi.org/10.1016/j.marpetgeo.2018.12.004

MacDonald, J., Faithfull, J.W., Roberts, N., Davies, A., Holdsworth, C., Newton, M., Williamson, S., Boyce, A., John, C. M., 2019. Clumped-isotope palaeothermometry and LA-ICP-MS U–Pb dating of lava-pile hydrothermal calcite veins, 174, 63.

Marques, F.O., Nogueira, F.C.C., Bezerra, F.H.R., Castro, D.L. 2014. The Araripe Basin in NE Brazil: an intracontinental graben inverted to a high-standing horst. Tectonophysics, 630, 251-264.

Martill, D.M., Bechly, G. and Loveridge, R.F., 2007. The Crato fossil beds of Brazil: window into an ancient world. Cambridge University Press.

Martill, D.M., Loveridge, R.F., Heimhofer, U., 2008. Dolomite pipes in the Crato Formation fossil lagerstätte (Lower Cretaceous, Aptian), of northeastern Brazil. Cretaceous Research, 29(1), 78-86.

Matos, R.M.D., Norton, I., Casey, K., Krueger, A., 2021. The fundamental role of the Borborema and Benin–Nigeria provinces of NE Brazil and NW Africa during the development of the south atlantic Cretaceous rift system. https://doi.org/10.1016/j. marpetgeo.2020.104872.

McKinnon, E., 2017. Structural diagenesis of bed-parallel and bed-normal fractures, Cretaceous Crato Formation carbonate rocks, NE Brazil. The Thesis Committee for Elizabeth McKinnon

Medeiros, V.C., Jardim de Sa, E.F., 2009. O Grupo Cachoeirinha (Zona Transversal, NE do Brasil) redefinição e proposta de formalização. Revista de Geologia, Universidade Federal do Ceará 22 (2), 124-136.

Menezes, C.P., Bezerra, F.H.R., Balsamo, F., Mozafari, M., Vieira, M.M., Srivastava, N. K., de Castro, D. L., 2019. Hydrothermal silicification along faults affecting

carbonate-sandstone units and its impact on reservoir quality, Potiguar Basin, Brazil. Marine and Petroleum Geology, 110, 198-217.

Miranda, T.S. De, Magalhães, J.R.G., Barbosa, J.A., Correia Filho, O., Alencar, M.L.,2014. Araripe Basin, NE Brazil: a rift basin implanted over a previous pull-apart system? In: 4th Atlantic Conjugate Margins Conference, vol. 3.

Miranda, T.S., Santos, R.F., Barbosa, J.A., Gomes, I.F., Alencar, M.L., Correia, O.J., Falcão, T.C., Gale, J.F.W. and Neumann, V.H., 2018. Quantifying aperture, spacing and fracture intensity in a carbonate reservoir analogue: Crato Formation, NE Brazil. Marine and Petroleum Geology, 97, pp.556-567.

Miranda, T.S., Neve, S.P., Celestino, M.A.L., Roberts, N. 2020. Structural evolution of the Cruzeiro do Nordeste shear zone: Brasiliano-Pan-African- ductile-to-brittle transition and Cretaceous brittle reactivation. J. Struct. Geol. 141, https://doi.org/10.1016/j.jsg.2020.104203

Mizusaki, A.M.P.; Thomaz-Filho, A.; Milani, E.J.; Césero, P., 2002. Mesozoic and Cenozoic igneous activity and its tectonic control in northeastern Brazil. J. South Amer. Earth Sci., 15: 183-198.

Neumann, V.H., Borrego, A.G., Cabrera, L. and Dino, R., 2003. Organic matter composition and distribution through the Aptian–Albian lacustrine sequences of the Araripe Basin, northeastern Brazil. International Journal of Coal Geology, 54(1-2), pp.21-40.

Neumann, V.H. and Assine, M.L. 2015. Stratigraphic proposal to the post-rift I tectonic-sedimentary sequence of Araripe Basin, Northeastern Brazil. In: 2nd International Congress on Stratigraphy, Graz, Austria.

Nuriel, P., Weinberger, R., Kylander-Clark, A.R.C., Hacker, B.R., Craddock, J.P., 2017. The onset of the Dead Sea transform based on calcite age-strain analyses, Geology, 45, 587-590, 10.1130/g38903.1.

Nuriel, P., Craddock, J., Kylander-Clark, A. R., Uysal, I. T., Karabacak, V., Dirik, R. K., Hacker, B. R., Weinberger, R. J. G., 2019. Reactivation history of the North Anatolian fault zone based on calcite age-strain analyses, 47, 465-469.

Nuriel, P., Wotzlaw, J.-F., Ovtcharova, M., Vaks, A., Stremtan, C., Šala, M., Roberts, N. M. W., and Kylander-Clark, A. R. C., 2020. The use of ASH-15 flowstone as a matrix-matched reference material for laser-ablation U-Pb geochronology of calcite, Geochronology Discuss., https://doi.org/10.5194/gchron-2020-22.

Okubo, J., Klyukin, Y.I., Warren, L.V., Sublett Jr, D.M., Bodnar, R.J., Gill, B.C., Xiao, S., 2020. Hydrothermal influence on barite precipitates in the basal Ediacaran Sete Lagoas cap dolostone, São Francisco Craton, central Brazil. Precambrian Research,340, 105628.

Onorati, G., Pascolieri M., Ventura R., Chiarini V., Crucillà U., 1992. The digital elevation model of Italy for geomorphology and structural geology Catena, 147-178

Pagel, M., Bonifacie, M., Schneider, D. A., Gautheron, C., Brigaud, B., Calmels, D., Cros, A., Saint-Bezar, B., Landrein, P., Sutcliffe, C., Davis, D. and Chaduteau, C. 2018. Improving paleohydrological and diagenetic reconstructions in calcite veins and breccia of a sedimentary basin by combining Δ47 temperature, δ18Owater and U-Pb age, Chemical Geology, 481, 1–17, 750 doi:10.1016/j.chemgeo.2017.12.026

Parrish, R. R., Parrish, C. M., Lasalle, S., 2018.Vein calcite dating reveals Pyrenean orogen as cause of Paleogene deformation in southern England, Journal of the Geological Society, 10.1144/jgs2017-107, 469.

Packard, J.J., Al-Aasm, I., Samson, I., Berger, Z. and Davies, J., 2001. A Devonian hydrothermal chert reservoir: the 225 bcf Parkland field, British Columbia, Canada. Am. Asso. Petrol. Geol. Bull., 85, 51–84.

Peacock, D.C.P., Dimmen, V., Rotevatn, A., Sanderson, D.J., 2017. A broader classification of damage zones. Journal of Structural Geology 102, 179–192. https://doi.org/10.1016/j.jsg.2017.08.004.

Peulvast, J.P., Bétard, F., 2015. A history of basin inversion, scarp retreat and shallow denudation: the Araripe basin as a keystone for understanding long-term landscape evolution in NE Brazil. Geomorphology 233, 20–40. https://doi.org/10.1016/j.geomorph.2014.10.009.

Phillips, W.J., 1972. Hydraulic fracturing and mineralization. Journal of the Geological Society (London), v. 128, p. 337–359.

Ponte F.C. and Ponte Filho F.C. 1996. Estrutura geológica e evolução tectônica da Bacia do Araripe. Recife, DNPM, 68 p.

Poros, Z., Jagniecki, E., Luczaj, J., Kenter, J., Gal, B., Correa, T.S., Ferreira, E., McFadden, K.A., Elifritz, A., Heumann, M., Johnston, M., Matt, V., 2017. Origin of silica in Pre-Salt carbonates, Kwanza Basin, Angola. American Association of Petroleum Geologists Annual Convention and Exhibition. Houston, Texas, USA.

Rand, H.M., 1983. Levantamento gravimetrico e magnetometrico da Bacia Araripe.Relatório interno da PETROBRAS, p. 11 (caderno de dados e mapas).

Rand, H.M. and Manso, V.A.V., 1984. Levantamento gravimétrico e magnetométrico da Bacia do Araripe. In: SBG, Congresso Brasileiro de Geologia, 4, Anais, pp. 2011–2016.

Ridley, J.R. and Diamond, L., 2000. Fluid chemistry of orogenic lode gold deposits and implications for genetic models. Rev. Econ. Geol., 13, 141–162.

Roberts, N.M. and Walker, R. J., 2016. U-Pb geochronology of calcite-mineralized faults: Absolute timing of rift-related fault events on the northeast Atlantic margin, Geology, 44, 531-534.

Roberts, N.M., Rasbury, E.T., Parrish, R.R., Smith, C.J., Horstwood, M.S., and Condon, D. J., 2017. A calcite reference material for LA-ICP-MS U-Pb geochronology, Geochemistry, Geophysics, 480 Geosystems.

Roberts, N.M., Drost, K., Horstwood, M.S., Condon, D.J., Chew, D., Drake, Milodowsk, A.E., McLean , N.M., Smye, A.J., Walker, R.J., Haslam, R., Hodson, K., Imber, J., Beaudoin, N., Lee, J.K., 2020. Laser ablation inductively coupled plasma mass spectrometry (LA-ICP-MS) U-Pb carbonate geochronology: strategies, progress, and limitations. Geochronology, 2(1), 33-61.

Rochelle-Bates, N., Roberts, N.M.W., Sharp, I., Freitag, U., Verwer, K., Halton, A., Fiordalisi, E., van Dongen, B.E., Swart, R., Ferreira, C.H. and Dixon, R., 2020. Geochronology of volcanically associated hydrocarbon charge in the pre-salt carbonates of the Namibe Basin, Angola. Geology. DOI:10.1130/G48019.1

Rohmer, J., Nguyen, K., Torabi, A., 2015. Off-fault shear failure potential enhanced by high stiff/low permeable damage zone during fluid injection in porous reservoirs. Geophys. J. Int. 202, 1566–1580.

Salamuni, E., Ebert, H.D., Hasui, Y., 2004. Morfotectônica Da Bacia Sedimentar De Curitiba. Revista Brasileira de Geociências 34, 469–478. https://doi.org/10.25249/0375-7536.2004344469478.

Salomon, E., Rotevatn, A., Kristensen, T. B., Grundvåg, S. A., Henstra, G. A., Meckler, A. N., Gerdes, A, Albert, R., 2020. Fault-controlled fluid circulation and diagenesis along basin-bounding fault systems in rifts–insights from the East Greenland rift system. Solid Earth, 11(6), 1987-2013.

Schueller, S., Braathen, A., Fossen, H., Tveranger, J., 2013. Spatial distribution of deformation bands in damage zones of extensional faults in porous sandstones: Statistical analysis of field data. Journal of Structural Geology 52, 148–162. https://doi.org/10.1016/j.jsg.2013.03.013.

Shukla, M.K. and Sharma, A., 2018. A brief review on breccia: it's contrasting origin and diagnostic signatures. Solid Earth Sci. 3, 50–59. https://doi.org/10.1016/j.sesci.2018.03.001.

Sial, A.N.; Long, L.E.; Pessoa, D.A.R.; Kawashita, K., 1981. Potassium-argon ages and strontium isotope geochemistry of Mesozoic and Tertiary basaltic rocks, Northeastern Brazil. An. Acad. Bras. Ciênc, 53: 115 -122.

Sibson, R., 1987. Earthquake rupturing as a mineralizing agent in hydrothermal systems. Geology, 15, 701–704.

Sibson, R.H., 1990. Faulting and fluid flow, in B. E. Nesbitt, ed., Fluids in tectonically active regimes of the continental crust. Mineralogical Association of Canada Short Course Handbook, v. 18, chapter 4, p. 93–132.

Silva, da L.C., Armstrong, R., Noce, C.M., Carneiro, M.A., Pimentel, M., Soares, A.C.P., Leite, C.A., Vieira, V.S., Silva, M.A., Paes, V.J .C., Filha, J.M.C., 2002. Reavaliação da evolução geológica em terrenos pré-cambrianos brasileiros com base em novos dados U–Pb SHRIMP, Parte III: províncias Borborema, Mantiqueira Meridional e Rio Negro-Juruena. Revista Brasileira de Geociências, 32, 529–544.

Tarasewicz, J.P.T., Woodcock, H.H., Dickson, J.A.D., 2005. Carbonate dilation breccias: Examples from the damage zone of the Dent fault, northwest England. Geological Society of America Bulletin, v. 117, no. 5 –6, p. 736– 745.

Turner, J.P., Green, P.F., Holford, S.P., Lawrence, S.R., 2008. Thermal history of the Rio Muni (West Africa)-NE Brazil margins during continental breakup. Earth Planet. Sci. Lett. 270, 354–367. https://doi.org/10.1016/j.epsl.2008.04.002.

Viegas, L.G.F., Archanjo, C.J., Hollanda, M.H.B.M., Vauchez, A., 2014. Microfabrics and zircon U-Pb (SHRIMP) chronology of mylonites from the Patos shear zone (Borborema Province, NE Brazil). Precambrian Res. 243, 1–17. https://doi.org/10.1016/j.precamres.2013.12.020.

Wibberley, C.A.J., and Shipton, Z. K., 2010. Fault zones: A complex issue. Journal of Structural Geology, 32(11), 1554–1556. doi:10.1016/j.jsg.2010.10.006.

Wu, G., Gao, L., Zhang, Y., Ning, C., Xie, E., 2019. Fracture attributes in reservoir-scale carbonate fault damage zones and implications for damage zone width and growth in the deep subsurface. Journal of Structural Geology 118, 181–193. https://doi.org/10.1016/j.jsg.2018.10.008.

3.3 CLASSIFICAÇÃO DAS ROCHAS DE FALHA DA FALHA TRIUNFO

Zonas de falhas são compostas por três elementos arquiteturais: a) zona de dano, b) núcleo e c) protólito (CAINE *et al*., 1996; LIN & YAMASHITA, 2013; CHOI *et al*., 2016; LIAO *et al*., 2019). A zona de dano ocorre em ambos os lados da falha e é dominada por uma maior frequência de estruturas rúpteis. O núcleo de falha é caracterizado pela presença de rochas de falhas, como cataclasistos, brechas e gouges, e por superfícies de deslizamento. Nesta região as texturas originais da rocha não são preservadas. O protólito representa a rocha não deformada ou pouco deformada.

3.3.1 Núcleo da Falha Triunfo

O núcleo da Falha Triunfo é caracterizado pela ocorrência de rochas de falha, como cataclasitos e brechas tectônicas, com protólito metamórfico (ortognaisses do Complexo Granjeiro) e sedimentar (arenitos da Formação Cariri) (Fig. 7). O núcleo da Falha Triunfo apresenta localmente espessura de cerca de 30 m, e é composto essencialmente por brecha de falha.

A brecha de falha de composição ortognaíssica, que está associada ao núcleo da Falha Triunfo, apresenta fragmentos angulosos com tamanhos que variam de centímetros a milímetros (Fig. 7- A). Esta rocha de falha também pode ocorrer localmente foliada. A textura milonítica, dos ortognaisses do embasamento cristalino, pode ser utilizada como guia na observação da rotação dos fragmentos das brechas de falha. Esta observação é mais evidente com a utilização da catodolunescência (Fig. 8- A). A matriz das brechas de falha é composta por fragmentos inequigranulares dispostos de forma difusa, sem a possibilidade de rearranjo. O cimento das brechas é marcado pela a ocorrência de argilominerais e de óxidos de ferro. As brechas da Falha Triunfo também apresentam uma forte cimentação por calcita ao longo de toda rocha ocupando os espaços vazios (Fig. 8- B). A calcita também ocorre como veios cortando a matriz e os fragmentos, indicando que possivelmente corresponda a uma segunda fase de entrada de fluido carbonático associado às brechas da Falha Triunfo (Fig. 8- C e D).

Figura 7- A) Brecha tectônica do embasamento cristalino, ortognaisse milonítico; B) Brecha tectônica da Formação Cariri composta por inúmeras bandas de deformação marcando o núcleo da Falha Triunfo. C) Cataclasito bastante fraturado e D) Detalhe do cataclasito ilustrando a ocorrência de veios de calcita.

Fonte: Autor (2020).

Figura 8- Fotomicrografia da brecha tectônica do embasamento cristalino. A) Fragmentos do ortognaisse milonítico imersos no cimento de calcita. Na porção central é possível observar que os clastos apresentam deslocamentos indicativos de esforço transtensional, setas em branco. Esses clastos apresentam uma foliação milonítica que ocorre de forma contínua mesmo após o faturamento da rocha indicando que não ocorreu rotação significativa entre os clastos; B) Fragmentos angulosos de quartzo e feldspato, cortados por veios de calcita e imersos em cimento calcítico, que preenche toda a rocha; C) Fragmento milonitizado da brecha tectônica, cortado por veio de calcita. Observe que este veio corta o clasto e o cimento (calcita), indicando duas gerações de calcita; D) Veio de calcita, seta azul, ocorre deslocando o cimento de calcita com sentido de movimento sinistral. Nicóis cruzados. Objetiva 5x. Frg- fragmento; Ca- calcita.

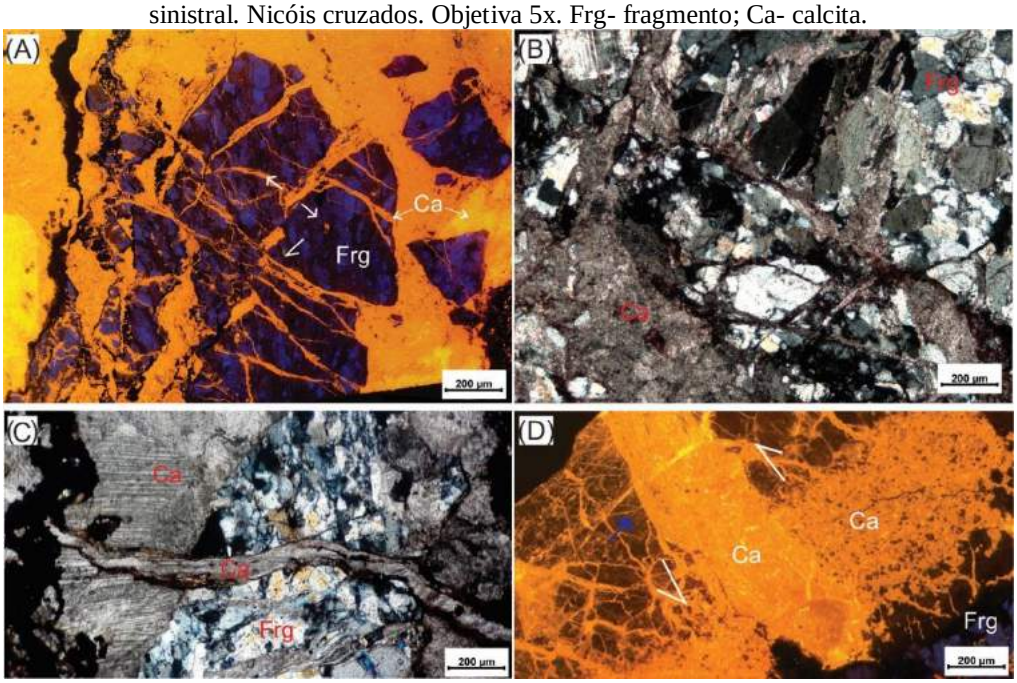

Fonte: Autor (2020).

A partir da análise de catodoluminescência foi possível observar de forma mais clara a ocorrência da calcita em duas fases distintas: a) veios; e b) cimento. A catodomuminescência contribuiu para observação do padrão de fraturamento e arranjo dos clastos nas rochas de falha. Na Figura 9-A, é possível observar uma série de falhas de cinemáticas distintas (sinistrais e dextrais), que é comum em rochas intensamente fraturadas. Estes falhamentos tendem a ocorrer com e sem envolvimento de calcita.

O cataclasito observado na área de estudo, possivelmente está associado às falhas de idade Paleozoica de direção N-S (Fig. 7-C,D). Esta rocha apresenta fragmentos angulosos, granulação mais fina e são compostos por ortognaisses. As ocorrências de calcita nessas rochas ocorrem principalmente como veios, diferente das brechas tectônicas associadas à Falha Triunfo (Fig. 7-D e 9- B-D). Sua matriz apresenta uma granulação muito fina com alguns fragmentos de quartzo e feldspatos se destacando.

Figura 9- A) Fotomicrografia ilustrando cimento de calcita na porção esquerda da imagem e de veios de calcita dispersos. Setas rosas indicam a ocorrência de fraturamento da rocha com e sem interação com calcita. Nesta rocha os clastos ocorrem deslocados, com sentido de movimento sinistral e destral. Na porção direita da imagem há a ocorrência de falhas em dominó com cinemática destral. As linhas brancas correspondem aos planos de microfalhas; B) Fotomicrografia do cataclasito. Fragmento do ortognaisse e uma matriz de granulação fina inequigranular com veio de calcita no centro. C) e D) Fotomicrografia do cataclasito ilustrando a ocorrência de veio preenchido por calcita com algumas inclusões de quartzo e feldspato. Nicóis cruzados. Objetiva 5x. Frg- fragmento; Ca- calcita.

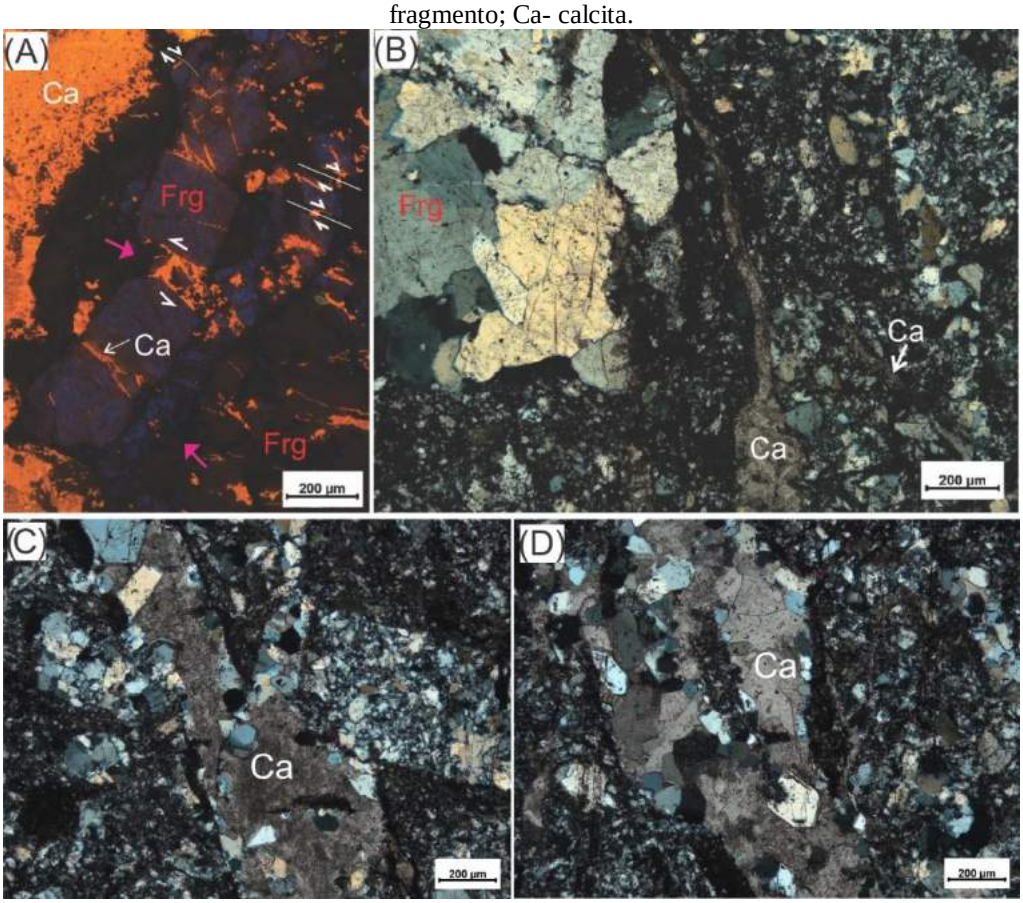

Fonte: Autor (2020).

3.3.2 Análise de DRX

A análise de DRX foi realizada com intuito de mapear as diferentes composições do material que preenche os planos de falha (gouge) da zona de dano da Falha Triunfo. A partir dessa análise observou-se que os difratogramas de DRX obtidos para as 20 amostras coletadas de planos de falhas e fraturas no embasamento cristalino, Complexo Granjeiro, apresentam semelhança significativa nas posições dos picos e intensidades, que são refletidas na composição mineralógica semelhante (Fig. 10). Quatro difratogramas foram escolhidos como mais representativos dentre os 20 difratogramas analisados (Fig.11).

O afloramento analisado apresenta duas fácies: máfica, classificada como anfibolito, e uma félsica, classificada como um ortognaisse. A diferença composicional da rocha é reflita no material que preenche os planos de falhas e também no desenvolvimento de estruturas. Foram definidos três domínios composicionais que ocorrem preenchendo os planos de falha. O domínio 1 é marcado por fraturas preenchidas por calcita com ou sem presença de argilominerais do tipo 2:1, e ocorre na porção inferior do afloramento (Fig. 11- A e B). O domínio 2 ocorre na porção máfica da zona de dano, onde ocorre o maior desenvolvimentos de falhas. As composições dos gouges de falha refletem a composição original da rocha e alguns minerais de alteração (anfibólios, plagioclásio, epidoto, clorita, carbonatos, além de algumas argilas, como caulinita, e argilas 2:1) (Fig. 11- C). O domínio 3 está localizado na porção félsica da zona de dano, nessa porção a rocha apresenta um aspecto mais cataclasado. O preenchimento das estruturas rúpteis é composto basicamente por quartzo, feldspatos, biotita, anfibólio e piroxênios, e alguns minerais acessórios como, zircão, titanita, carbonato, rutilo e epidoto. Além de alguns argilominerais (e.g., caulinita) e argilas 2:1 (Fig. 11- D).

Figura 10- Modelo digital de afloramento da zona de dano da Falha Triunfo, Complexo Granjeiro, o qual foi utilizado para análise composicional do preenchimento das falhas e fraturas. Destaque para as estruturas rúpteis onde foi realizada a coleta do material para análise de DRX, exceto as falhas 10, 13, 18 e 19, que não apresentam rocha de falha (*gouge*). Em amarelo (domínio 1) estão evidenciadas as estruturas preenchidas por calcita; em vermelho (domínio 2) estão destacadas os planos das falhas preenchidas por anfibólio e plagioclásio em sua maioria, além de argilominerais; e as fraturas em verde (domínio 3), de composição quartzo-feldspáticas com presença de anfibólio, piroxênio, argilominerais e alguns minerais acessórios.

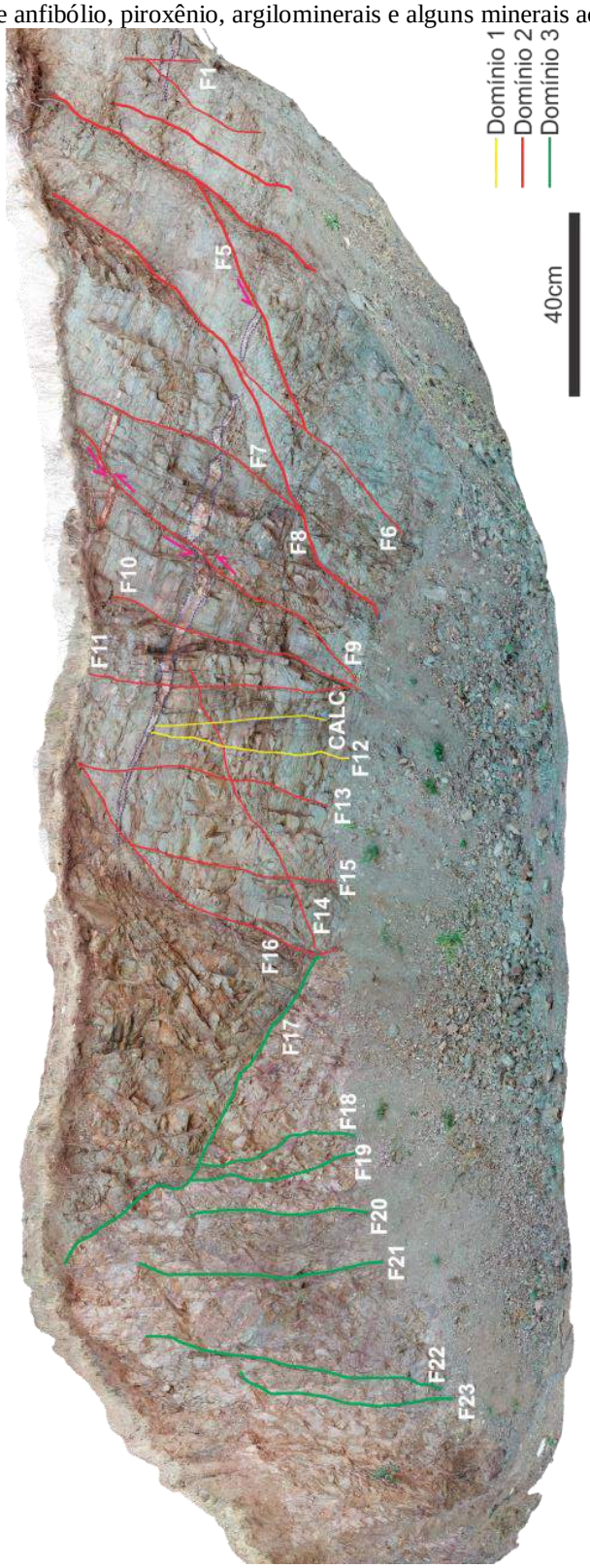

Fonte**:** Autor (2020)**.**

Figura 11- Difratogramas de amostras coletadas ao longo dos planos de falhas do Complexo Granjeiro. A) Difratograma de fratura preenchida por calcita; B) Difratograma de uma fratura preenchida por calcita e argilas 2:1; Difratogramas representativos de planos de falha localizadas na fácies C) máfica e D) félsica da rocha. Observar a clara diferença dos preenchimentos em cada fácies do embasamento cristalino.

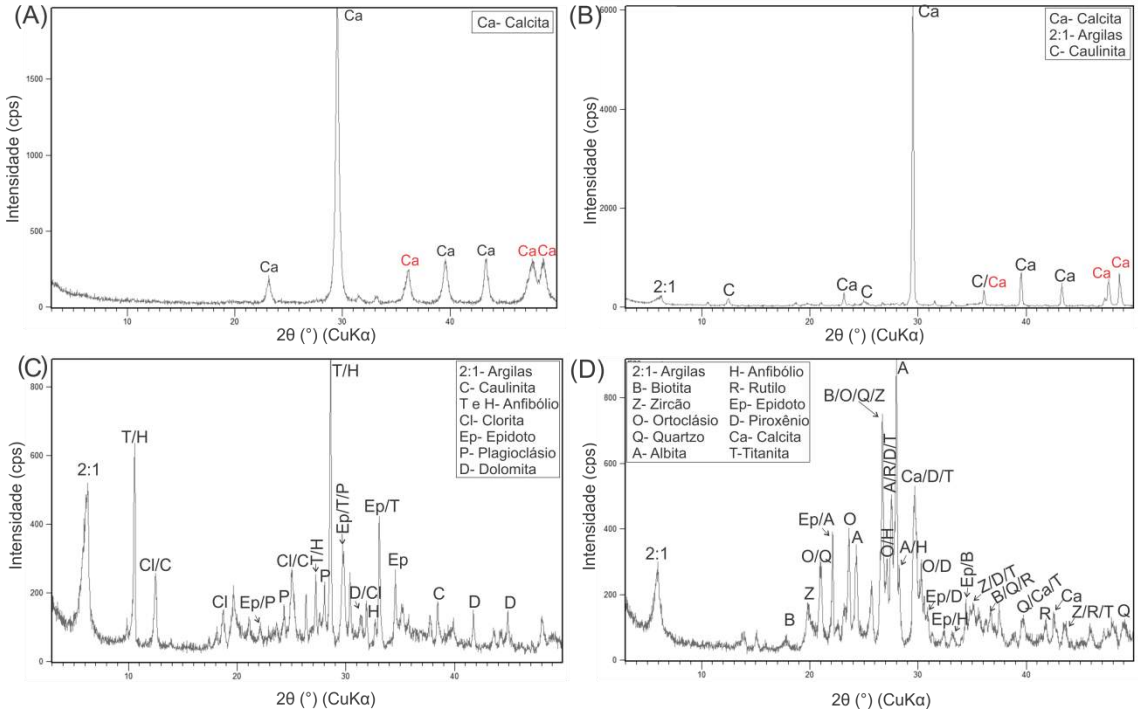

Fonte: Autor (2020).

4 CONCLUSÕES

Esta dissertação apresenta a análise estrutural multiescalar da zona de falha Triunfo e suas implicações na evolução tectônica da borda norte da BA. Para a identificação dos elementos arquiteturais da Falha Triunfo e definição dos seus eventos deformacionais foram utilizados dados topográficos de satélite e aeromagnéticos, mapeamento geológico- estrutural (1:25.000), com aplicação da técnica de *scanline*, microtectônica (catodoluminescência e EDX), geocronologia (U-Pb, carbonato) e DRX.

A zona de falha da Falha Triunfo apresenta três elementos arquiteturais: a) protólito, compreende a ortognaisses (*footwall*), arenitos e calcários (*hangingwall*) pouco deformados; b) zona de dano, composta por ortognaisses (*footwall*), arenitos e calcários (*hangingwall*), intensamente fraturados; c) núcleo, composto por brechas de falha e cataclasitos. A espessura da zona de dano foi estimada variando de 240 a 290 m no footwall e de 372 a 610 m no *hangingwall*, é assimétrica, refletindo possivelmente heterogeneidades mecânicas das rochas, bem como variação no padrão geométrico da falha.

O núcleo da Falha Triunfo no setor do embasamento é caracterizado pela presença de brechas tectônicas e cataclasitos, comumente com calcita ocorrendo como cimento e preenchendo veios. A relação temporal entre esses dois tipos de ocorrência de calcita foi observada, e reflete que ambos foram formados em períodos diferentes, possivelmente durante episódios de reativação das falhas com entrada de fluídos carbonáticos.

Este trabalho propõe três estágios deformacionais para borda norte BA: 1- Dn (Neoproterozoico), deformação dúctil; 2- Dn+1 (Paleozoico), deformação dúctil- rúptil e 3- Dn+2 (Cretáceo), rúptil. Os eventos deformacionais Dn+1 e Dn+2 refletem a transição da deformação dúctil- rúptil da zona de cisalhamento Patos e a consequente geração da zona de falha Triunfo. Esta pesquisa propõe que após o evento Dn+2 a Falha Triunfo continuou ativa durante a fase pós-rift da BA.

As brechas carbonáticas (*pipes*) da Formação Crato estão diretamente associadas ao sistema de falhas da zona de falha Triunfo. Os dados petrográficos e geocronológicos sugerem que o desenvolvimento estrutural dos *pipes* brechas teria ocorrido durante reativações episódicas (94.9 ± 3.8 Ma e 80.2 ± 3.0 Ma) das falhas, associadas à entrada de fluídos de diferentes composições químicas. Processo semelhante a este também ocorreu nas brechas tectônicas encontradas no *footwall* (embasamento) da Falha Triunfo. A associação mineral encontrada nos *pipes* (dolomita em sela, dolomita, calcita, galena, barita) se assemelha à paragênese mineral encontrada em reservatórios carbonáticos que apresentam

alterações hidrotermais (e.g., reservatório pré-sal, Bacia de Campos). No caso das brechas carbonáticas da Formação Crato, o sistema de falhas da borda norte da BA funcionou como condutos para o transporte de fluídos possivelmente vindos da Formação Cariri e/ou embasamento.

As análises DRX permitiram mapear na zona de dano (*footwall*) da Falha Triunfo os preenchimentos dos planos de falhas, classificando-os em três domínios composicionais. Os domínios analisados ilustram a ocorrência de calcitas preenchendo completamente fraturas ou associadas a outros minerais, além de argilas do tipo 2:1. Ambos minerais (calcita e argilas 2:1) são importantes no processo de datação de falhas e de rochas de falha, através dos métodos U-Pb, utilizando calcitas, ou K-Ar, utilizando ilitas (argila 2:1). Apesar de não ter sido realizado o tratamento para diferenciar o tipo de argila 2:1, as amostras analisadas ilustram um bom potencial para o método de datação K-Ar, além do método U-Pb utilizado neste trabalho.

Recomendo que sejam realizados estudos mais detalhados nos *pipes* brechas, visando identificar a origem dos fluídos, a partir da análise geoquímicas ($\delta^{13}C$, $\delta^{18}O$, $^{87}Sr/^{86}Sr$), além de inclusões fluídas para verificar a temperatura do fluído atuante na formação da dolomita. Recomendo também analisar os processos de silicificação que ocorre na Formação Cariri e analisar se existe alguma correlação com as deformações observadas na Formação Crato discutidas nesta dissertação.

REFERÊNCIAS

ALENCAR, M. L., **Mapeamento Geológico-Estrutural Da Borda Norte Da Bacia Do Araripe, Nova Olinda, Ceará.** 2014. Trabalho de conclusão de curso de Geologia. Universidade Federal de Pernambuco. Recife. p.153. 2014.

ALENCAR, M. L.; BARBOSA, J. A.; MIRANDA, T. S; SANTANA, F. R.; MAGALHÃES, J. R. G.; CORREIA FILHO, O. J. Análise De Estruturas Rúpteis Da Formação Crato, Município De Nova Olinda - CE. *In:* XIV Simpósio Nacional De Estudos Tectônicos, Chapada dos Guimarães. **Anais**. 2013.

ALENCAR, M. L. *et al*. Soft-Sediment Deformation Structures In Aptian Lacustrine Laminites: Evidence Of Post-Rift Paleoseismicity In The Araripe Basin, Ne Brazil. **Journal of South American Earth Sciences**, v.105, jan. 2020. DOI: 10.1016/j.jsames.2020.102955.

ASSINE, M. L. Bacia do Araripe, **Boletim de Geociências da Petrobras**, v.19, p.371-389. 2007.

ASSINE, M. L.; PERINOTTO, J. A.; CUSTÓDIO, M. A.; NEUMANN, V. H.; VAREJÃO, F. G.; MESCOLOTTI, P. C. Sequências Deposicionais do Andar Alagoas da Bacia do Araripe, Nordeste do Brasil. **Boletim de Geociências da Petrobras**, Rio de Janeiro, 22:3-28. 2014.

BALSAMO, F.; STORTI, F.; GROCKE, D. Fault-related fluid flow history in shallow marine sediments from carbonate concretions, Crotone Basin, south Italy. **J. Geol. Soc**., v.169, p.613–626, set. 2012.

BILLI, A.F.; SOLVINI, F.; STORTI, F. The damage zone-fault core transition in carbonate rocks: Implication for fault growth, structure and permeability. **Journal of Structural Geology**, v.25, p.1779– 1794, nov. 2003.

BISDOM, K.; GAUTHIER, B.D.; BERTOTTI, G.; HARDEBOL, N.J. Calibrating discrete fracture-network models with a carbonate three-dimensional outcrop fracture network: Implications for naturally fractured reservoir modeling. **AAPG Bulletin,** v.98, p.1351–1376. 2014. https://doi.org/10.1306/02031413060

CABRAL, F.A.; SILVEIRA, A.C.; RAMOS, G.M.; MIRANDA, T.S.; BARBOSA, J.A.; NEUMANN, V.H. Microfacies and diagenetic evolution of the limestones of the upper part of the Crato Formation, Araripe Basin, northeastern Brazil. **Brazilian Journal of Geology**, v.49(1), dez. 2019.

CAINE, J.S.; EVANS, J.P.; FORSTER, C.B. Fault zone architecture and permeability structure (supplemental data). **Geology**, v.24, p.1025-1028, nov. 1996. https://doi.org/10.1130/0091-7613(1996)024<1025

CASTRO, D.L.; CASTELO BRANCO, R.M. Caracterização da arquitetura interna das bacias rifte do Vale do Cariri (NE do Brasil), com base em modelagem gravimétrica 3-D. **Revista Brasileira de Geofísica**, v.17, p.129-144, nov.1999.

CATTO, B.; JAHNERT, R.J.; WARREN, L.V.; VAREJAO, F.G.; ASSINE, M.L. The microbial nature of laminated limestones: lessons from the Upper Aptian, Araripe Basin, Brazil. **Sedimentary geology**, v.341, p.304-315, maio 2016.

CELESTINO, M.A.; MIRANDA, T.S.; CORREIA FILHO, O. J.; BARBOSA, J. A. Aspectos Tectônicos Da Borda Ne Da Bacia De Fátima, Província Borborema- Ne Do Brasil. **Estudos Geológicos,** v.27, p.3–19. 2018. https://doi.org/10.18190/1980-8208/estudosgeologicos.v27n2p3-19

CELESTINO, M.A. *et al*. Fault damage zones width: implications for the tectonic evolution of the Araripe Basin, Brazil. **Journal of Structural Geology**, v.138, p.104–116, set.2020. https://doi.org/10.1016/j.jsg.2020.104116

CHANG, H.K.; KOSWMANN, R.O.; FIGUEIREDO, A.M. New concepts on the development of East Brazilian marginal basins. **Episodes**, v.11(3), p.194, set. 1988.

CHEN, P.Y. Table of key-lines in X-ray power diffraction patterns of minerals in clay and associeted rocks. Bloomington, Departament of Natural Resources. **Geological survey occasional paper**, v.21. p.67, 1977.

CHOI, J.H.; EDWARDS, P., KO, K.; KIM, Y.S. Definition and classification of fault damage zones: A review and a new methodological approach. **Earth-Science Reviews,** v.152, p.70–87, jan. 2016. https://doi.org/10.1016/j.earscirev.2015.11.006

DERSHOWITZ, W. S.; EINSTEIN, H. H. Characterizing rock joint geometry with joint system models. **Rock Mechanics and Rock Engineering**, v. 21, p. 21–51, jan. 1988. doi:10 1007/BF01019674.

DE LIMA, F.G.; DE SÁ, E.F. Controle estrutural da borda sudeste da Bacia do Parnaíba, Nordeste do Brasil: relação com eventos geodinâmicos no Gondwana. **Geologia USP - Serie Cientifica,** v.17, p.3–21, out.2017. https://doi.org/10.11606/issn.2316-9095.v17-125909

DIMMEN, V.; ROTEVATN, A.; PEACOCK, D.C.; NIXON, C.W., NÆRLAND, K. Quantifying structural controls on fluid flow: Insights from carbonate-hosted fault damage zones on the Maltese Islands. **Journal of Structural Geology,** v.101, p.43–57, ago.2017. https://doi.org/10.1016/j.jsg.2017.05.012

FRANÇOLIN J.B.; COBBOLD P.R.; SZATMARI P. Faulting in the Early Cretaceous Rio do Peixe Basin (NE Brazil) and its significance for the opening of the Atlantic. **Journal of Structural Geology**, v.16, p.647-661. 1994.

GARCIA, X.; JULIÀ, J.; NEMOCÓN, A.M.; NEUKIRCH, M. Lithospheric thinning under the Araripe Basin (NE Brazil) from a long-period magnetotelluric survey: Constraints for tectonic inversion. **Gondwana Research,** v.68, p.174–184, abr. 2019. https://doi.org/10.1016/j.gr.2018.11.013

LIAO, Z.; LIU, H.; CARPENTER, B.M.; MARFURT, K.J.; RECHES, Z. Analysis of fault damage zones using three-dimensional seismic coherence in the Anadarko Basin, Oklahoma. **AAPG Bulletin,** v.103, p.1771–1785, ago. 2019. https://doi.org/10.1306/1219181413417207

LIMA, B.E.; ROS. L.F. Deposition, diagenetic and hydrothermal processes in the Aptian Pre-Salt lacustrine carbonate reservoirs of the northern Campos Basin, offshore Brazil. **Sedimentary Geology**. v.383, p.55-81, abr. 2019. doi:10.1016/j.sedgeo.2019.01.006.

LIMA, B.E. *et al*. Deep-burial hydrothermal alteration of the Pre-Salt carbonate reservoirs from northern Campos Basin, offshore Brazil: Evidence from petrography, fluid inclusions, Sr, C and O isotopes. **Marine and Petroleum Geology**, v.113,104143, mar.2020. doi:10.1016/j.marpetgeo.2019.104143.

LIN, A.; YAMASHITA, K., Spatial variations in damage zone width along strike-slip faults: An example from active faults in southwest Japan. **Journal of Structural Geology,** v.57, p.1–15, dez. 2013. https://doi.org/10.1016/j.jsg.2013.10.006

MARQUES, F.O.; NOGUEIRA, F.C.; BEZERRA, F.H.; CASTRO, D.L. The Araripe Basin in NE Brazil: an intracontinental graben inverted to a high-standing horst. **Tectonophysics**, v.630, p.251-264, set.2014.

MARTILL, D.M.; LOVERIDGE, R.F.; HEIMHOFER, U. Dolomite pipes in the Crato Formation fossil lagerstätte (Lower Cretaceous, Aptian), of northeastern Brazil. **Cretaceous Research**, v.29(1), p.78-86, fev. 2008.

MARTILL, D.M.; BECHLY, G.; LOVERIDGE R.F. The Crato Fossil Beds of Brazil: Window into an ancient world. Cambridge University Press, Cambridge, p.625. 2007.

MATOS, R.M.D. The Northest Brasilian rift system. **Tectonics**, v.11(4), p.776-791, ago. 1992.

MATOS, R.M.D. History of the Northeast Brazilian rift system: kinematic implications for the break-up between Brazil and West Africa. In: N.R. Cameron, R.H. Bate, V.S. Clure (eds.). The Oil and Gas Habitats of the South Atlantic. **Geol. Soc., London**, Spec. Publ., v.153, p.55-73, jan. 1999.

MEDEIROS V.C. **Evolução geodinâmica e condicionamento estrutural dos terrenos Piancó-Alto Brígida e Alto Pajeú, Domínio da Zona Transversal, NE do Brasil.** 2004. Tese de Doutorado, Programa de Pós-Graduação em Geodinâmica e Geofísica, Universidade Federal do Rio Grande do Norte. Natal. 200p. 2004.

MIRANDA, T.S.; MAGALHÃES, J.R..; BARBOSA, J.A.; CORREIA FILHO, O.; ALENCAR, M.L. Araripe Basin , NE Brazil : A rift basin implanted over a previous pull-apart system ? 4th **Atlantic Conjugate Margins Conference 3**. 2014.

MIRANDA, T. S. **Caracterização geológica e geomecânica dos depósitos carbonáticos e evaporíticos da Bacia do Araripe, NE Brasil**. 2015. Tese de doutorado. Programa de Pós-Graduação em Geociências, Universidade Federal de Pernambuco. Recife. p. 268. 2015.

MIRANDA, T. S. *et al*. Petrophysics and petrography of aptian tight carbonate reservoir, Araripe Basin, NE Brazil. **78th EAGE Conference and Exhibition**, maio 2016. https://doi.org/10.3997/2214-4609.201600890.

Miranda, T. S. *et al*. Quantifying aperture, spacing and fracture intensity in a carbonate reservoir analogue: Crato Formation, NE Brazil. **Marine and Petroleum Geology**, v. 97, p. 556-567, nov. 2018.

MUNIZ, M. C.; BOSENCE, D. W. Pre-salt microbialites from the Campos Basin (offshore Brazil): image log facies, facies model and cyclicity in lacustrine carbonates. **Geological Society, London, Special Publications**, v.418(1), p.221-242, jul. 2015.

NEUMANN, V. H. **Estratigrafia, Sedimentologia, Geoquimica y Diagenesis de los Sistemas Lacustres Aptiense-Albienses de la Cuenca de Araripe**. 1999. Tese de Doutorado. P.244. 1999.

NEUMANN, V.H.; BORREGO, A.G.; CABRERA, L.; DINO, R. Organic matter composition and distribution through the Aptian–Albian lacustrine sequences of the Araripe Basin, northeastern Brazil. **International Journal of Coal Geology**, v.54(1-2), p.21-40, abr. 2003.

OLIVEIRA, R. G. **Arcabouço Geofísico, Isostasia e Causas do Magmatismo Cenozóico da Província Borborema e de Sua Margem Continental (Nordeste do Brasil)**. 2008. Tese de doutorado, Pós-graduação em Geodinâmica e Geofísica – Universidade Federal do Rio Grande do Norte. Natal. 415p. 2008.

ONORATI, G.; PASCOLIERI M.; VENTURA, R.; CHIARINI, V.; CRUCILLÀ, U. The digital elevation model of Italy for geomorphology and structural geology. **Catena**, v.19, p.147-178, abr. 1992.

ORTEGA, O.J.; MARRETT, R.A.; LAUBACH, S.E. A scale-independent approach to fracture intensity and average spacing measurement. **AAPG Bulletin**, v.90, p.193–208. 2006. https://doi.org/10.1306/08250505059

OSÉS, G.L. *et al*. Deciphering pyritization-kerogenization gradient for fish soft-tissue preservation. **Scientific Reports**, v.7, p.1468, dez. 2017.

PEACOCK, D.C.; DIMMEN, V.; ROTEVATN, A.; SANDERSON, D.J. A broader classification of damage zones. **Journal of Structural Geology,** v.102, p.179–192, set. 2017. https://doi.org/10.1016/j.jsg.2017.08.004

PEULVAST, J.P.; BÉTARD, F. A history of basin inversion, scarp retreat and shallow denudation: The Araripe basin as a keystone for understanding long-term landscape evolution in NE Brazil. **Geomorphology,** v.233, p.20–40, mar. 2015. https://doi.org/10.1016/j.geomorph.2014.10.009

PONTE, F.C.; PONTE FILHO, F.C. Estrutura geológica e evolução tectônica da Bacia do Araripe. Recife, **DNPM**, p.68, 1996.

RAND, H.M. Levantamento gravimetrico e magnetometrico da Bacia Araripe. **Relatório interno da PETROBRAS**, 11 p., caderno de dados e mapas. 1983.

RAND, H.M.; MANSO, V.A. Levantamento gravimétrico e magnetométrico da Bacia do Araripe. In: SBG, Congresso Brasileiro de Geologia, 4, **Anais**, p.2011-2016. 1984.

ROBERTS, N.M.; WALKER, R. J. U-Pb geochronology of calcite-mineralized faults: Absolute timing of rift-related fault events on the northeast Atlantic margin, **Geology**, v.44, p.531-534, 2016.

ROBERTS, N.M.; RASBURY, E.T.; PARRISH, R.R.; SMITH, C.J.; HORSTWOOD, M.S.; CONDON, D. J. A calcite reference material for LA-ICP-MS U-Pb geochronology, Geochemistry, **Geophysics**, **Geosystems**, v.480, maio 2017.

ROTEVATN, A. *et al*. Structural Inheritance and Rapid Rift-Length Establishment in a Multiphase Rift: The East Greenland Rift System and its Caledonian Orogenic Ancestry, **Tectonics,** v.37, p.1858–1875, maio 2018. https://doi.org/10.1029/2018TC005018.

SALAMUNI, E.; EBERT, H.D.; Hasui, Y. Morfotectônica Da Bacia Sedimentar De Curitiba. **Revista Brasileira de Geociências,** v.34, p.469–478, dez.2004. https://doi.org/10.25249/0375-7536.2004344469478

SALOMON, E. *et al*. Fault-controlled fluid circulation and diagenesis along basin bounding fault systems in rifts–insights from the East Greenland rift system. **Solid Earth Discussions**, v.11, p.1987-2013, nov. 2020.

SANTOS, R.F. *et al*. Characterization of natural fracture systems: analysis of uncertainty effects in linear scanline results. **AAPG (Am. Assoc. Pet. Geol.) Bull,** v.99 (12), p.2203–2219, dez. 2015. https://doi.org/10.1306/05211514104.

SCHOBBENHAUS, C. (org). Programa Geologia do Brasil. **Carta Geológica do Brasil ao Milionésimo** – Folha Jaguaribe. CPRM – Serviço Geológico do Brasil. 2004.

SCHUELLER, S.; BRAATHEN, A.; FOSSEN, H.; TVERANGER, J. Spatial distribution of deformation bands in damage zones of extensional faults in porous sandstones: Statistical analysis of field data. **Journal of Structural Geology,** v.52, p.148–162, jul.2013. https://doi.org/10.1016/j.jsg.2013.03.013

SILVA, A. L. **Estratigrafia Física e Deformação do Sistema Lacustre Carbonático Aptiano-Albiano da Bacia do Araripe em Afloramento Selecionados**. Dissertação de Mestrado, Programa de Pós-Graduação em Geociências – Universidade Federal de Pernambuco. 118p. 2003.

TORABI, A.; ALAEI, B.; LIBAK, A. Normal fault 3D geometry and displacement revisited: Insights from faults in the Norwegian Barents Sea. **Marine and Petroleum Geology**, v.99, p.135-155, jan. 2019.

VAREJÃO, O.F.; WARREN, L.V.; SIMÕES, M.G.; FÜRSICH, F.T.; MATOS, S.A.; ASSINE, M.L. Exceptional preservation of soft tissues by microbial entombment: Insights into the taphonomy of the Crato Konservat-Lagerstätte. **Palalios**, v.34, p.331-348, 2019.

WARREN, L.V. *et al*. Stromatolites from the Aptian Crato Formation, a 1hypersaline lake system in the Araripe Basin, northeastern Brazil. **Facies**, v.63(1), p.3, nov.2017.

WU, G.; GAO, L.; ZHANG, Y.; NING, C.; XIE, E. Fracture attributes in reservoir-scale carbonate fault damage zones and implications for damage zone width and growth in the deep subsurface. **Journal of Structural Geology,** v.118, p.181–193, 2019. https://doi.org/10.1016/j.jsg.2018.10.008